PREFACE

A programme of measurement of horizontal drifts by the spaced aerial method was initiated at the Physical Research Laboratory, Ahmedabad as early as 1954. The first equipment was designed and built for taking observations on 5.0 Mc/s by N.G.Nanda (1955) and later was modified to operate on 2.6 Mc/s and 4.0-4.4 Mc/s by R.Sethuraman (1958). The present author further modified the equipment in 1959 to send and receive signals from 4.5 Mc/s to 7.5 Mc/s in addition to the existing ones on 2.6 Mc/s and 4.0-4.4 Mc/s. The author continued to take observations on all these frequencies from 1959.

The author made a large number of observations of drift on different frequencies in 1960-62 and has analysed them in this thesis. It may be mentioned that not many observations on a higher frequency like 7.0 Mc/s had been taken before.

The reading of the films, the reduction of data and correlation analysis were all done by the author. The thesis discusses observations in two parts : 1956-59 and 1959-62.

Scope of the thesis

The thesis contains a description of the experimental technique used for obtaining fading records of the diffraction pattern of radio waves reflected from ionospheric irregularities

in E and F regions and the results of analysis of the fading records obtained at Ahmedabad over a period covering 1956-62.

The essential contents are :

(1) Results of analysis of drift speed and direction of irregularities in the E and F regions of the ionosphere.

(2) Amplitude and time analysis of singly-reflected downcoming waves from the E region.

(3) Correlation methods of analysis and size of the irregularities in the ionosphere.

(4) Comparison with results obtained by Sethuraman (1956-59) at Ahmedabad and by others elsewhere.

C M Patel
Author

Countersigned

K R Ramanathan

27/4/66.

ACKNOWLEDGEMENT

I take great pleasure in expressing my indebtedness to Professor K.R.Ramanathan for his guidance and interest in the problem and to Dr.S.S.Degaonkar for his whole-hearted assistance in putting the thesis into proper shape. I acknowledge with grateful thanks the help and supervision rendered by Dr.R.G.Rastogi towards the analysis of the drift data, to Dr.J.S.Shirke for advice on technical matters and to Mr.C.T.Patel for his help in taking the observations.

The financial support for this work came from the Council of Scientific and Industrial Research, Govt. of India till 1962 and later from the Department of Atomic Energy, Govt. of India to both of whom I express my sincere thanks.

C M Patel

(C.M.Patel)

C O N T E N T S

LIST OF TABLES

LIST OF FIGURES

CHAPTER I

Evidence for winds in Upper Atmosphere

Brief review of radio methods used for their study

1. General

The existence of strong winds of the order of 50-100 m/sec. in the upper atmosphere has been known for a long time. Visual observations of the movement of noctilucent clouds (Störmer 1935, Hoffmeister, 1946) and of meteor trails (Oliver 1942, 1947) give direct observational evidence of the existence of such winds. The dynamo theory of diurnal geomagnetic variations requires the presence of a world-wide wind system in the ionosphere. The semidiurnal oscillations of barometric pressure at the surface of the earth, also implies a world-wide wind system which extends to the upper atmosphere. Developments in radio techniques (Mitra 1949, Briggs and Spencer, 1954) for measuring drifts of electrons have shown movements of ionisation irregularities in the ionosphere. The information provided by the movements of noctilucent clouds and of meteor trails relate to the neutral atmosphere while drift velocities of ionospheric irregularities may be caused either by a mass movement of the gas as a whole or by the movement of electrons due to an electric field. The motion of electrons is affected by the presence of the earth's magnetic field (Ratcliffe, 1960).

2. Motion of ionospheric irregularities in relation to the movement of the neutral atmosphere and a feeble background plasma

In considering ionospheric drift measurements, it has to be noted that radio observations refer to movements of ionisation irregularities in a neutral atmosphere in which is embedded a feeble background plasma. If the neutral air moves as a whole it cannot in general be taken to mean that the plasma has the same movement. In the D and lower E regions, where the collision frequencies are high the plasma and the ionospheric irregularities can be moved relatively more easily by air movements than by electric fields, and at these levels it may be considered that the drift observations provide information about air movements. In the F region, however, it is relatively easier to move the electrons by means of an electric field. It is therefore probable, though not certain, that the irregularities will move with the plasma. It is generally agreed at present that the observed horizontal drifts in the F region represent movements of plasma caused by electric fields.

Dynamical sources such as planetary, tidal and internal gravity waves play an important role in upper atmospheric movements. It is now believed that thermal wind equation alone cannot explain the observed variations in winds observed in meteor trails (Hines, 1963). In short, it appears that the drift movements obtained by radio methods may have

to be viewed with caution and should not in general be taken to mean neutral winds, except perhaps in the height range 80-120 km.

In the following sections, some of the important radio methods used to study the horizontal drifts in the ionosphere are briefly reviewed.

3. Experimental methods for studying horizontal drifts in the ionosphere using radio techniques

There are many radio methods used to study horizontal drifts in the ionosphere. They are (a) method of similar fades using closely spaced aerials and receivers, (b) method of widely spaced transmitters and a receiver, (c) radio study of ionised meteor trails, and (d) method of radio-star scintillations.

(a) Method of closely spaced receivers

The amplitude of a radio wave singly reflected from the ionosphere generally varies in a random fashion with time. This phenomenon is known as the fading of a radio wave. Pawsey (1933) found that the fading patterns of radio waves recorded at two closely spaced receivers were similar in shape but were displaced in time with respect to one another. He explained such time-shifts by assuming that the reflecting layer of the ionosphere was moving horizontally. Ratcliffe (1948) suggested that the ionosphere contains in it irregularities of ionisation

which act as an irregular diffracting screen for the incident radio waves and the reflected radio waves produce an irregular diffraction pattern on the ground. Any wind in the ionosphere would cause the diffraction pattern to move past the receiving point producing fading of radio waves received by an antenna. In this simple case, the fading recorded at two nearby points would be similar in appearance but displaced in time. Any random movements of the ionospheric irregularities would produce random changes of the diffraction pattern on the ground and the fading patterns recorded at two nearby points would lose similarity.

In general, the two mechanisms mentioned above operate simultaneously so that, although the diffraction pattern moves on the ground with a steady drift velocity, it is subject to random changes of form as it moves. Under these conditions the fading recorded by two receivers separated by a small distance is similar but displaced in time, and the degree of similarity decreases as the separation is increased; at a sufficiently great distance any similarity would vanish.

Following the ideas of Pawsey (1933) and Ratcliffe (1948), Mitra (1949) developed a method of closely spaced receivers for the measurement of speed and direction of the ionospheric irregularities from the fading records produced by the moving irregular diffraction pattern across the ground.

Mitra's method of closely spaced receivers for

investigating horizontal drifts has been used in many laboratories and also at Ahmedabad. A brief description of the method is given in the following paragraphs.

Mitra's method involves the measurement of time delays between corresponding maxima or minima of the fading records. Knowing the separation between the receivers which record the fading pattern, the velocity and direction of the diffraction pattern can be calculated. This concept of similar fades is explained with the aid of Figure 1.1(a).

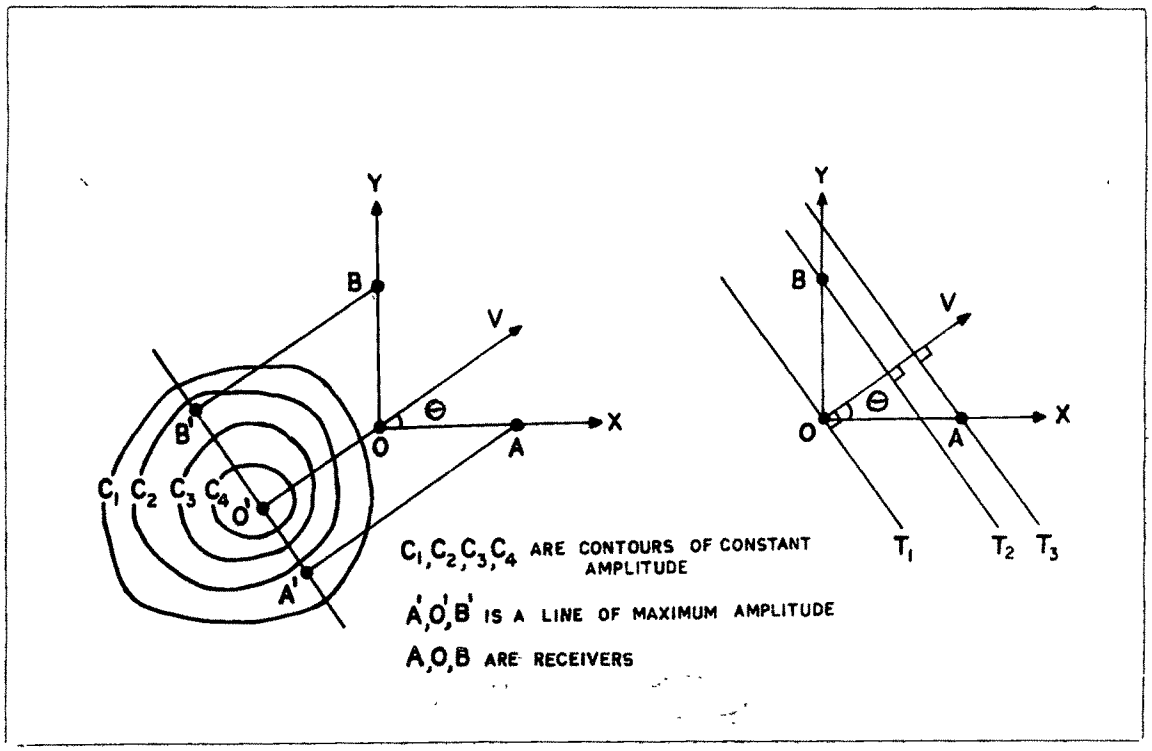

Fig.1.1(a) Fig.1.1(b)

Contours of constant amplitude showing line of maximum amplitude.

Three receivers 0, A and B are located at the vertices of a right angled triangle. The origin of the co-ordinate system is located at 0 with the positive X-axis in the direction from 0 to A and with the positive Y-axis from 0 to B.

Assuming that the diffraction pattern produced by the ionospheric irregularities drifts across the ground with a steady velocity and without any change of form as it moves and that the diffraction pattern on the ground is isometric in nature, i.e. its statistical properties are identical in all directions, then the diffraction pattern can be conveniently represented by contours of constant amplitude and it is possible to construct a line of maximum amplitude such that when this line passes over the receivers 0, A and B amplitude peaks are observed. The line of maximum amplitude passes through the point of contact between a line parallel to the direction of drift and the amplitude contours. As the line of maximum amplitude drifts over the triangular arrangement of receivers with speed V and direction at an angle θ with the X-axis, the receiver at 0 will record an amplitude variation along the line 00' as time passes. When the point 0' passes over 0 a maximum in amplitude will be recorded by the receiver at 0. The point 0' is the point at which the line 00' is tangent to the contour with the largest amplitude. Similarly the receiver at A will record a maximum at point A' and the receiver B, at the point B'. If the contours of constant amplitude are approximately circular and the receiver separation

is small compared to the size of the diffraction pattern, then the points A', O' and B' will lie on a straight line perpendicular to the direction of the drift velocity. The line A'O'B' is known as the "line of maximum amplitude". If only the time delays of maxima or minima are considered, the motion of the diffraction pattern across the ground can be replaced by the motion of the line of maximum amplitude. In Figure 1.1(b) the contours are replaced by the line of maximum amplitude moving at times T_1, T_2 and T_3. From Figure 1.1(b) the following apparent velocities can be deduced :-

$$V_1 = \frac{a}{T_3 - T_1} = \frac{a}{T_x} \qquad (1)$$

$$V_2 = \frac{a}{T_2 - T_1} = \frac{a}{T_y} \qquad (2)$$

where $a = OA = OB$

T_x = The time delay between the arrivals of the line of maximum amplitude at receivers O and A respectively.

T_y = The time delay between the arrivals of the line of maximum amplitude at the receivers O and B respectively.

Now $$T_x = \frac{a \cos \theta}{V} \qquad (3)$$

and $$T_y = \frac{a \sin \theta}{V} \qquad (4)$$

Substituting in equations (1) and (2) yields

$$V_1 = \frac{V}{\cos\theta} \qquad (5)$$

$$V_2 = \frac{V}{\sin\theta} \qquad (6)$$

Eliminating θ between (5) and (6) we get,

$$\frac{1}{V^2} = \frac{1}{V_1^2} + \frac{1}{V_2^2} \qquad (7)$$

Dividing equation (5) by equation (6) we get

$$\tan\theta = \frac{V_1}{V_2} \qquad (8)$$

Thus knowing a, the receiver separation and measuring the mean time delays T_x and T_y, the drift velocity V and direction θ can be easily calculated. The conventional direction is expressed in degrees east of north. This we may denote by ϕ which is equal to $(90-\theta)$. The velocity calculated by equation (7) refers to the velocity of the ground diffraction pattern which is twice the velocity of the ionospheric irregularities and so to get the velocity of the ionospheric irregularities the magnitude of the velocity obtained by equation (7) should be divided by two.

Mitra's method is simple in application but has several drawbacks owing to the simplifying assumptions. Although the pattern is assumed statistically isometric, the individual contours of constant amplitude may not be circular,

or the line of maximum amplitude may not be normal to the drift direction. This will lead to a variability in time shifts. The assumption that there are no random movements superimposed on the steady drift is not often true. The diffraction pattern may not possess the statistically isometric or circular symmetry at all times and it may have any shape.

Ratcliffe (1954) has shown that if the speed and direction of the diffraction pattern remain constant, there will not be any error in speed or direction due to random orientation of the line of maximum amplitude with respect to the drift direction, provided the averaging is done over a sufficiently large number of time delays. Briggs, Phillips and Shinn (1950) and Phillips and Spencer (1955) have developed correlation methods of analysing the fading records which permit the deduction of the true and random velocities and the shape and orientation of the diffraction pattern. These methods take a long time for computation. It is not possible to apply them to a large number of records. So the method of similar fades is applied for routine scaling of the speed and direction of the irregularities following the recommendations regarding the selection of fading records suggested by Beynon and Brown (1957).

(b) <u>The method of widely spaced transmitters and a single receiver for measuring ionospheric winds</u>

The amplitude variation of the received echo becomes

completely uncorrelated if the receiving points are separated by more than a few wavelengths. But some other measurable characteristics of received echoes corresponding to large scale irregularities in the reflecting layer can be detected by taking observations at points separated by several wavelengths to a few hundred kilometers apart. Munro (1948, 1950) has developed a method for measuring the horizontal movements in the F region from the records taken with widely separated points of reflection in the ionosphere. The system consists of three transmitters spaced in a triangular array. These transmitters are operated on the same radio frequency, and with the same repetition frequency, and are so phased, by either mains synchronisation or pulse triggering technique, that the three pulses are spaced about 50 km apart on a normal type of time base such as are used for ionospheric observations. It is thus possible to record the virtual heights of three sets of echoes simultaneously at one receiving station on a single film. It has been frequently observed that several types of clearly defined changes occur in echoes from the F region which show a time difference of occurrence at the spaced points. Such changes usually occur in the form of :

(1) Some characteristic patterns due to splitting of reflected echoes.

(2) Peaks and dips in difference of virtual heights in ordinary and extraordinary echoes.

(3) Changes in virtual heights of the two components observed at vertical incidence.

Knowing the time difference in the occurrence of similar characteristics of the echo at different points, the speed and direction of large scale irregularities in the F region can be calculated.

Munro (1950, 1953) has reported the results obtained by the use of widely spaced transmitters and a receiver showing the movements of large scale irregularities of the size of about 400-500 km. These appear at F region heights. He has shown that these large scale irregularities move with speeds of 100-200 m/sec. towards the northeast direction in winter and southeast direction in summer at Sydney in Australia. The direction of movement shows a small diurnal variation. On the other hand, Bramley (1953) working at Slough did not find the seasonal change reported by Munro. Bramley's results show that irregularities of the size of 100-500 km. move with a velocity of 35-350 m/sec. with a tendency to move towards east.

(c) Measurement of horizontal drifts in the upper atmosphere by means of ionised meteor trails

Meteors enter the earth's atmosphere with velocities of 12 to 40 km/sec. They are vaporized by collision with air molecules leaving ionised meteor trails with density of the order of 10^{10} electrons/cm^3. These ionized columns or trails have an initial radius of a few centimeters and lengths of approximately 10 km. and disperse by ambipolar diffusion at a rate which in the height range 80-120 km is sufficiently slow for the trails to behave as scatterer of radio waves in

the UHF range. They have been used extensively for the investigation of drift movements of the atmosphere at levels in which the trails are embedded.

Investigation of drifts in the upper atmosphere by observations of these changes in the radio echoes of drifting meteor trails was first made by Manning, Villard and Peterson (1950) at Stanford. Later, two techniques were developed for the systematic study of horizontal drifts by using drifting meteor trails as reflectors of high frequency radio waves in the height range of 80-120 km : (i) a continuous wave method developed at Adelaide by Robertson, Liddy and Elford (1953) and (ii) a coherent pulse method developed at the Jodrell Bank Experimental Station by Greenhow (1953) and Greenhow and Neufeld (1955).

The continuous wave method gives the position and height of the meteor trails with greater accuracy than the coherent pulse method, while the latter has the advantage of single station operation and freedom from unwanted short range echoes. A brief description of the methods is as follows.

(i) Pulse method of measuring horizontal drifts using ionized meteor trails

In the coherent pulse method, the transmitter is triggered to radiate pulses of about 80-100 μs duration at a repetition rate of 150 pulses per second at a frequency of about 36 Mc/s. The reflected signal from the drifting meteor

trail is received by a conventional superheterodyne receiver operating at the same frequency. The receiver has a gating circuit for selecting out the wanted signal. The received signals are fed into four oscilloscopes from which information regarding the echo range, amplitude and phase variations can be collected. The first of these has a type A display of the ground pulse and of the received echo. These enable range measurements to be made. The amplitude variations in the received signals are displayed in the second C.R.O. in which the reflected echo is applied to the Y-plates with a short period time base (0.3 ms.) initiated by the echo to the X-plate. This gives a Fresnel diffraction pattern as the meteor crosses the aerial beam and is used to determine the speed of the meteor. The ground pulse and the received signals are mixed together and the resultant beat signal is applied to two other scopes with a phase lag of 90° to one. They record the phase variations as the ionised trial drifts towards, or away from, the receiving station. A complete cycle of change in these two represents a phase reversal caused by the drift of the trail in a distance $\lambda/2$. Knowing the frequency, it is possible to determine the speed of the drift along the line of sight. The sense of the drift is obtained by comparing the patterns obtained in the two oscilloscopes and by seeing which of them leads. Having obtained the radial component of the movement in a particular direction, the aerials are directed in a perpendicular direction or in two other directions for periods of the order of 10 minutes and the radial components

are obtained along these directions also. If the heights of the meteors are within small, defined limits, the actual velocity and direction of drift in the atmospheric layer at which these drifting trails are observed can be determined.

(ii) Continuous wave method of measurements of horizontal drifts

Robertson et al (1953) and Elford and Robertson (1953) have described a continuous wave method of determining drifts with the help of meteor trails. This equipment operates on a frequency of 25 Mc/s with a power output of 250 watts. The receiving station is situated at a distance of about 12 miles from the transmitter and consists of three dipoles placed at the corners of a right angled triangle with a separation of The heights of the aerials are adjusted so that the ground signal is of comparable magnitude with the sky wave signals. There would however be a phase difference between the ground signal and the meteor signal at each aerial and this phase difference would undergo periodic change as the reflecting column of ionisation drifts. This results in a periodic change in amplitude showing beats. Knowing the period t of the beat, and the wavelength λ , the radial component of speed V_r can be computed from the relation $V_r = \frac{\lambda}{2t}$. To determine the sense of the radial velocity, i.e. whether it moves towards or away from the receiving aerials, a sudden phase shift of 900 is introduced in the transmitted signals periodically, followed by a gradual recovery. The sudden change in the phase shift

affects the ground wave earlier than the sky wave, producing a resultant signal which appears in the form of a spike in the beat signal. From the positions of these spikes, it is possible to determine the sense of the drift. The range is measured in the conventional manner and the direction of arrival is measured by a direction finder consisting of three receiving aerials. The actual speed of the drift can then be determined with the help of simple transformations.

Results obtained from radio observations of the drifting meteor trails

Manning, Villard and Peterson (1950) working at Stanford have observed that the meteor trails drift with a velocity of the order of 50 m/sec and the most frequent directions are towards northeast and north. The results of Elford and Robertson (1953) for Adelaide show that the trails drift with a velocity of the order of 70 m/sec. The results of these authors have shown that there is a velocity gradient of the order of 3.6 m/sec per km. The results obtained by Greenhow and Neufeld (1961) show that, at the Jodrell Bank Experimental station, the steady drift and the semidiurnal drift vectors predominate over the diurnal vector and that the phase and amplitude of the prevailing drift vector change with height. The results of these workers also show that the diurnal and semi-diurnal drift vectors rotate in a clockwise direction. Elford (1959) has summarised the results of drifting meteor trails observed at Adelaide. He reports that the

prevailing, diurnal and semi-diurnal drift vectors are of comparable amplitude. The magnitude of the prevailing E-W drift is found to be higher than the prevailing N-S drift. Large height gradients in the prevailing winds are also noted. The diurnal and the semi-diurnal vectors rotate in an anticlockwise direction.

(d) Drift measurements by the method of radio-star scintillations

The amplitude of electromagnetic waves emitted by radio stars when observed on meter wavelengths are found to fluctuate rapidly in an irregular manner with respect to time. This phenomenon is known as scintillations of radio star. Little and Maxwell (1951) and Ryle and Hewish (1950) have found that the occurrence of these fluctuations shows a high degree of correlation with the presence of the spread F and it is now generally agreed that they result from irregular diffraction of the incoming radiation as it passes through the ionisation irregularities present under spread F conditions.

When observations are carried out with similar receiving equipments spaced over base lines of a few kilometers, it is possible to detect small displacements in the time of occurrence of the individual fluctuations recorded at the various receiving stations. These time delays are due to the drift of the diffraction pattern across the ground due to the movements of the irregularities in the F region.

The motion of the diffraction pattern is calculated from a comparison of the records taken at three receivers, and after making necessary corrections for the rotation of the earth, the horizontal drift can be deduced.

Results obtained by the method of radio star scintillations

Ryle (1951) has reported that the irregularities producing radio star scintillations move with velocities of the order of 100 m/sec. He observed a complete reversal of the direction of drift along the eastwest line within a period of about half an hour. The results obtained by Maxwell and Little (1952) and by Hewish (1951) show that in the upper part of the F region at night the direction of drift is towards the west. This changes to an eastward direction after midnight during magnetically disturbed periods.

CHAPTER II

Experimental Set-up

1. Introduction

The experimental set up used at Ahmedabad for ionospheric drift work is the spaced receiver method developed by Mitra (1949). The first equipment was designed and built by Nanda (1955). It was later modified by Sethuraman (1958) to operate on 2.6 and 4.0-4.4 Mc/s and by the author in 1959 to operate on 4.5 to 7.5 Mc/s.

The essential parts of the equipment are (1) aerial system, (2) transmitting unit and (3) receiving and recording units.

The transmitting, receiving and recording units are built on unit construction system and are mounted in racks. They can be removed from the rack for servicing. The essential parameters of the equipment are given in Table 2.1.

Table 2.1

Peak transmitter power	-- 1.5 KW.
Pulse duration	-- 200-350 μsec.
Pulse repetition frequency	-- 50 c/s
Bandwidth of the receiver	-- $\pm$10 Kc/s
Receiver gain	-- 3 x 10^6
Transmitting aerials	-- (i) Inverted delta for 4.5 to 7.5 MHZ
	(ii) Half-wave dipole for 2.6 and 4.0 to 4.4 MHZ
Receiving aerials	-- Half-wave dipoles designed for 2.6 MHZ.

A brief description of the different units is given in the following sections.

2. Aerial system

The schematic plan of the aerial system used at Ahmedabad for investigating drifts in the ionosphere is shown in Figure 2.1. All the aerials are erected in the open field behind the main building of the laboratory.

The transmitting aerials are the half-wave center-fed dipoles designed for the operation on 2.6 Mc/s and 4.0-4.4 Mc/s. The inverted delta aerial is used as a transmitting aerial for the frequency range 4.5 to 7.5 Mc/s. The transmitting aerials are oriented in east-west direction.

The receiving aerials are half-wave center-fed dipoles designed for 2.6 Mc/s and are oriented in the north-south direction. The aerials are separated by distance of 120 meters along E-W and N-S directions as shown in Figure 2.1.

3. Transmitter

The transmitter consists of a pulse-modulated master oscillator feeding a power amplifier stage and covers the frequency range of 2 to 7.5 Mc/s in three bands. It is pulsed at the mains frequency of 50 cycles per second. The pulse width is variable between 200-350 μsec in four steps. The peak power of the transmitter is about 1.5 KW. A schematic block

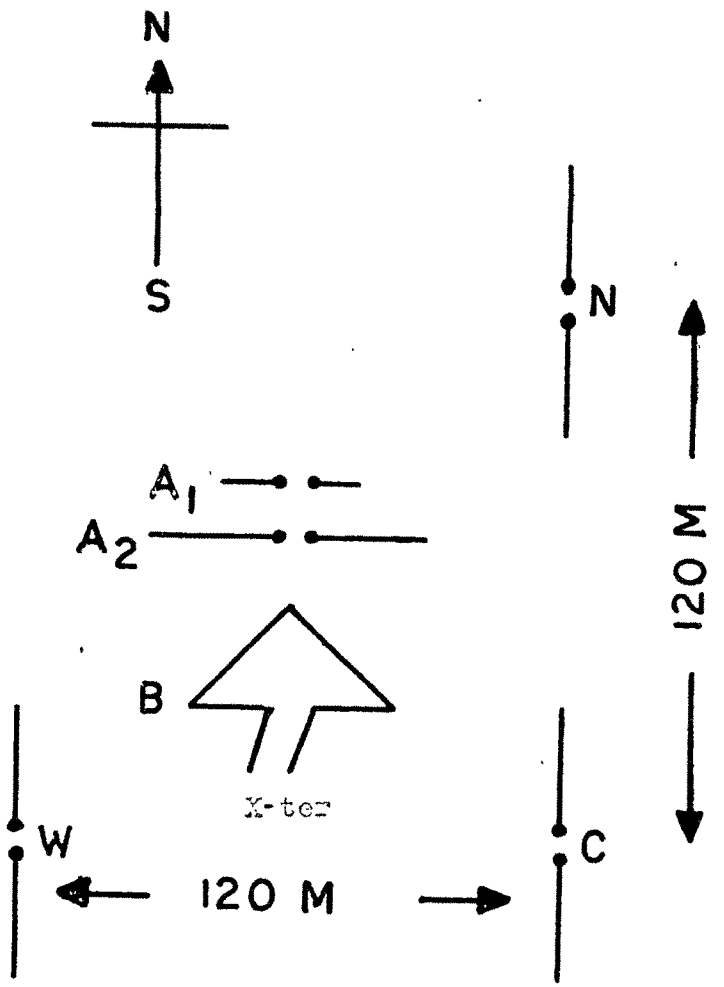

Figure 2.1 Schematic diagram of the aerial system for transmitter and the receiver.

A_1 - transmitting dipole for 4.0-4.4 MHz

A_2 - transmitting dipole for 2.6 MHz

B - Inverted delta for transmitting 4.5-7.5 MHz

C, W and N - receiving dipoles for all the frequencies

C-W forms E-W pair

N-C forms N-S pair

diagram of the transmitter is shown in Figure 2.2 and the details of the circuit diagram are shown in Figure 2.3.

4. Receiving and recording unit

This unit incorporates an assembly of

(1) B.C. 312 USA Army Receiver modified for pulse work.
(2) Triggering unit.
(3) Switching circuit and sweep generator.
(4) Two delayed pulse generators.
(5) Display units.
(6) Camera unit and time marker.
(7) Sweep generator.

The pulses returned from the ionosphere are received at three spaced aerials and are brought to the receiving and recording unit by means of R.F. cables of 72 ohms impedance. A block diagram showing the various parts of the receiving and recording unit and the manner in which they are interlinked is shown in Figure 2.4.

The pulses from each of the three aerials C, W and N are fed in sequence to the receiver by means of an electronic switch which operates in such a way that one pulse is received from each aerial in turn. The output of the receiver is applied to the vertical deflection plates of the monitoring cathode ray tube and to the horizontal deflection plates of the recording cathode ray tube. Delayed pulse generators 1 and 2

BLOCK DIAGRAM OF THE TRANSMITTER

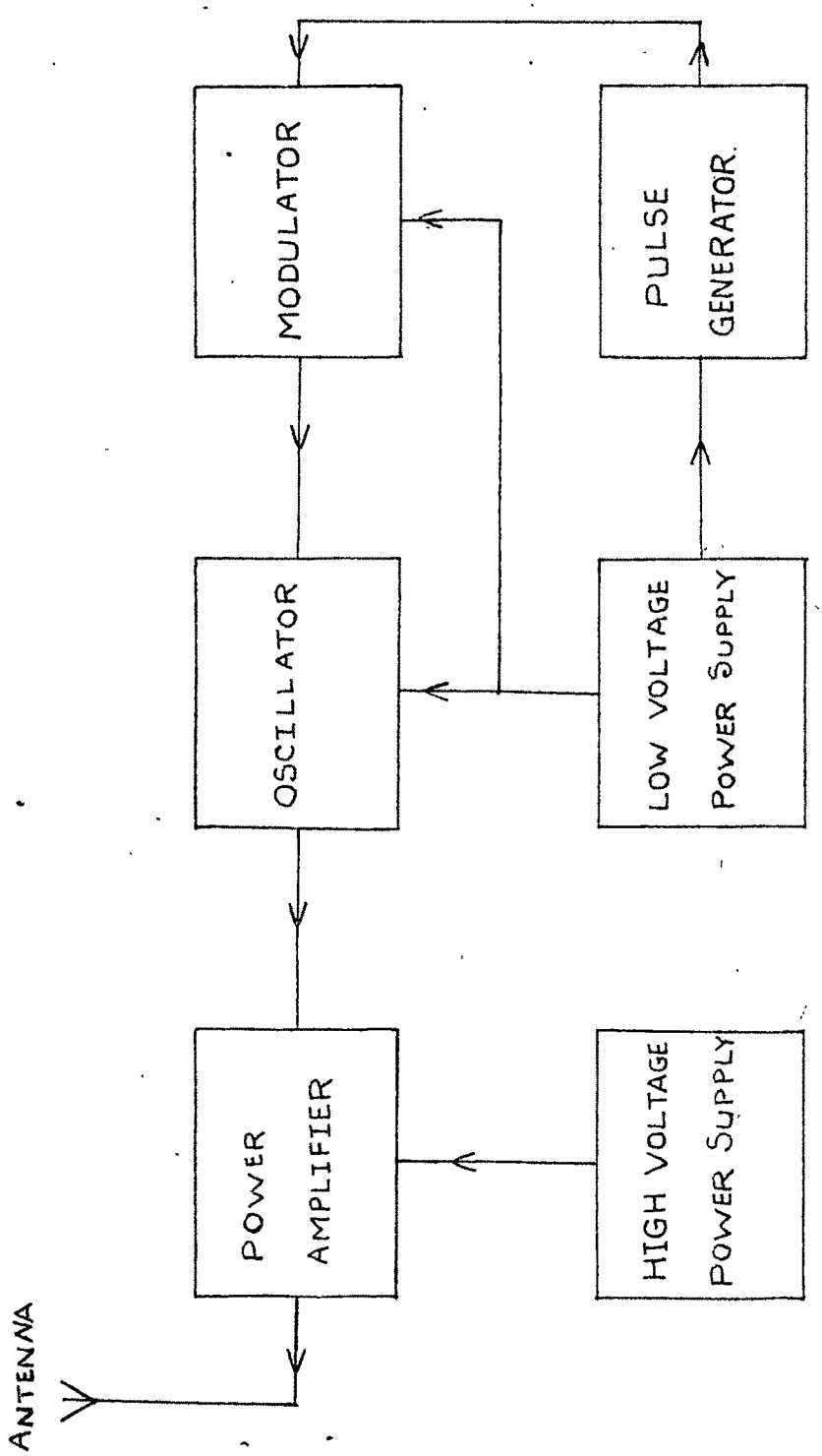

FIGURE 2·2

TRANSMITTER

Type 2

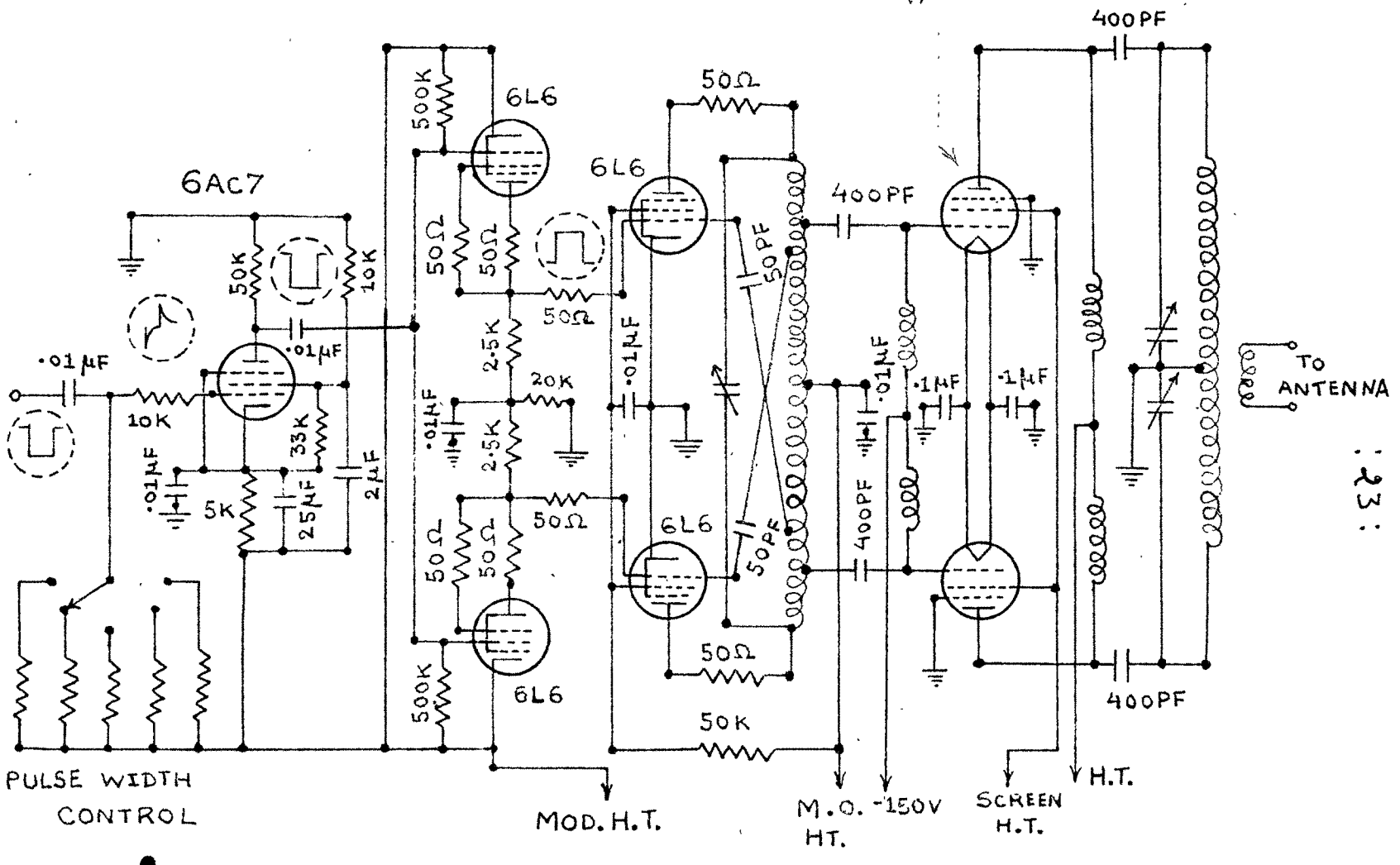

FIGURE 2·3

BLOCK DIAGRAM OF RECEIVING & RECORDING UNIT

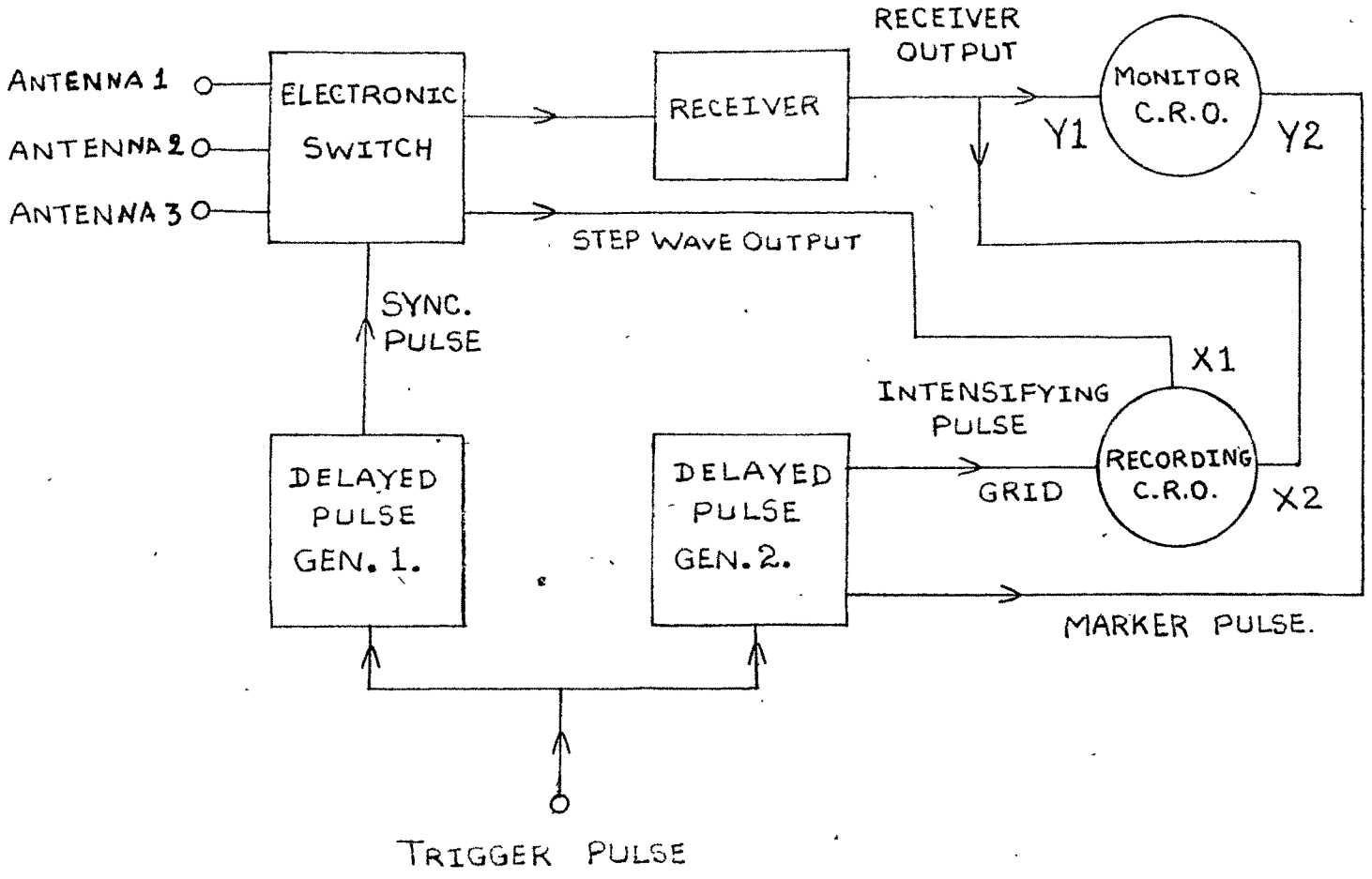

FIGURE 2·4

produce rectangular D.C. pulses delayed by a fixed time with respect to the start of the transmitted pulse. One of these is used to synchronise the electronic switch so that the change-over from one aerial to another takes place midway in the interval between two consecutive transmitted pulses. The other is used as a gate pulse to select the desired echo simultaneously; a pulse is applied to the grid of recording CRO generally beyond cut-off so that the spot appears on the screen only during the presence of the gate pulse. A part of the same pulse is fed to the Y-plate of the monitor tube for visual adjustment of the position of the gate pulse. The fading of the echo at three aerials which is displayed on the recording cathode ray tube is photographed on 35 mm film, moving in a direction perpendicular to the direction of deflection at a speed of 4 in/min. A brief description of the various sub-units of the receiving and recording system is presented in the following sections.

(1) Receiver

The receiver used is an U.S. Army disposal type BC-312 which is a superheterodyne receiver employing two stages of R.F. amplification, two stages of I.F. amplification followed by a conventional second detector and one stage audio amplifier. To use it for pulse operation, the following modifications were made :

(a) The gain of the R.F. stages was increased by replacing

the existing 6K7 tubes by 6AC7 tubes which have a much higher transconductance and are capable of delivering higher gain. Suitable changes were made in the circuit values for operating them under optimum condition. Since most of the receiver noise originates in the mixer stage, the gain of the mixer stage was reduced in order to maintain a good signal to noise ratio at the output of the receiver.

The A.V.C. control of these tubes was removed as we are interested in studying the fading of the echo amplitude.

(b) Desensitising of the R.F.Stages

A negative rectangular D.C. pulse coincident in time with the transmitted r.f. pulse was applied to the suppressor grids of the two R.F. amplifier tubes of the receiver. Thus the gain of the receiver is greatly reduced during the time the transmitter was on so that blocking of the receiver was prevented.

(c) Gain control

The R.F. and mixer stage gain was fixed in order to maintain a good signal to noise ratio. The gain of the receiver was controlled by a resistor common to the cathode of the all I.F. amplifier tubes.

(d) Second detector

In order to avoid any unfavourable discrimination between the strong and the weak signals because of the curvature

in the detector characteristics at low levels, the detector was fed with a high amplitude signal and operated as nearly as possible as a linear device.

The time constant of the load was so fixed as to effect a compromise between steepness of the edges of the pulse which requires a short time constant and obtaining the largest possible pulse envelope with minimum I.F. component which requires a long time constant. A load resistance of 50 k ohms and a condemsor of 100 pf. have been used.

The detected output was further amplified in a video amplifier stage, the output of which was fed to the display units.

The receiver so converted had a gain of approximately 3×10^6 with a good signal-to-noise ratio and an over-all bandwidth of 20 kc which fulfills all the necessary requirements for pulse receptions.

Circuit diagram of the receiver is shown in Figures 2.5(A) and 2.5(B).

(2) Trigger generator

This unit supplies a triggering pulse to start the time-base and after a suitable delay, two more coincident pulses, one for the modulation pulse generator for the transmitter unit and the other to trigger the delayed pulse generators. The circuit diagram of the trigger generator is shown in Figure 2.6.

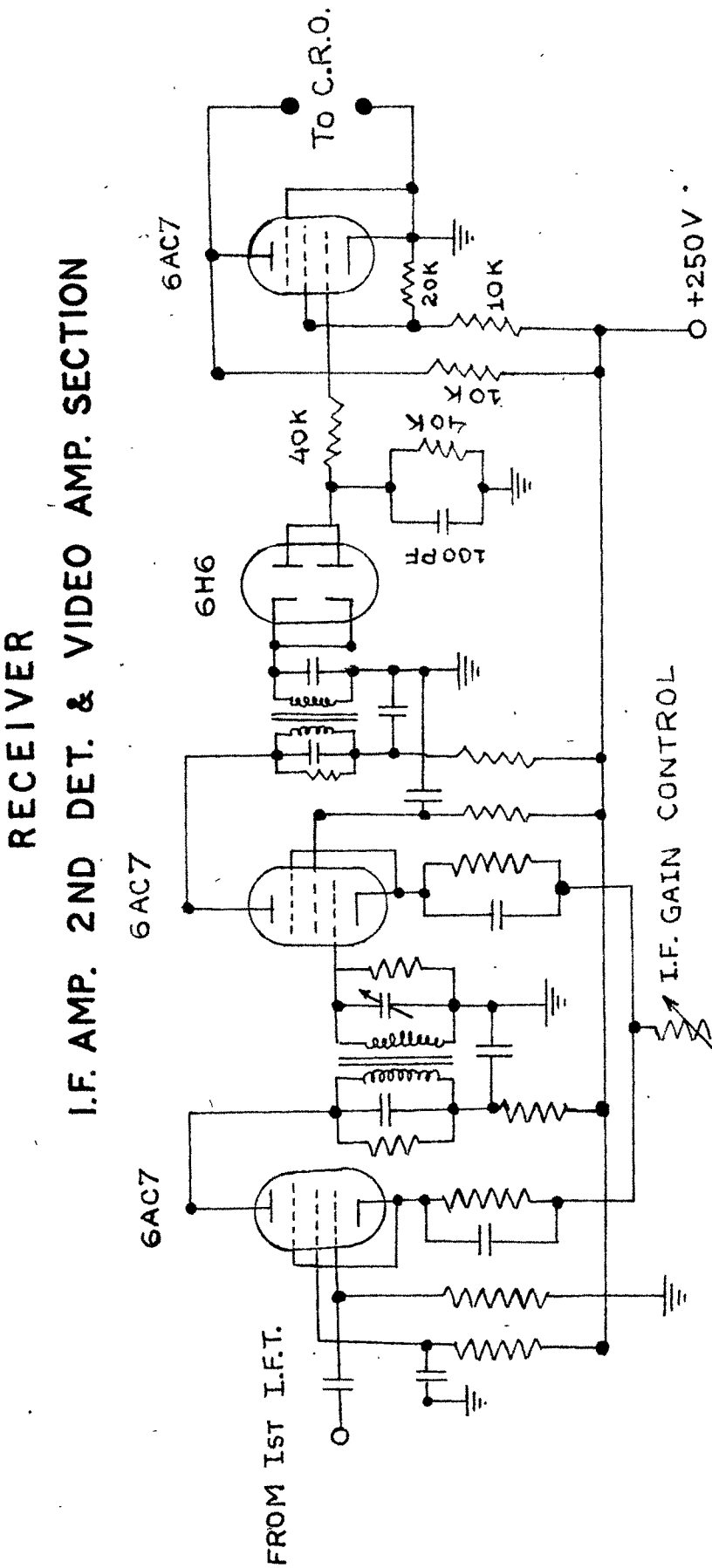
RECEIVER
I.F. AMP. 2ND DET. & VIDEO AMP. SECTION
TO C.R.O.
6AC7
20K
10K
+250V
10K
40K
40K
100 PF
6H6
6AC7
I.F. GAIN CONTROL
6AC7
FROM IST I.F.T.

FIGURE 2.5 (A)

RECEIVER

R.F. AMP. & MIXER SECTION

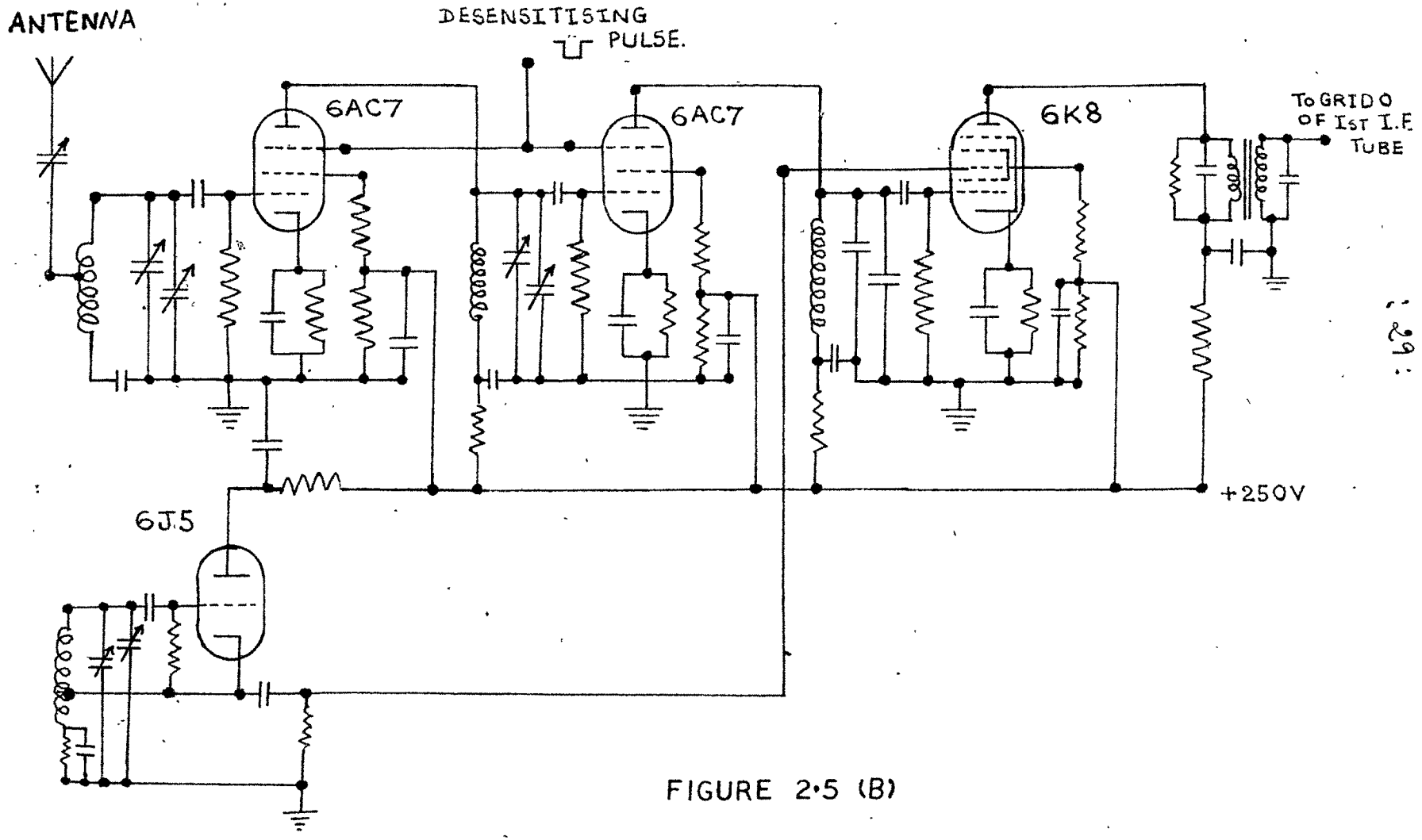

FIGURE 2·5 (B)

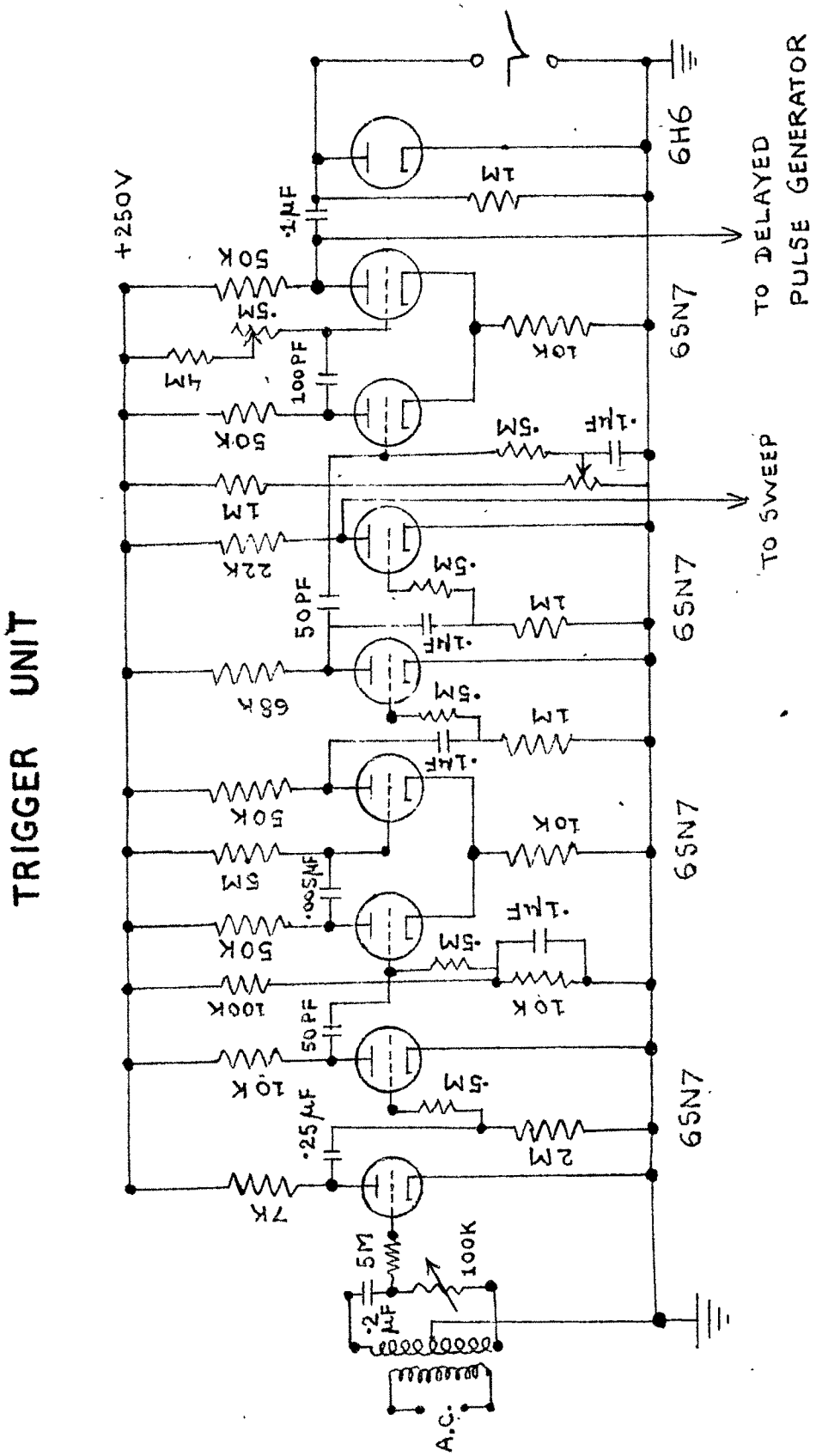
TRIGGER UNIT
+250V
6H6
6SN7
6SN7
6SN7
6SN7
1M
.1μF
50K
.5M
4M
100PF
50K
10K
.5M
.1μF
1M
22K
50PF
.1μF
.5M
1M
68K
.5M
1M
.1μF
50K
10K
5M
.005μF
.1μF
50K
.5M
100K
10K
100K
50PF
10K
.5M
2M
.25μF
7K
5M
100K
.2μF
A.C.
TO DELAYED PULSE GENERATOR
TO SWEEP

FIGURE 2·6

(3) Delayed pulse generators

This unit consists of two identical circuits producing two pulses at different and adjustable times after the transmitter pulse. The input is derived from the trigger unit. The output pulse of one of the two generators is at amplitudes of 15V and 150V. The larger output pulse (150V) is fed to the grid of the cathode ray tube used for photographic recording. This tube is bright only for the duration of the intensifying pulse which is synchronous to the gate pulse. The small output pulse (15V) is fed to one of the Y-plates of the monitor cathode ray tube, as a marking pulse. The length and time of occurrence of these pulses are adjustable.

The output of the other pulse generator is used to synchronise the electronic switch.

The circuit diagram of the delayed pulse generator is shown in Figure 2.7.

(4) Electronic switch

Electronic switching unit is built according to the details supplied by Briggs (Private communications). The unit consists of a synchronised ring multivibrator which produces the three switching wave forms one after the another in succession to switch on the grounded grid amplifiers one after the another. The switching waveforms are added together to generate a stepwave for the recording cathode ray tube. The

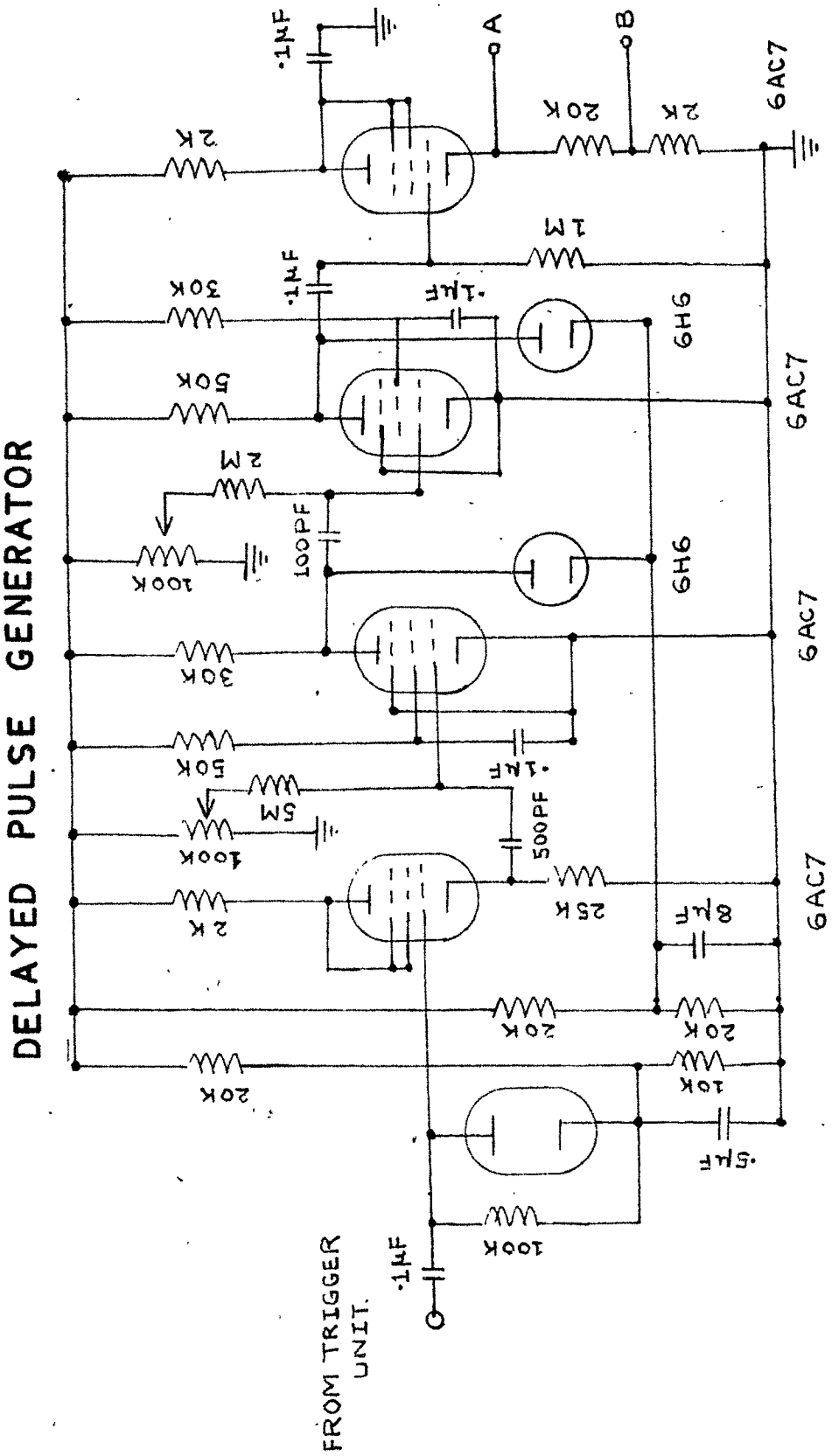
DELAYED PULSE GENERATOR
FROM TRIGGER UNIT.
·1μF
100K
1M
·5μF
10K
20K
8μF
25K
500PF
5M
100K
2K
50K
30K
·1μF
100PF
2M
100K
·1μF
·1μF
30K
50K
2K
1M
2K
20K
2K
A
B
·1μF
6AC7
6H6
6AC7
6H6
6AC7
6AC7

FIGURE 2·7

circuit diagram of the electronic switch is given in Figure 2.8. The three tubes V_1, V_2 and V_3 are connected to operate as a ring multivibrator and each of these is synchronised by the pulse derived from the delayed pulse generator. At any instant, one of the tubes is nonconducting and the other two tubes are conducting and this process repeats in a sequential manner. The waveforms appearing at the anodes of the ring multivibrator are connected via diodes to the cathodes of the grounded grid amplifier tubes V_4, V_5 and V_6. The cathodes of these tubes are returned to a point at +27 volts with respect to the ground and thus during the positive portions of the pulses it conducts. The cathodes of the tubes V_4, V_5 and V_6 are kept at a large positive potential with respect to the grid, thereby preventing it from conducting. During the negative portions of the pulses, however, the diodes stop conducting and the grid voltage in the grounded grid amplifier tubes is only that due to the 0.9 kΩ resistance connected in the cathode circuits. The tubes therefore conduct and the R.F. voltage applied to the cathode circuit appear in the output circuit. The anodes of the three tubes are connected to a common load consisting of an R.F. choke and a 15 kΩ resistance. The output from each of the aerials thus appears across the load in succession. This output is taken to the common pulse receiver through a 0.1 μF capacitor.

A step wave form is also generated from the switching wave forms of the ring multivibrator by adding through a

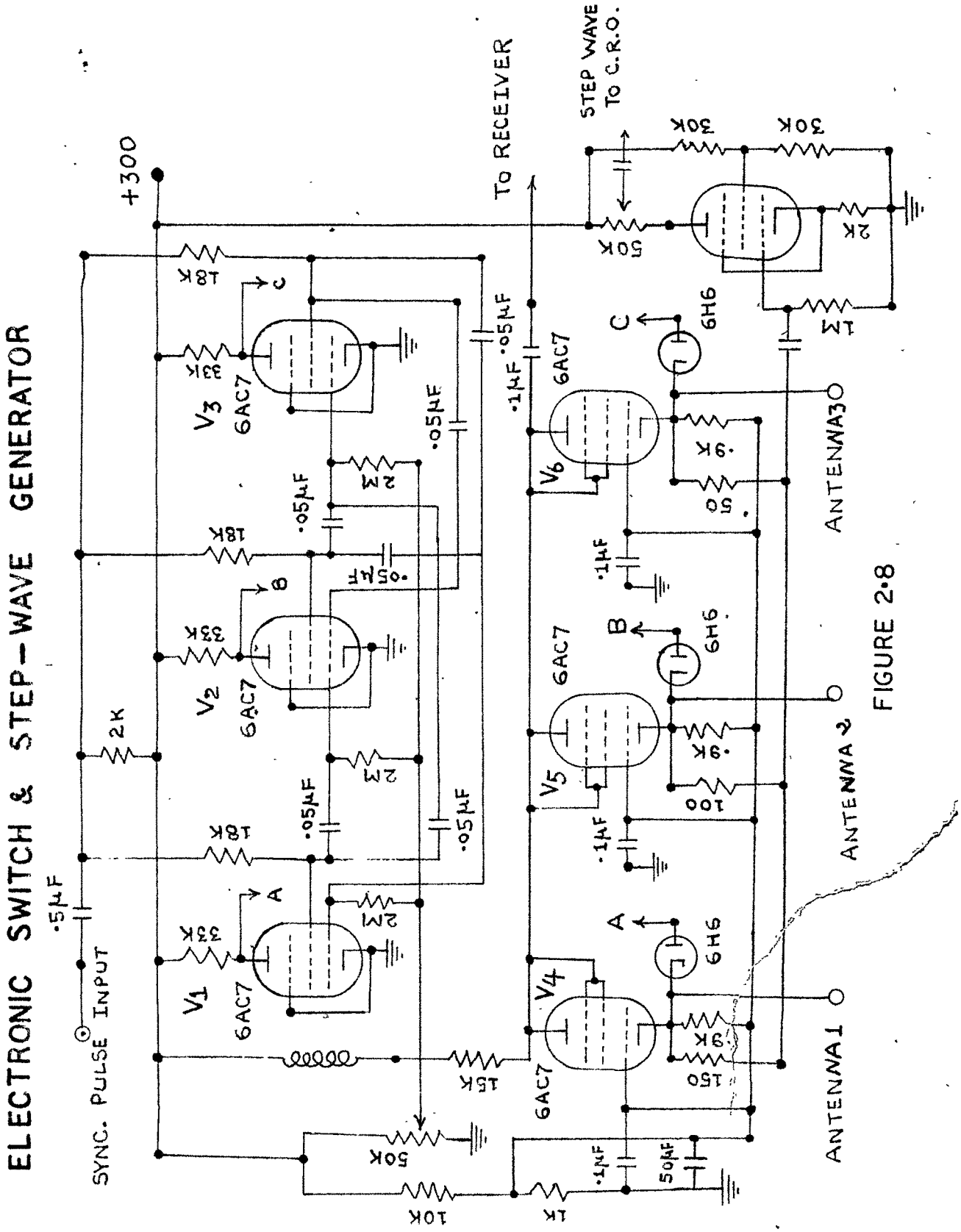
ELECTRONIC SWITCH & STEP-WAVE GENERATOR
SYNC. PULSE INPUT
.5μF
+300
TO RECEIVER
STEP WAVE TO C.R.O.
V1 6AC7
V2 6AC7
V3 6AC7
V4 6AC7
V5 6AC7
V6 6AC7
6H6
6H6
6H6
ANTENNA1
ANTENNA2
ANTENNA3
A
B
C
18K
33K
2K
2M
.05μF
15K
50K
10K
1K
.1μF
50μF
9K
100
150
30K
1M

FIGURE 2·8

potential divider arrangements having a common resistor of 100 kΩ at the grid of tube V10 and individual resistor of 50 kΩ , 100 kΩ and 150 kΩ to which the three wave forms are amplified by this tube and the desired amplitude of the stepwave, which determines the spacing between the traces in the recording oscilloscopes, is obtained with the help of potentiometer load at the anode of the amplifier.

(5) Display units

The display arrangement consists of two 5" cathode ray tubes 5BP1 for visual monitoring and for photographic recording.

The monitor oscilloscope is brought out on the front pannel to enable visual observations of the reflected echo and the adjustment of the various controls in the equipment, while the recording oscilloscope unit which is enclosed in a light-proof box is mounted with its screen on the side of the rack to enable the proper mounting of the camera assembly.

The static operating condition for the monitor tube is such that in the absence of any sweep voltage, it is blanked out. An intensifying pulse derived from the sweep circuit is applied to the grid of the monitor tube, rendering the trace visible for the duration of the sweep. The signal voltage from the receiver and the marker pulse (15V) from the delay pulse generator for selecting the required echo are applied to the plates of the CR tube so as to give an upward deflection of the trace.

A 150V pulse from the delay pulse generator (corresponding to the marker pulse on the monitor tube but of higher amplitude) is fed to the grid of the recording CR tube so that there is a bright trace on the screen only for the duration corresponding to the marker pulse. This gating pulse enables us to eliminate the initial ground pulse and the various multiple hop echoes which may be present.

The recording CR tube is not provided with any time base. It has its beam switched to three different positions by means of deflecting voltage (stepwave) produced by the electronic switch and fed to one of the X-plates. The signal voltage from the receiver is fed to the other X-plate so that three horizontal lines appear on the tube screen, each line being proportional in length to the strength of the echo at one of the aerials. The variations in the echo amplitudes are recorded photographically on a 35 mm film of high sensitivity. The circuit diagram of only one display unit is shown in Figure 2.9.

(6) Camera unit and time marker

The camera unit is mounted on two angle iron rails of approximately two feet length, projecting from the side of the rack just in front of the recording cathode ray tube panel. The camera is mounted on a wooden platform together with the synchronous motor which is coupled to the camera for moving the film. This forms the camera unit.

The camera is a conventional 35 mm cine camera modified

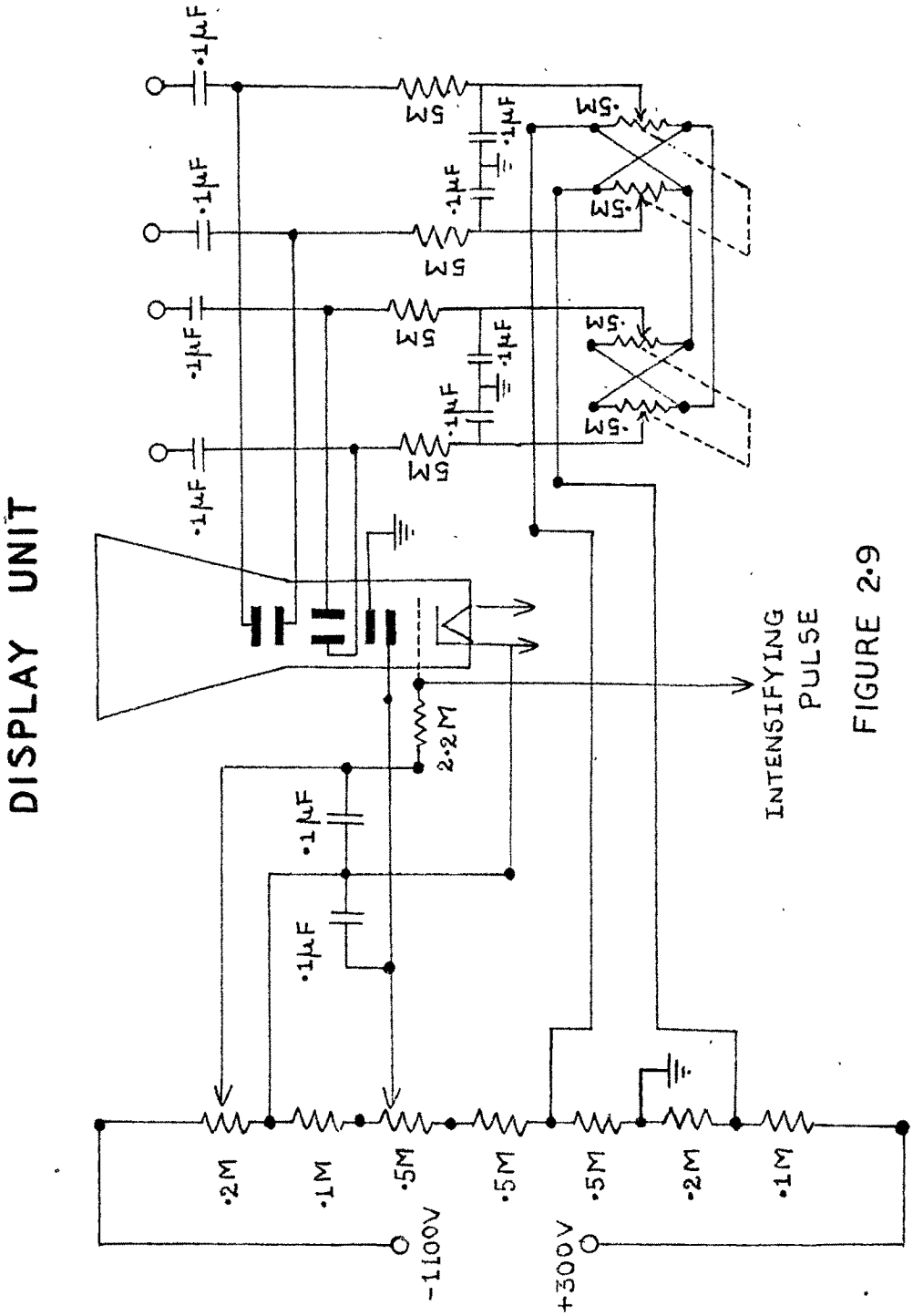
DISPLAY UNIT
·1μF
5M
·5M
2·2M
INTENSIFYING PULSE
·2M
·1M
·5M
-1100V
+300V

FIGURE 2·9

in the following manner. An F/2.8 lens of focal length 2" was substituted in place of the original lens. The original drive mechanism was disconnected because the speed was too high and an external synchronous motor was suitably coupled. The motor speed can be adjusted by means of suitable gears and is fixed to move at a rate of 4" per minute. The original revolving shutter was disconnected so that continuous exposure could be had and on the shaft left free by the removal of the shutter, a vane of suitable width was attached which interrupts the exposures every twelve seconds to provide the time marks. A light-proof hood extending from the side of the rack up to the camera prevents fogging of the film due to any external light. A small window was provided for controlling intensity, focus and positioning of the spots.

(7) Sweep generator

Figure 2.10 miller intergator circuit is used for generating sweep voltage for the time base of the recording cathode ray tube. It generates a single stroke sweep voltage in a pushpull manner and also provides a rectangular pulse, having precisely the same duration as the sweep which is used to brilliance modulate the monitor cathode ray tube.

In order to achieve high stability in the working of the various electronic circuits all the d.c. voltages, except the H.T. for cathode ray tubes and the H.T. for the transmitter power amplifier stage, were electronically stabilized against load variations and/or against the voltage fluctuations.

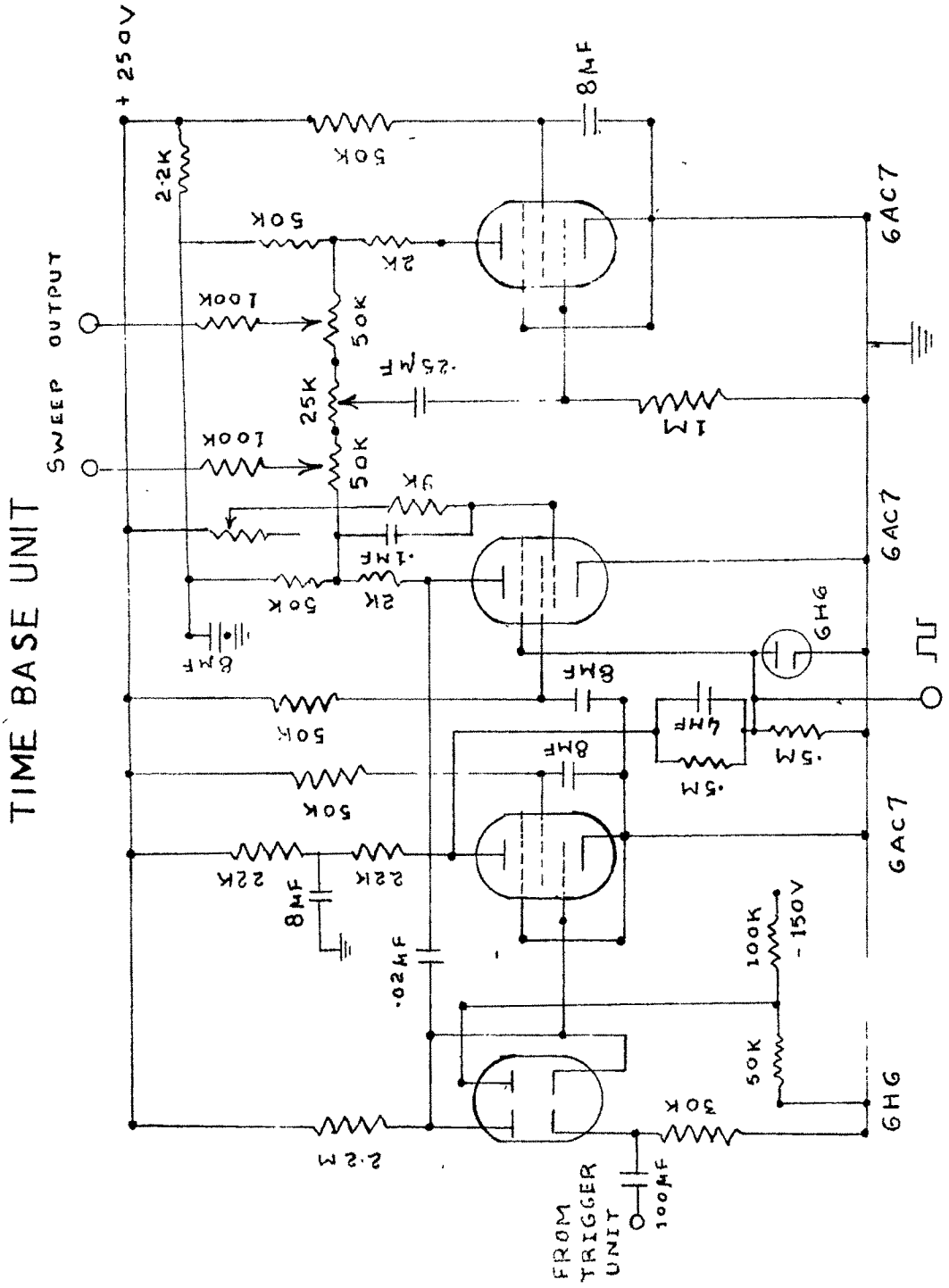

INTENSIFYING PULSE
FIGURE 2·10

5. Programme of ionospheric drift measurements at Ahmedabad

A routine programme of investigating horizontal drift speed and direction in the E and F regions of the ionosphere over Ahmedabad was undertaken early in 1956. Observations have been continued since then and we shall concern ourselves in this thesis with observations on 2.6 MHZ and 4.0-4.4 MHZ during September 1956 - February 1959 and on frequencies 2.6, 5.7 and 7.0 MHZ during November 1959 - February 1962. Round the clock observations were taken for a period of 3 to 9 days in a month including the Regular World Days. During day the reflections on 2.6 MHZ were from normal E and/or from the sporadic E; and from sporadic E or F during night. The observations taken on 4.0-4.4 MHZ refer to either F or E_s and those on 5.7 and 7.0 MHZ to mostly F during day.

Owing to the low power of the transmitter and high absorption during noon hours, only a few readings are available between 1100 hrs and 1400 hrs, particularly on 2.6 MHZ and 4.0-4.4 MHZ. On many occasions, it was not possible to take observations on these frequencies because of interference from broadcasting stations or from atmospherics. There are also a few occasions when the critical frequency of the normally reflecting layer was below the operating frequency. Hence the useful data available for analysis are not uniformally distributed at different hours of the day.

6. Some typical examples of fading records obtained at different frequencies at Ahmedabad

The fading records obtained from the E and F regions at different frequencies showed generally regular fading patterns, but there were quite a few irregular ones. A few sample fading records showing different characteristics are presented in Figures 2.11, 2.12, 2.13, 2.14 and 2.15. In each of these, starting from simple fading records, we have shown the fading pattern which becomes more and more complex. We shall describe here briefly the nature of the fading as can be judged visually from the records beginning from A.

I. Figures 2.11 and 2.12

Figure 2.11 refers to the E region reflections at 2.6 Mc/s and Figure 2.12 to that from the F region at the same frequency. We note here the main features :

(1) The records of the type marked A and B show regular wavelike fading characteristic and show almost one to one correlation. Such records can be analysed with great accuracy.

(2) Type C and D do not show one to one similarity all along the fading curve but show recognizable similarity in maxima and minima.

(3) Type E, F and G (in Figure 2.11) show quick and random fading. Similarity between fading records is very variable with different time sequence of the record.

(4) Type H and I (Figure 2.11) and type E, F and G (Figure 2.12) show very slow fading. It is often difficult to locate maxima and minima in such records and hence are unsuitable for analysis.

II. Figures 2.13 and 2.14

Figures 2.13 and 2.14 show fading pictures on 5.7 and 7.0 MHZ respectively reflected from the daytime F region. The variations in the fading pattern are almost of the same type on both the frequencies and the fading is usually periodic in nature. We note that :

(1) The fading records of type A and B show good correspondence between themselves and the correlation is almost one to one.

(2) Records of type C and D show fading periods longer than that in type A and B. However the similarity between different fading records is still close.

(3) Type E shows slow fading similar to that in Figure 2.12. Such records are difficult to analyse and are not considered in the subsequent analysis.

III. Unusual records

An unusual sequence of record of reflections on 7.0 MHZ from F region is shown in Figure 2.15. Here it may be seen that the usual slow fading suddenly changes to quick

fading in a matter of few minutes and then returns to its original slow fading after some time. The degree of rapidity in fading and the change in the amplitude of fading as shown in Figure 2.15 is most dramatic. However such records though interesting to look at cannot be used for normal analysis work to find drift speed and direction.

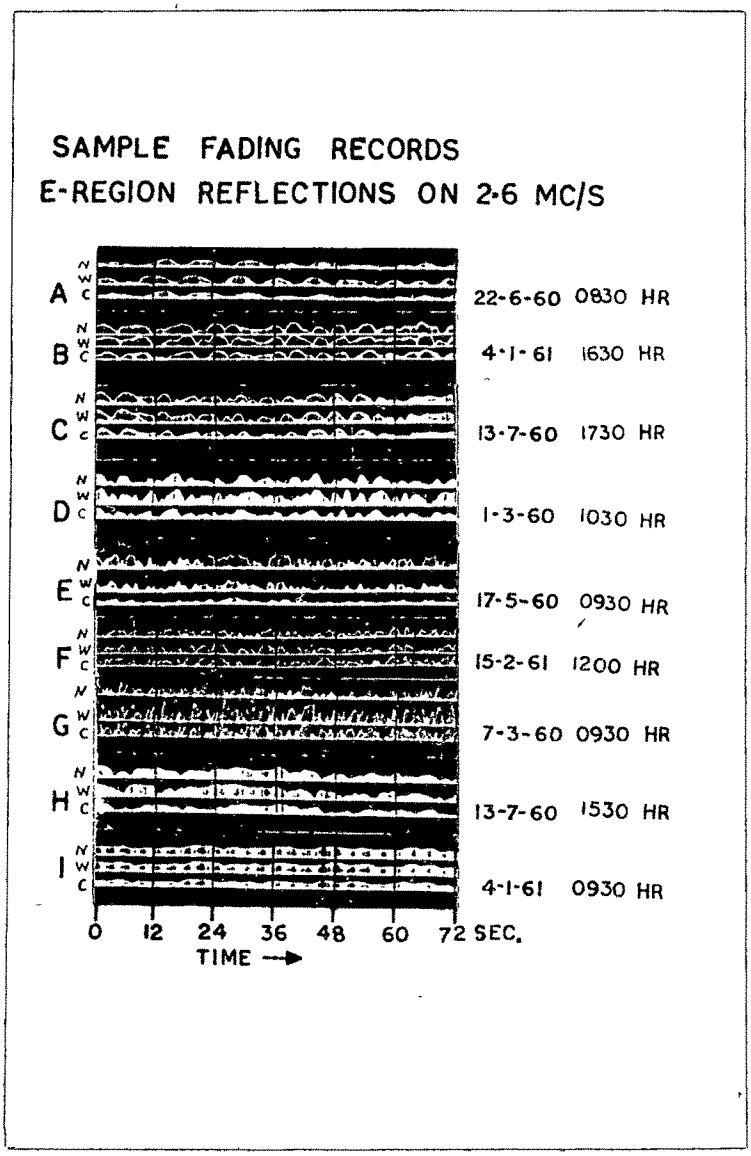

Figure 2.11 Sample fading record from E region on 2.6 Mc/s.

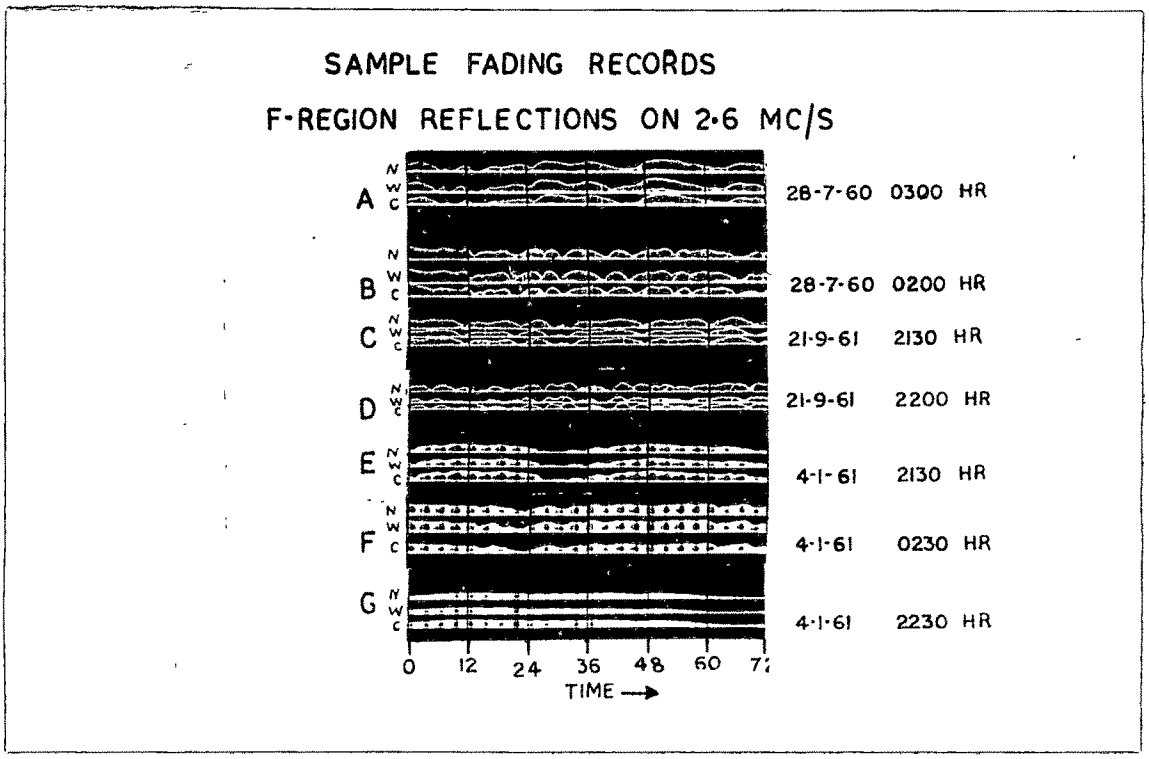

Figure 2.12 Sample fading record from F region on 2.6 Mc/s.

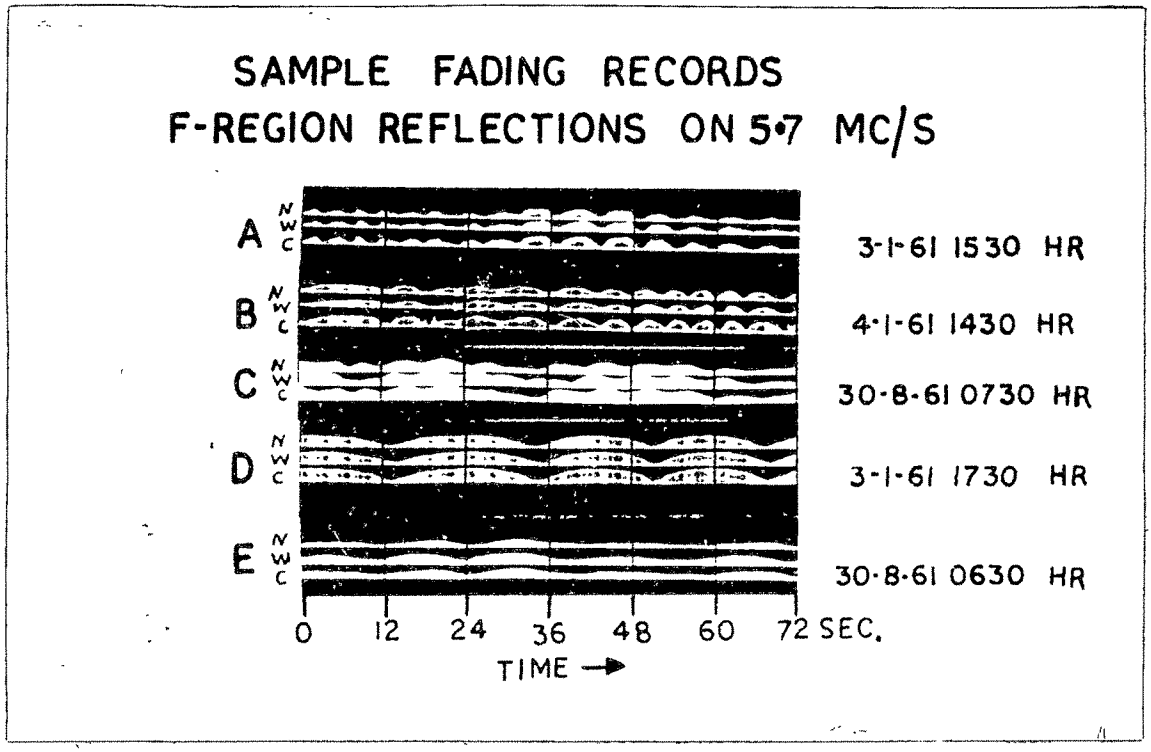

Figure 2.13 Sample fading record from F region on 5.7 Mc/s.

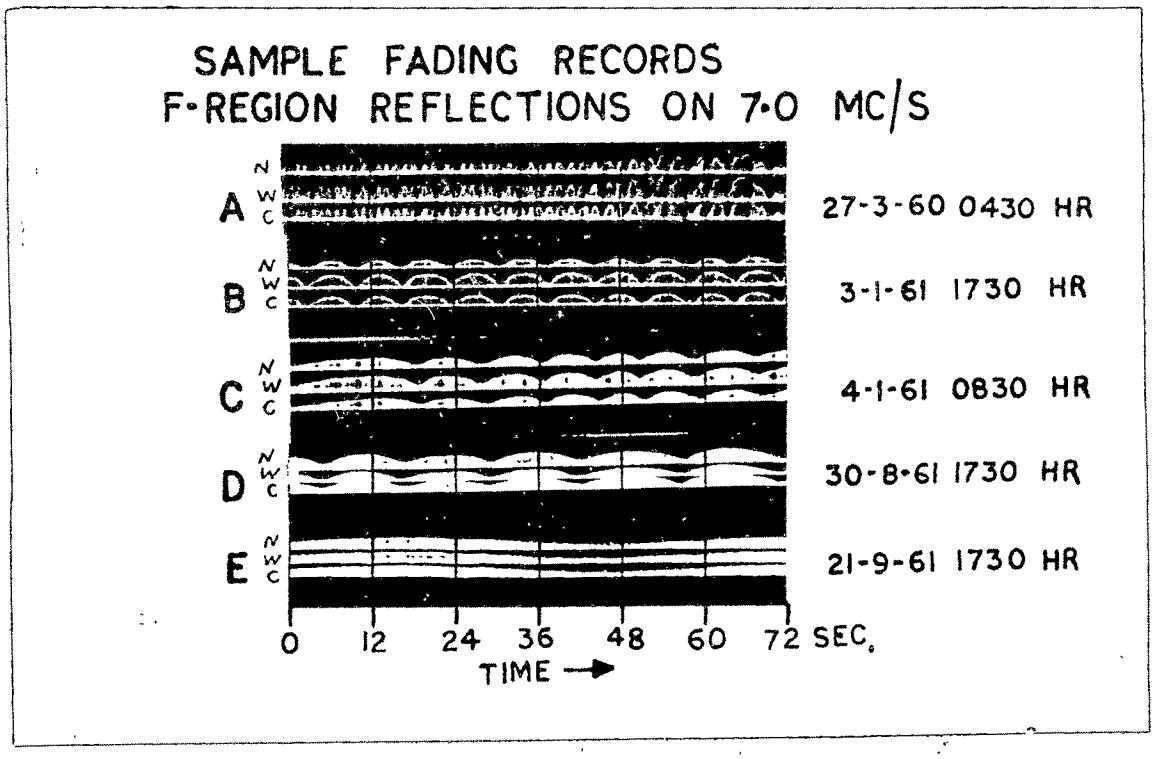

Figure 2.14 Sample fading record from F region on 7.0 Mc/s.

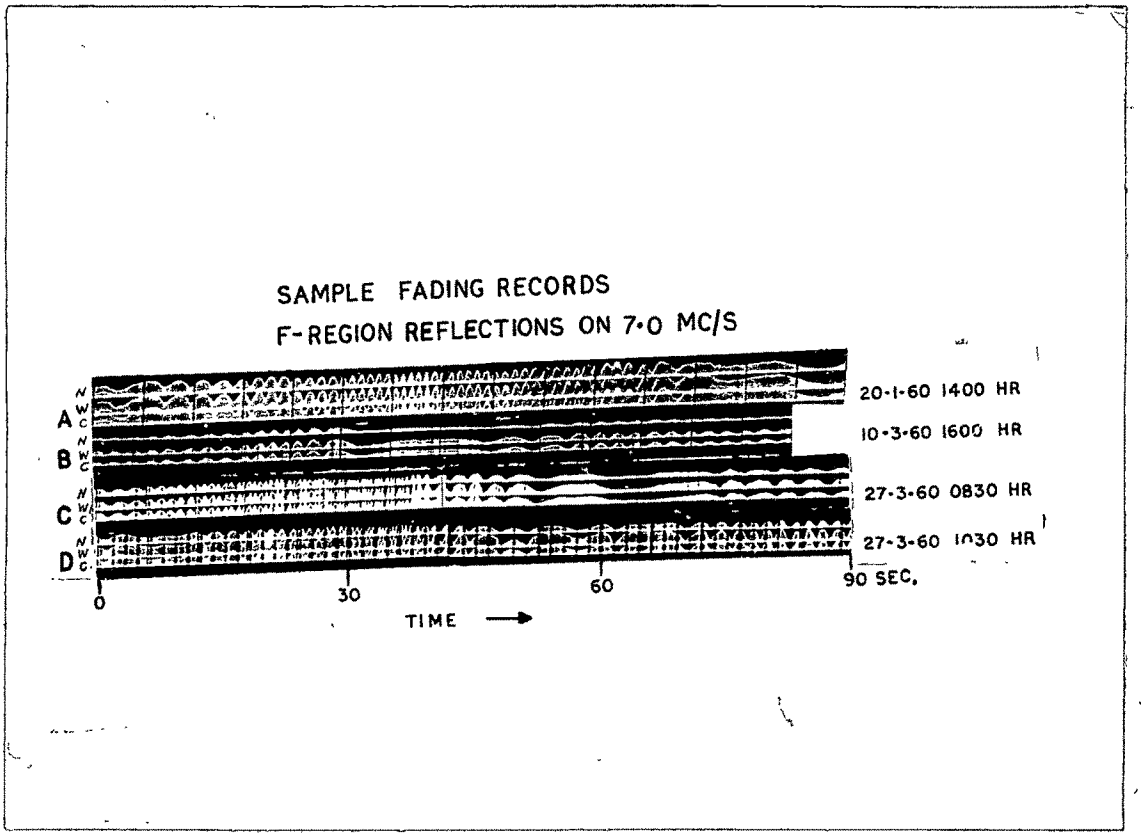

Figure 2.15 Sample fading record (quick fading) from F region on 7.0 Mc/s.

CHAPTER III

Measurement of horizontal drifts in the E region over Ahmedabad from September 1956 to February 1962

The total period of observations on E and F region drifts ~~are~~ is divided in two parts, since the results on drift speed and direction differ in some respects in the two groups. Thus we shall consider the following two periods separately :-

(1) September 1956 to February 1959

(2) November 1959 to February 1962.

In each of these periods, the data were analysed separately for the E and F regions. We shall first present the results for the E region and in the next chapter we shall do for the F region.

To study the seasonal variation in drift speed and direction the data were grouped according to season, equinoxes (March, April, September and October), summer (May, June, July and August) and winter (November, December, January and February). In each of these seasons, the diurnal variation of drift speed and direction was also studied. It was generally found that there was no significant difference between the changes in speed or direction in the same season of the different years in each period and hence combined histograms for each season were prepared for each of the two periods (1) and (2). A similar

procedure of grouping the data was adopted to study the diurnal variation of drift speed and its components along E-W and N-S directions.

The total number of observations (No) used in the preparation of the histograms and so also the arithmetic mean $\overline{V}$ and the median value V^{x} of the drift speed are shown on the appropriate diagrams.

Results of analysis of horizontal drifts in the E region

1. Mean annual variation in speed and direction at 2.6 Mc/s during day and night

(i) 1956-59

Figure 3.1(a) shows histograms of the percentage occurrence of drift speed and direction for night and day. During night, the most frequent values of speed lie between 60 and 80 m/s with mean and median value 85 m/s and 74 m/s respectively. During day the most frequent values lie in the range 40-60 m/s with mean and median at 79 m/s and 68 m/s respectively. This shows that the average speed is higher during night than during day. The histograms show sharp rise and slow fall in frequency of occurrence of different speeds with a peak between 20 and 140 m/s.

The histograms of drift directions show two peaks, one towards N-W and the other towards S-E. The former appears to be more prominent than the latter. However the nighttime

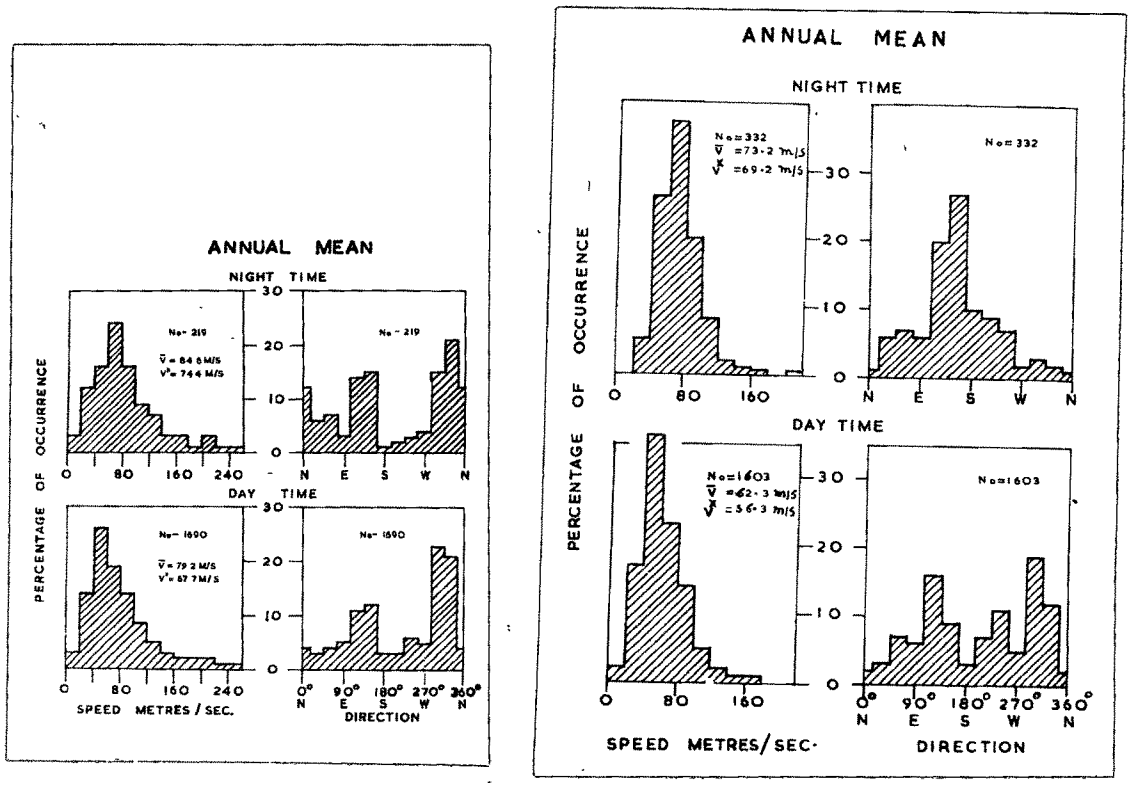

(a) - 1956-59 (b) - 1959-62

Figure 3.1 Histograms showing annual mean variation of E region drift speed and direction on 2.6 Mc/s during day and during night.

histograms show comparatively larger percentage of occurrence towards north or east.

(ii) 1959-62

Figure 3.1(b) shows the histograms of percentage occurrence of drift speed and direction for night and day during 1959-62. The histograms for drift speed show sharp rise and sharp fall with most frequent occurrences in the range 40-60 m/s. The mean speed is 73 m/s during night and 62 m/s during day.

The drift direction shows a single maximum towards S-E during night. In daytime the direction is not so well defined but in the majority of cases it is towards N-W or S-E.

2. Drift speed and direction at 4.0-4.4 Mc/s

On some occasions reflections on 4.0-4.4 Mc/s were obtained from sporadic E during daytime. A comparison is made in Figure 3.2 of the results obtained on 2.6 Mc/s and 4.0-4.4 Mc/s reflections from E region during day. Apart from small differences in speed and direction at the two frequencies the general features are not significantly different.

3. Seasonal variation

(i) Drift speeds 1956-62

To study the seasonal variations in speed and direction

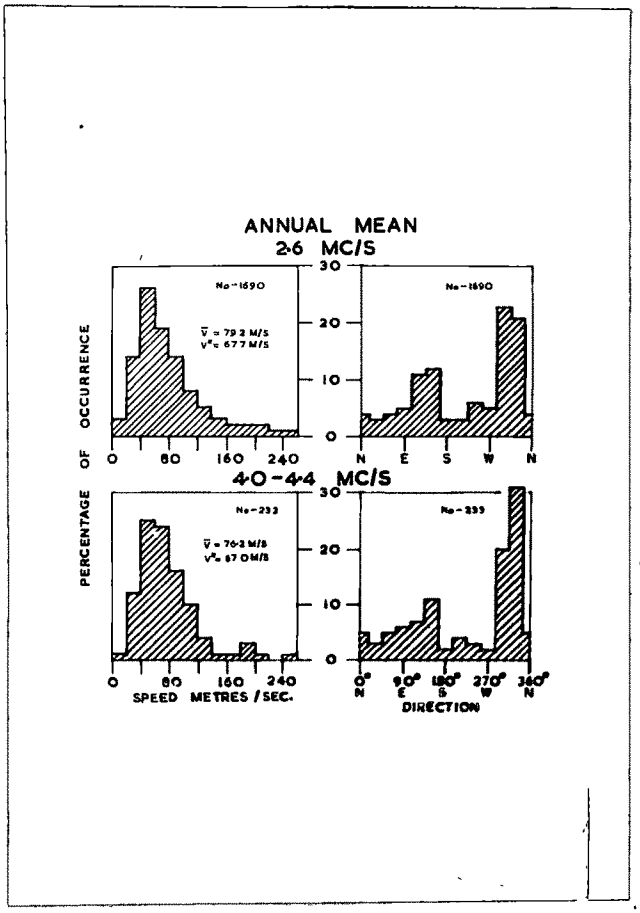

1956-59

Figure 3.2 Histograms showing annual mean variation of E and/or E_s region drift speed and direction on 2.6 and 4.0-4.4 Mc/s during daytime.

of daytime and nighttime drifts histograms were constructed for three seasons, equinoxes, winter and summer. These are shown in Figure 3.3(a) for 1956-59 and in Figure 3.3(b) for 1959-62. In all seasons the histograms for daytime speeds show rapid rise and gradual fall with maximum occurrence in the range 40-60 m/s. The nighttime histograms show a more gradual rise and the peak is shifted to the range 60-80 m/s.

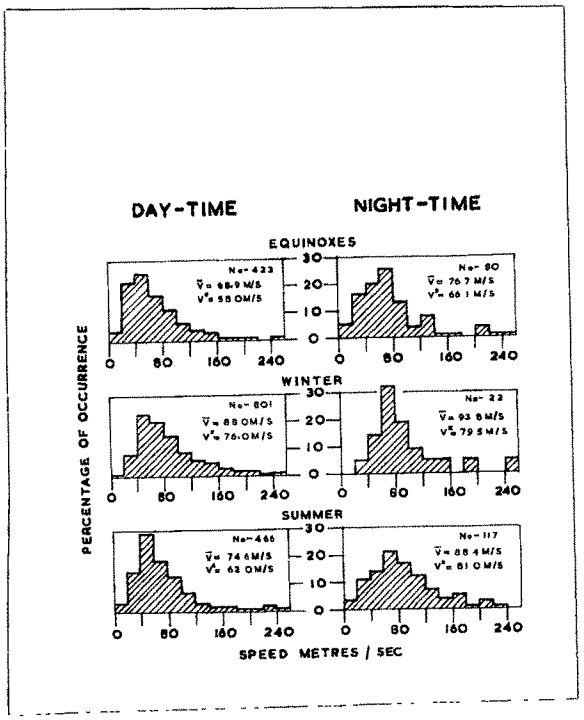

(a) - 1956-59

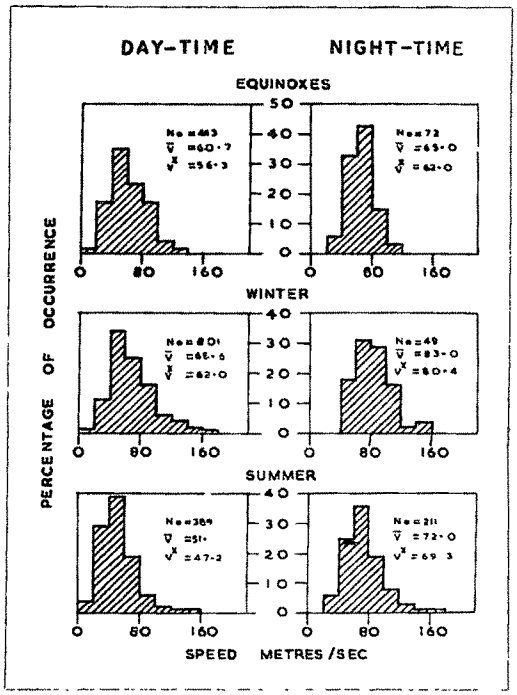

(b) - 1959-62

Figure 3.3 Histograms showing seasonal variation of E region drift speed on 2.6 Mc/s.

The findings are summarised in Table 3.1 for the entire period 1956-62. It may be seen that seasonwise, the average speed is maximum in winter and minimum in equinoxes except during daytime in 1959-62 where the minimum speed is found in summer. Diurnally the average speed is higher during night than during day in all seasons.

Table 3.1

Average value of drift speeds in the E region for daytime and nighttime hours in different seasons of the years (1956-59) and (1959-62).

Season	1956-59 Night m/s	1956-59 Day m/s	1959-62 Night m/s	1959-62 Day m/s
Equinoxes	77 ± 5	69 ± 2	65 ± 2	61 ± 1
Winter	94 ± 10	88 ± 2	83 ± 3	69 ± 1
Summer	88 ± 4	75 ± 2	72 ± 2	51 ± 1
Annual Mean	85 ± 3	79 ± 1	73 ± 1	62 ± 1

(ii) Drift direction 1956-62

The histograms of percentage occurrence of drift directions are shown in Figure 3.4(a) for 1956-59. The frequency of occurrence is distributed nearly equally towards S-E and N-W during daytime in equinoxes and summer, while in winter it is more towards N-W

than towards S-E. Reverse is the case for nighttime except in summer when it is more towards N-W.

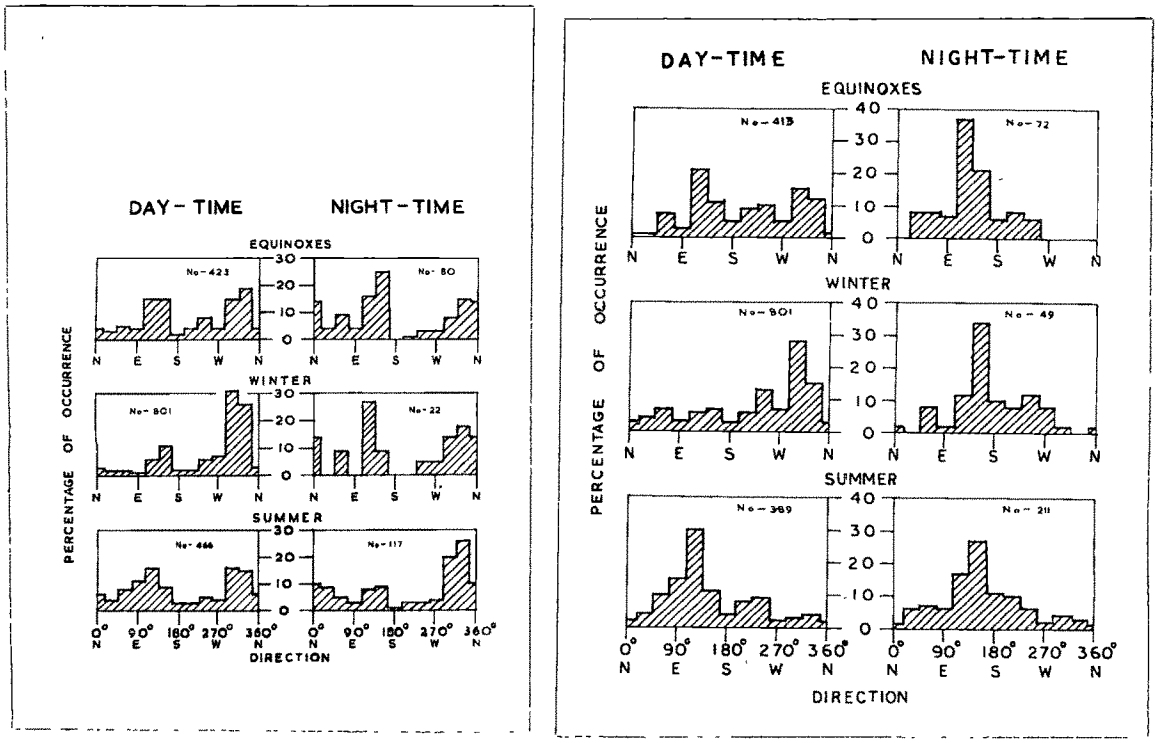

(a) - 1956-59 (b) - 1959-62

Figure 3.4 Histograms showing seasonal variation of E region drift direction on 2.6 Mc/s.

Figure 3.4(b) shows the results for 1959-62. Here the peak towards S-E is very prominent during night in all seasons. The daytime directions are very variable, but there is a tendency towards S-E in summer and towards N-W in winter.

4. Mean hourly variation in drift speed

To obtain average hourly variation in drift speed, the hourly values of speeds were averaged for all days in each season as well as for the whole year to get the annual average curve. These curves are shown in Figure 3.5(a) and Figure 3.5(b). The open circles indicate that the number of observations in that hourly interval were few. A clear diurnal variation appears in summer with a maximum at midnight and a minimum at midday; in winter of 1959-62, a weak semidiurnal variation is observed. During equinoxes and winter the nighttime values show large scatter. The yearly average curve shows a diurnal variation with a maximum between 22 and 04 hours and a flat minimum during day.

To find the diurnal variation in drift direction, histograms were prepared for 06-07 hrs, 08-10 hrs, 11-13 hrs, 14-15 hrs and 16-18 hrs. We had to resort to this sort of grouping because of fewer number of observations at one particular time. The results for 1956-59 are shown in Figure 3.6(a). No histograms are shown for 11-13 hrs and 14-15 hrs in summer and equinoxes and for nighttime in any season since sufficient data do not exist. The figures show

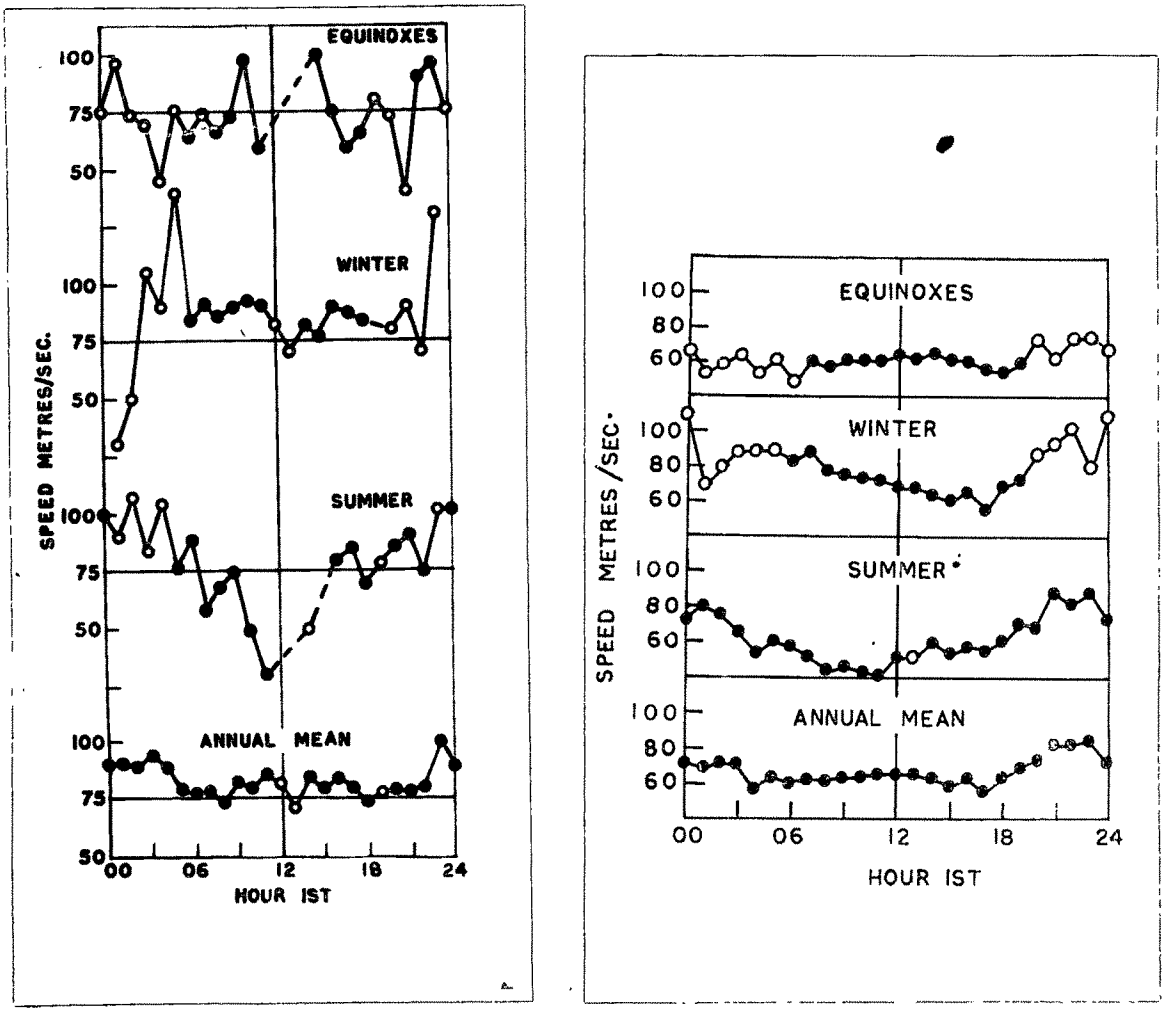

(a) - 1956-59 (b) - 1959-62

Figure 3.5 Curves showing diurnal variation of average drift speed in the E region.

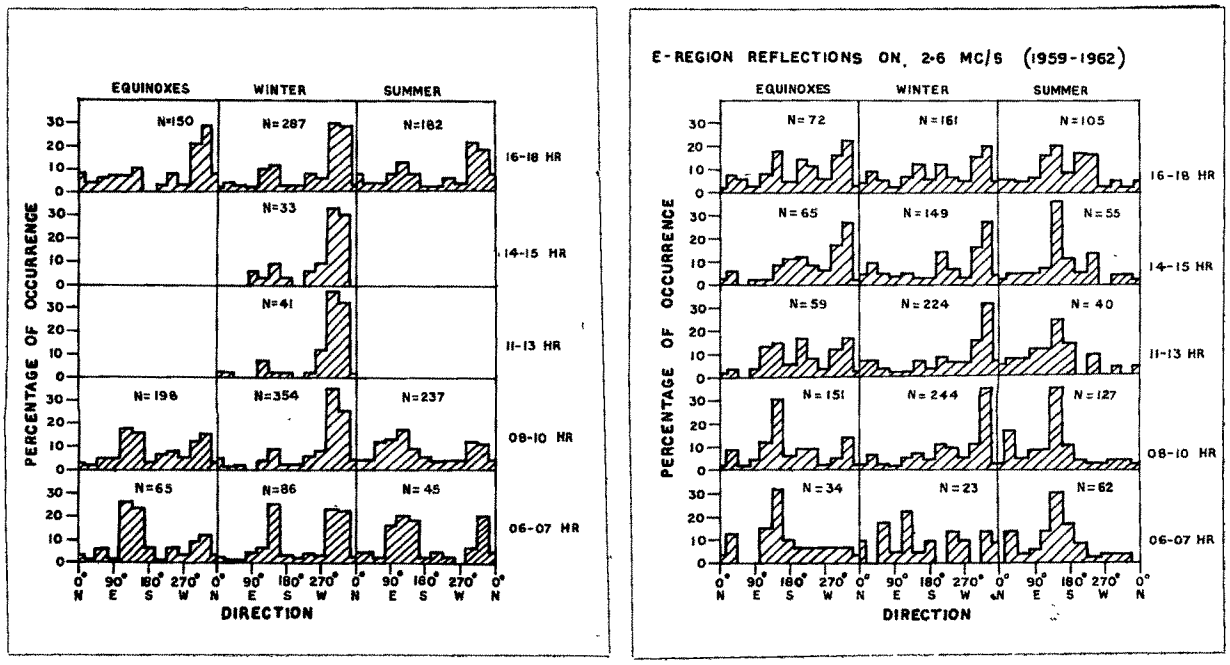

(a) - 1956-59 (b) - 1959-62

Figure 3.6 Histograms showing the variation of E region drift direction for few hours during day.

a strong peak in the N-W direction during daytime in winter and a small secondary peak in the S-E direction in the early morning hours (06-07 hr). In summer and equinoxes, N-W and S-E directions are equally probable in the forenoon hours but change towards N-W in the afternoon hours.

Figure 3.6(b) shows the results for 1959-62. The prevailing directions are S-E in summer and N-W in winter. The scatter is very large at 16-18 hrs in all seasons and at 06-07 hrs in winter. During equinoxes, the predominant direction changes from S-E in the forenoon hours to N-W in the afternoon hours.

5. Diurnal variation of E-W and N-S components of drift

The components of drift velocity along E-W and N-S directions (positive towards north and towards east) were obtained and the average diurnal variation of the E-W and N-S component was averaged for each season and for the whole year. These curves are shown in Figure 3.7(a) and Figure 3.7(b). As before open circles in the figure are based on few observations. An inspection of these curves shows :

(i) During 1956-59 - Figure 3.7(a)

The E-W component is generally towards west during most of the day, except early morning when the drift is eastwards. The N-S component is generally towards north except for few hours in the morning and late evening.

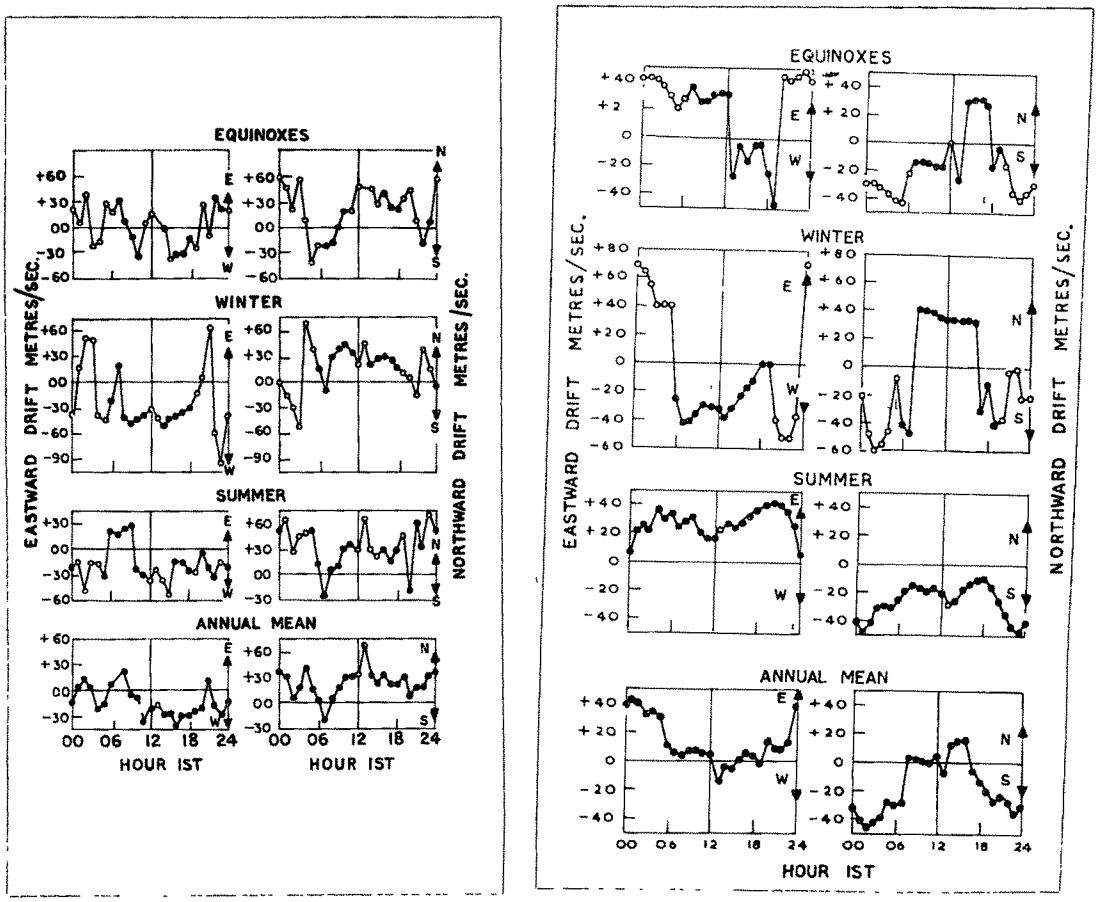

(a) - 1956-59 (b) - 1959-62

Figure 3.7 Curves showing diurnal variation of E-W and N-S components of E region drifts.

(ii) During 1959-62 - Figure 3.7(b)

The E-W component is generally towards west during daytime and towards east during nighttime and the N-S component towards north during day and south during night in winter and equinoxes. In summer the E-W component is towards east and the N-S component towards south at all hours of the day.

6. Harmonic analysis of E-W and N-S components during 1959-62

We have attempted here to present the results of harmonic analysis of individual curves shown in Figure 3.7(b). We obtained the diurnal and semidiurnal vectors in the E-W and the N-S components from the following well known relation;

$$V = V_0 + V_1 \sin(t + \theta_1) + V_2 \sin(2t + \theta_2) \qquad (1)$$

where V_0 is the amplitude of steady component, V_1, θ_1 and V_2, θ_2 are the amplitudes and phases of the 24 hr and 12 hr waves. The results are given in Table 3.2 and are shown on harmonic dials in Figure 3.8. It can be seen that the diurnal component is in general more prominent than the steady or the semidiurnal component except in summer.

The same results are shown in polar plots in Figure 3.9. Here it can be seen that the steady vector is prominent towards S-E in summer and in equinoxes, but changes to S-W in winter. The diurnal vector traces an ellipse of high

Table 3.2

Coefficients of harmonic analysis of E region drifts during 1959 to 1962

Season	Steady Component		Diurnal Component				Semidiurnal Component			
	E-W drift	N-S drift	E-W drift		N-S drift		E-W drift		N-S drift	
	V_o m/s	V_o m/s	V_1 m/s	Phase angle θ_1	V_1 m/s	Phase angle θ_1	V_2 m/s	Phase angle θ_2	V_2 m/s	Phase angle θ_2
Equinoxes	+19.5	-15.2	25.0	44°	25.4	231°	17.4	132°	10.3	330°
Winter	- 9.1	- 5.4	31.1	62°	39.3	261°	31.5	6°	18.1	123°
Summer	+27.2	-25.6	4.1	144°	12.2	258°	8.5	251°	8.9	265°
Annual Mean	+12.5	-15.5	18.6	59°	24.9	250°	6.3	27°	0.7	147°

Positive sign refers to direction towards east & negative sign towards west in E-W component.

Positive sign refers to direction towards north & negative sign towards south in N-S component.

V_1, θ_1 and V_2, θ_2 refer to the amplitude and phase ~~at which maximum~~ of the eastward or northward drift ~~is observed.~~ according to the equation $V = V_o + V_1 \sin(t + \theta_1) + V_2 \sin(2t + \theta_2)$

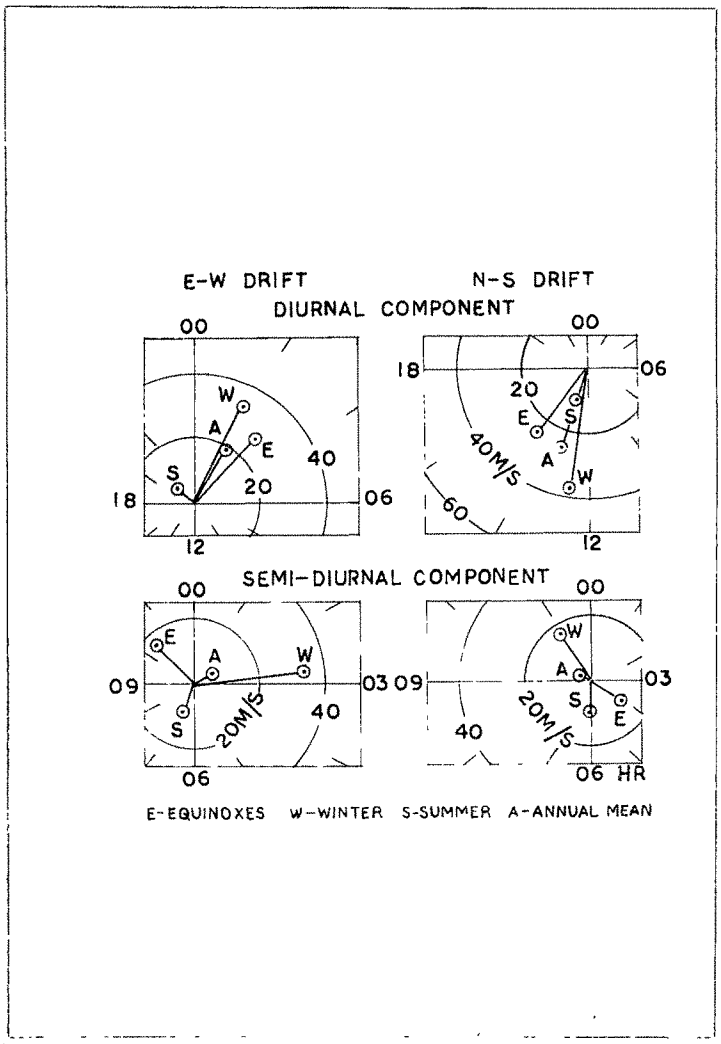

1959-62

Figure 3.3 Harmonic dial of E-W and N-S drift vectors in the E region, when magnitude and time of maximum amplitude are plotted.

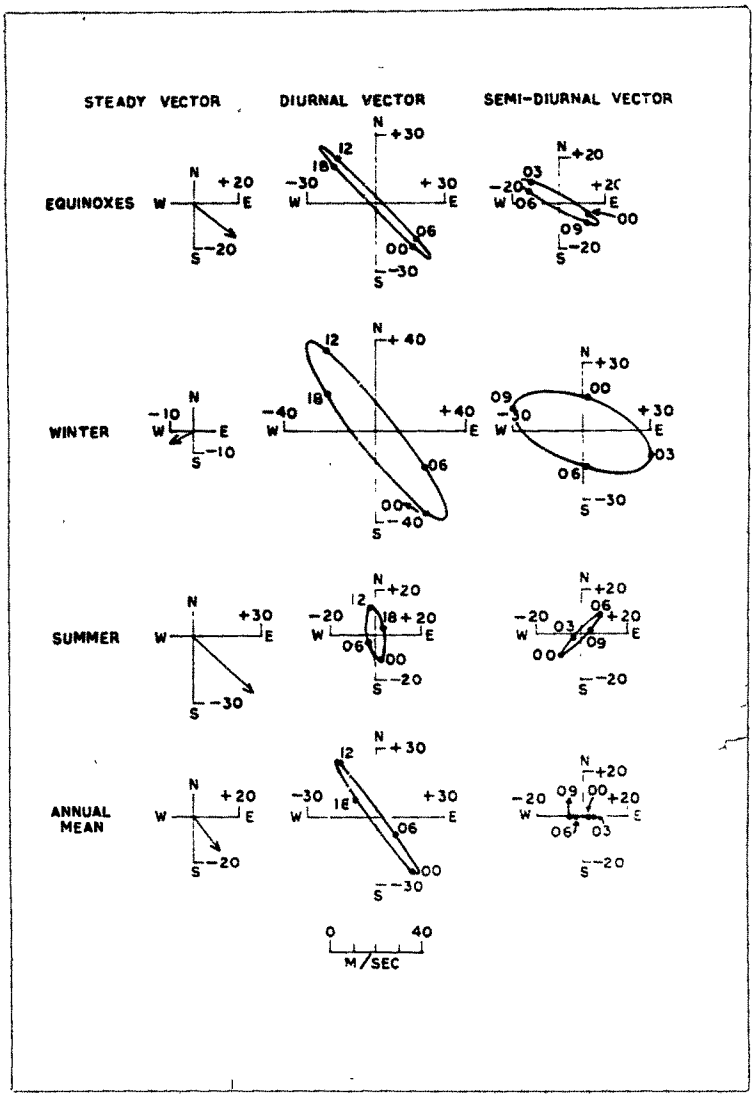

1959-62

Figure 3.9 Polar plots of steady, diurnal and semidiurnal drift vectors in the E region.

eccentricity and rotates anticlockwise in winter and equinoxes, but clockwise in summer.

In the case of the semidiurnal component, its vector also traces an ellipse with a sense of rotation in a clockwise direction in winter and in summer but in anticlockwise direction in equinoxes. The amplitude of the diurnal and semidiurnal vector is maximum in winter but minimum in summer.

7. Discussion

Summarising all the available data upto 1953 from the high latitude stations, Briggs and Spencer (1954) report that 80 m/s could be taken as a representative value for the drift speed in the E region and that it is higher in winter than in summer. Later papers on the subject [Tsukamoto and Ogata (1959), Mitra et al (1960), Rao and Rao (1961), Piggott and Barclay (1962)] show the results at Yamagawa, Delhi, Waltair and Halley Bay for the IGY period. All these stations except Waltair showed higher winter drift speeds. At Waltair, Rao and Rao (1961) did not find any significant variation in the drift speed. The most probable value of the speed ranged from 89 m/s at Yamagawa, 83 m/s at Waltair, 65 m/s at Halley Bay to 55 m/s at Delhi. At Ahmedabad during the same period the most frequent value of drift speed was about 82 m/s. This shows that at Delhi the speed was minimum.

Rao and Rao (1965) have analysed the drift data of Waltair, Yamagawa, De Bilt, Brisbane and Wellington for the

period 1958 and they find that the most probable range of drift speed is 60-80 m/s except at Brisbane where it is only 20-40 m/s. Their analysis also shows that at all the stations they studied, the nighttime average drift speed ~~is~~ was higher than during day and that the difference between nighttime and daytime speed was higher at Yamagawa than at any other place. Our results at Ahmedabad are consistent with the above findings as we have seen earlier that the average speed here is 85 m/s during night and 79 m/s during day.

Latitudinally, we find that the most probable drift speed is minimum at Delhi and Ahmedabad and increases towards equator and high latitudes. A summary of the results at different places is given in Table 3.3.

Table 3.3

Comparison of drift speeds in the E region of the ionosphere at different places

Station	Geomag. lat.	Most probable range of speed	Mean Speed Day	Mean Speed Night	Source
		m/s	m/s	m/s	
Waltair	7°N	60-80	81	88	Rao & Rao (1965)
Ahmedabad	14°N	40-60	74	85	Patel (present thesis)
Delhi	19°N	50-60	—	—	Mitra et al (1960)
Yamagawa	20°N	60-80	73	82	Rao & Rao (1965)
De Bilt	59°N	60-80	90		Rao & Rao (1965)
Brisbane	36°S	20-40	51	52	Rao & Rao (1965)
Wellington	52°S	60-80	78	86	Rao & Rao (1965)

The mean hourly values of drift speed when plotted with the time of the day do not show any significant periodicity in any season except at Waltair where a semidiurnal trend is seen (Rao and Rao, 1965). Such a plot for Ahmedabad shows only diurnal variation in summer but no significant periodicity in other seasons. This means that there is diurnal or semidiurnal variation in some seasons at low latitude stations like Ahmedabad and Waltair but no clear periodicity at high latitude stations.

Comparison of E region drifts during 1956-59 and 1959-62 at Ahmedabad

Comparing the results at Ahmedabad from 1956 through 1962 we find that the average drift speed has decreased both during day and during night with decrease in sunspot activity. This is in agreement with that reported by Rao and Rao (1964) at Waltair.

The average drift speed shows seasonal variation during both the periods with maximum in winter and minimum in equinoxes for nighttime observations. During daytime it is maximum in winter; the minimum is in equinoxes during 1956-59 and in summer during 1960-62.

The diurnal variation of average speed during 1956-59 shows 24 hourly variation in summer and no significant diurnal or semidiurnal variation in winter and equinoxes. However during 1959-62 there is diurnal and weak semidiurnal change

in summer and in winter respectively and no clear periodicity in equinoxes. This may be regarded as a variation with solar activity.

8. Summary and conclusions

We may draw the following conclusions from the study of E region drifts :

(1) There is no significant difference between the speed and the direction of the drift measured on 2.6 Mc/s and 4.0-4.4 Mc/s.

(2) The average drift speed is about 80 m/s and is maximum in winter and minimum in equinoxes except during daytime in 1959-62; and is higher during night than during day.

(3) In 1956-59 most probable direction is towards N-W in winter daytime and summer nighttime. In other seasons the N-W and S-E directions occur equally frequently. In 1959-62 the most probable direction is towards S-E during nighttime. During daytime the most probable direction is towards N-W in winter and towards S-E in summer. In equinoxes, the majority of the directions occur towards N-W and S-E in daytime.

(4) There is no diurnal variation in drift speed in winter and equinoxes, but we find a diurnal variation with minimum around noon and maximum around midnight in summer and semidiurnal variation in winter during 1959-62.

(5) In general, the E-W component is more towards west and the N-S component more towards north during day and towards east and towards south during night. In summer of 1959-62, the E-W component is towards east all the time and N-S component is towards south all the time.

(6) From the harmonic analysis it appears that the diurnal variation of drift is more prominent than the steady or the semidiurnal wave except in summer when the steady vector predominates.

(7) The rotation of diurnal drift vector with time is anticlockwise in winter and equinoxes, but clockwise in summer.

(8) The rotation of semidiurnal drift vector with time is clockwise in winter and summer, but anticlockwise in equinoxes.

CHAPTER IV

Measurement of horizontal drift in the F region over Ahmedabad from January 1957 to February 1962

We shall present in this chapter the results of analysis of horizontal drift in the F region. The analysis was done on similar lines as that for the E region as described in the previous chapter.

1. Mean annual variation in speed and direction at 4.0-4.4 Mc/s during day and at 2.6 Mc/s during night

(i) 1957-59

Figure 4.1(a) shows histograms of the percentage of occurrence of drift speed and direction for night (2.6 Mc/s) and day (4.0-4.4 Mc/s) and for the year as a whole. We notice from this figure that the histograms rise quickly to the peak occurrence value and decline slowly afterwards during night; whereas during day it shows rapid rise and rapid fall. Though the speed values range from 20 to 240 M/s, the most probable range is 40-60 m/s both during night and day. However the mean and median values are 79 m/s and 69 m/s during night and 71 m/s and 65 m/s during day respectively. Thus the average drift speed is little higher during night than that during day.

The histograms of drift directions show two peaks,

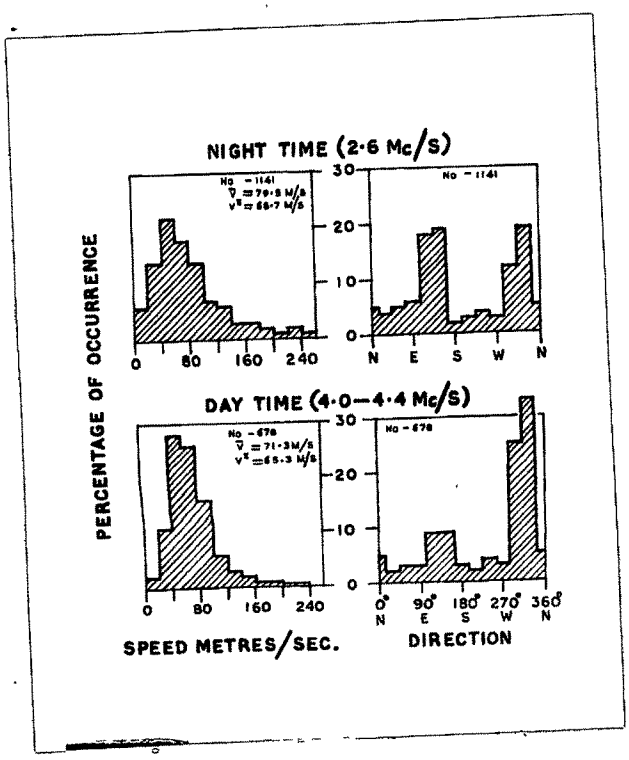

(a) - 1957-59

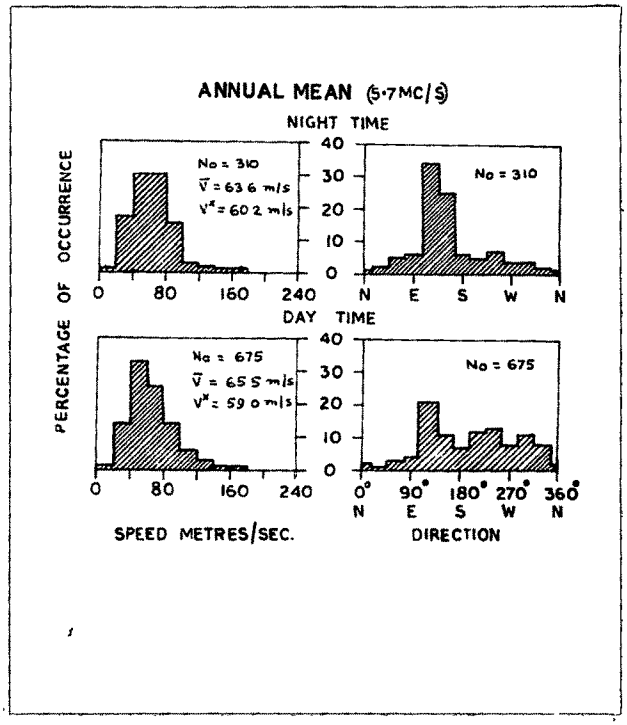

(b) - 1960-62

Figure 4.1 Histograms showing annual mean variation of F region drift speed and direction during day and night.

one towards N-W and the other S-E equally prominent during night; but the N-W direction is the most prominent during day.

(ii) 1960-62

Figure 4.1(b) shows the histograms of percentage occurrence of drift speed and direction during night and day on 5.7 Mc/s. The results indicate that during night there is a rapid rise and rapid fall of drift speeds to and from its peak occurrence values; whereas the decline is not so fast during day. The speed values lie in the range 20-180 m/s with maximum occurrence between 20-80 m/s during night and 40-60 m/s during day. The mean and median values are about 65 m/s and 60 m/s respectively and therefore there does not appear to be any significant diurnal variation in drift speed at this frequency.

The drift direction as can be seen in the figure is mostly towards S-E during night, whereas it cannot be said to be so during day.

Figure 4.2 shows the comparison of drift speed and direction for nighttime only, obtained on two frequencies 2.6 and 5.7 Mc/s. It can be seen that there is no significant difference between these two quantities at these frequencies although their heights of reflection may be quite different.

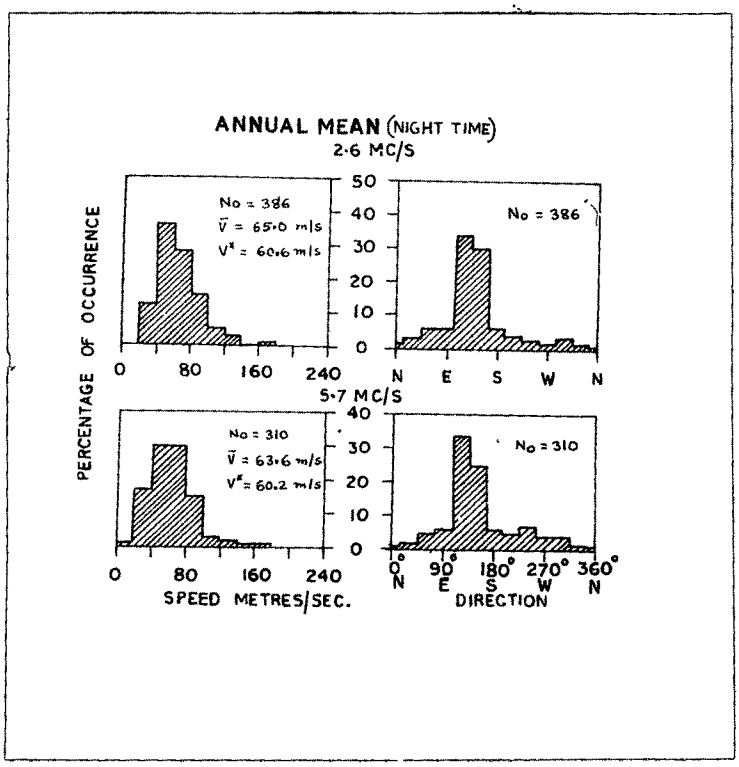

1960-62

Figure 4.2 Histograms showing annual mean variation of F region drift speed and direction on 2.6 and 5.7 Mc/s during nighttime.

2. Seasonal variation

Drift speed : 1957-62

The histograms of percentage occurrence of drift speed during day (at 4.0-4.4 Mc/s) and night (at 2.6 Mc/s) are shown seasonwise (equinoxes, winter and summer) in Figure 4.3(a) for 1957-59 and Figure 4.3(b) for 1960-62.

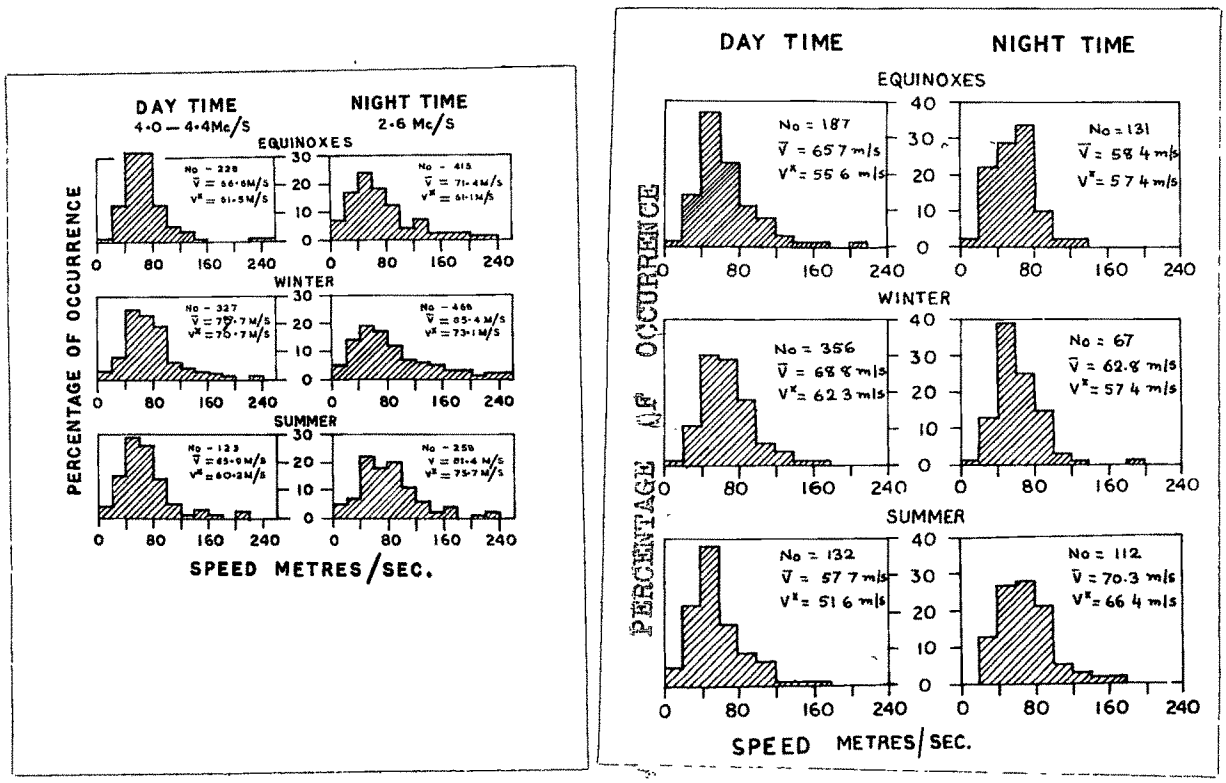

(a) - 1957-59 (b) - 1960-62

Figure 4.3 Histograms showing seasonal variation of F region drift speed.

One distinct difference that may be seen from the figures is that during the period 1957-59, the nighttime percentage occurrences drop off gradually as compared to these in the 1960-62 group where there is sharp fall in occurrence of high drift speed beyond about 100 m/s. The average values of drift speed in different seasons are given in Table 4.1. We find from Table 4.1 that the average drift speed $\overline{V}$ is considerably higher during night than during day in all seasons except in winter and equinoxes during 1960-62. It is interesting to note that the speeds are higher during night than during day in summer from 1957 through 1962.

Table 4.1

Average value of drift speeds in the F region for the daytime and nighttime hours in different seasons for the years 1957-62

Season	1957-59 Night m/s	1957-59 Day m/s	1960-62 Night m/s	1960-62 Day m/s
Equinoxes	71 ± 2	67 ± 2	58 ± 2	66 ± 2
Winter	85 ± 2	77 ± 2	63 ± 3	69 ± 1
Summer	81 ± 1	66 ± 3	70 ± 3	58 ± 2
Annual Mean	79 ± 2	71 ± 1	64 ± 1	65 ± 1

Drift direction: 1957-62

From the histograms of drift directions shown in Figures 4.4(a) and 4.4(b), we see interesting features in the two cases. In the first group (1957-59) in all seasons, the direction is predominantly N-W during daytime, but equally frequent towards N-W and S-E during night. However in the second group (1960-62), the direction has shown preference towards S-E during daytime and nighttime in summer and in equinoxes but only during nighttime in winter.

We have shown in Figure 4.5 the histograms of nighttime F region drift speeds and direction from observations on a single frequency, viz. 2.6 Mc/s. This shows clearly the maximum frequency of occurrence between 40-80 m/s and direction towards S-E in all seasons.

3. Average hourly variation of drift speed and direction

Figures 4.6(a) and 4.6(b) show the average hourly variation of speed and also the annual mean curve.(a) and (b) refer as usual to observations during 1957-59 and 1960-62 respectively. The observations made on two frequencies, 2.6 Mc/s and 5.7 Mc/s, are combined in Figure 4.6(b) since there was not much difference in the results obtained at the two frequencies. The variation is semidiurnal in equinoxes but largely diurnal in winter and summer. The annual mean curve shows a semidiurnal tendency. However, it is not so clear during 1957-59.

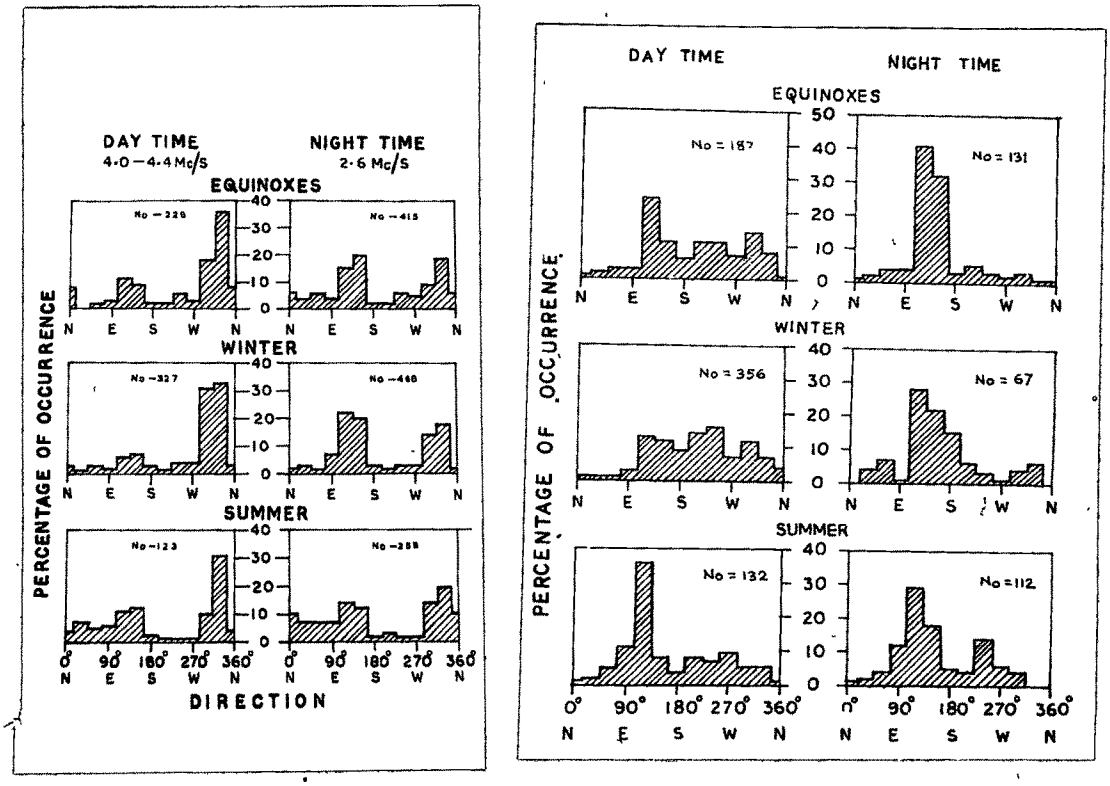

(a) - 1957-59 (b) - 1960-62

Figure 4.4 Histograms showing seasonal variation of F region drift direction.

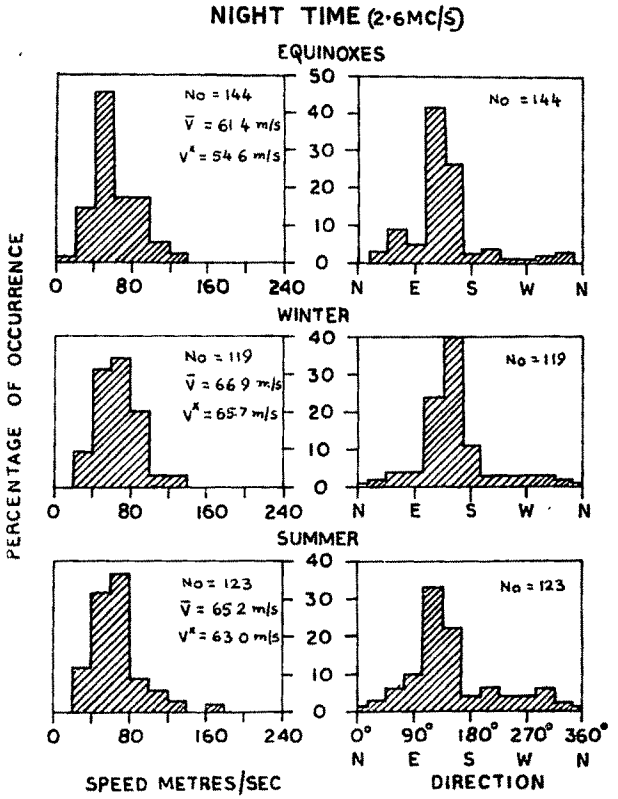

1960-62

Figure 4.5 Histograms showing seasonal variation of F region drift speed and direction on 2.6 Mc/s.

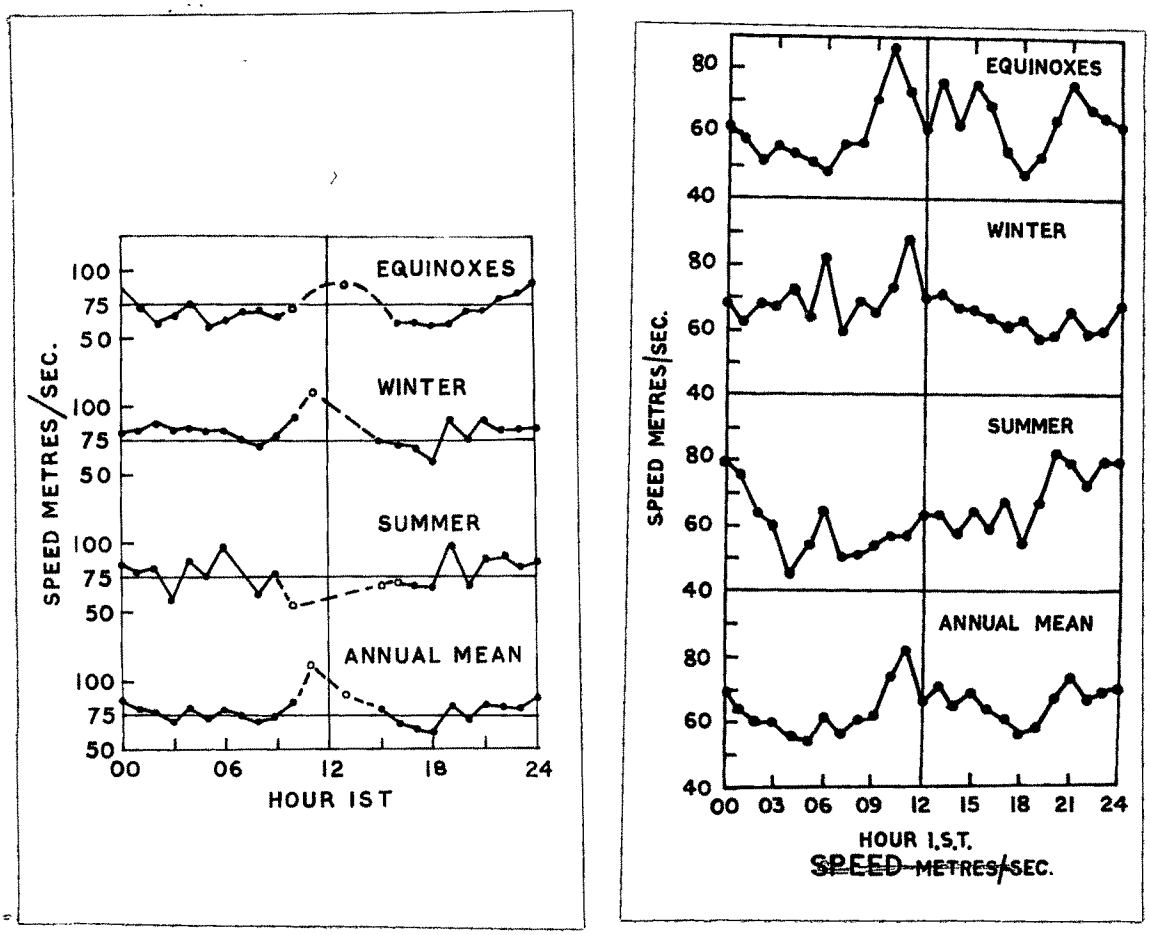

(a) - 1957-59 (b) - 1960-62

Figure 4.6 Curves showing diurnal variation of average drift speed in the F region.

Figures 4.7(a) and 4.7(b) show the average hourly values of E-W and N-S components of the drift direction in each season and the year as a whole. During 1957-59, the variation of E-W component is clearly westward during day and eastward during night and that of N-S component is northward during day and southward during night. This is also so regarding the E-W component during 1960-62 except in summer when it is eastward all the time and the N-S component is consistently towards south in that period. The change over from one direction to the other generally takes around 06 hrs and 18 hrs local time. The variation is mostly diurnal type with a weak semidiurnal component in summer.

4. Harmonic analysis of E-W and N-S components of F region drift speeds

To evaluate steady, diurnal and semidiurnal vectors of the E-W and the N-S drifts, the individual curves in Figure 4.7(b) were subjected to Fourier analysis as described for the E region in the previous chapter.

Table 4.2 gives the results of such an analysis. It shows the amplitude and phase of the diurnal and semidiurnal vectors. It may be seen that in the N-S direction, the steady drift is large as compared to the diurnal or semidiurnal component and is directed towards the south. In the E-W direction, the diurnal component is quite large (except in summer) compared to the steady or semidiurnal

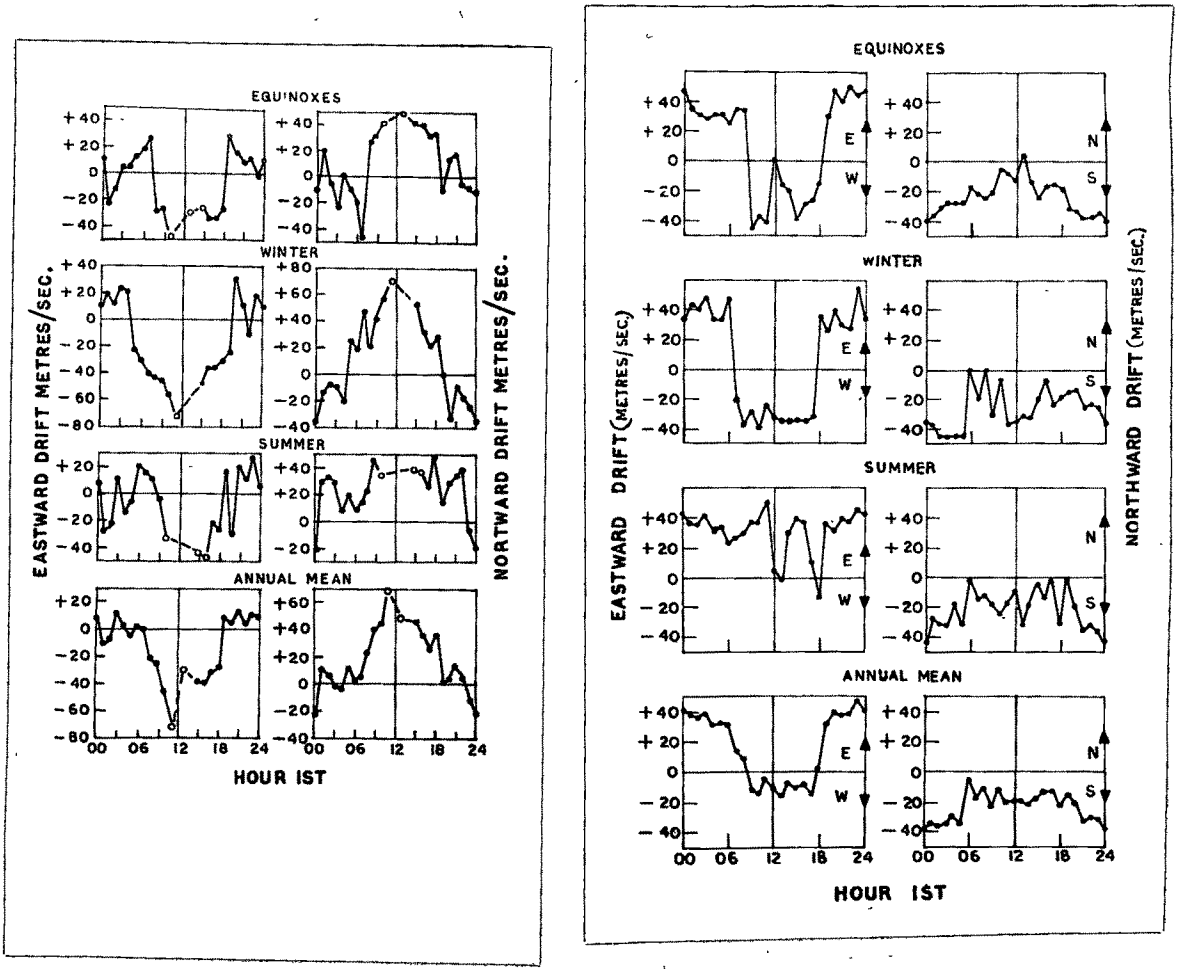

(a) - 1957-59 (b) - 1960-62

Figure 4.7 Curves showing diurnal variation of E-W and N-S components of F region drift.

Table 4.2

Coefficients of harmonic analysis of F region drifts during March 1960 to February 1962.

Season	Steady Component		Diurnal Component				Semidiurnal Component			
	E-W drift	N-S drift	E-W drift		N-S drift		E-W drift		N-S drift	
	V_o m/s	V_o m/s	V_1 m/s	θ_1	V_1 m/s	θ_1	V_2 m/s	θ_2	V_2 m/s	θ_2
Equinoxes	+10.0	-23.7	38.9	78°	13.5	275°	8.9	200°	1.7	20°
Winter	+ 5.9	-25.7	45.1	86°	6.9	229°	5.0	283°	11.6	224°
Summer	+30.0	-20.8	8.4	60°	8.4	262°	6.1	120°	8.4	276°
Annual Mean	+15.0	-23.5	31.4	81°	9.1	261°	3.8	208°	5.6	250°

Positive sign refers to direction towards east & negative sign towards west in E-W component.
Positive sign refers to direction towards north & negative sign towards south in N-S component.
V_1, θ_1 and V_2, θ_2 refer to the amplitude and phase ~~at which maximum~~ of the eastward or northward drift ~~is observed~~. according to the equation $V = V_o + V_1 \sin(t + \theta_1) + V_2 \sin(2t + \theta_2)$

component and the direction of flow is towards east. The same results can be seen more clearly in the form of harmonic dials as shown in Figure 4.8.

The polar plots in Figure 4.9 show the steady, diurnal and semidiurnal vectors in component form with the time of the day. This is a better representation which cannot be seen in detail in Table 4.2. We see here that the steady drift is towards S-E in all seasons. The diurnal vector rotates in a clockwise fashion in winter and in an anticlockwise direction in summer and equinoxes. The semidiurnal vector rotates clockwise in summer and anticlockwise in winter but collapses into a single line in equinoxes.

5. Observations of drift speed and direction at 7.0 Mc/s

We have taken a good number of observations on 7.0 Mc/s during day. We shall give here a brief account of the results of analysis of F region drift speed and direction on 7.0 Mc/s during 1959-62.

Figure 4.10(a) shows the annual mean variation of drift speed and direction between 07-17 hours of the day. It can be seen that the histograms of drift speed show steep rise and gradual fall. The most probable range in speed is observed between 20 and 120 m/s. The average drift speed is 68 m/s with a median value 62 m/s.

Figure 4.10(b) shows that the direction of the drift

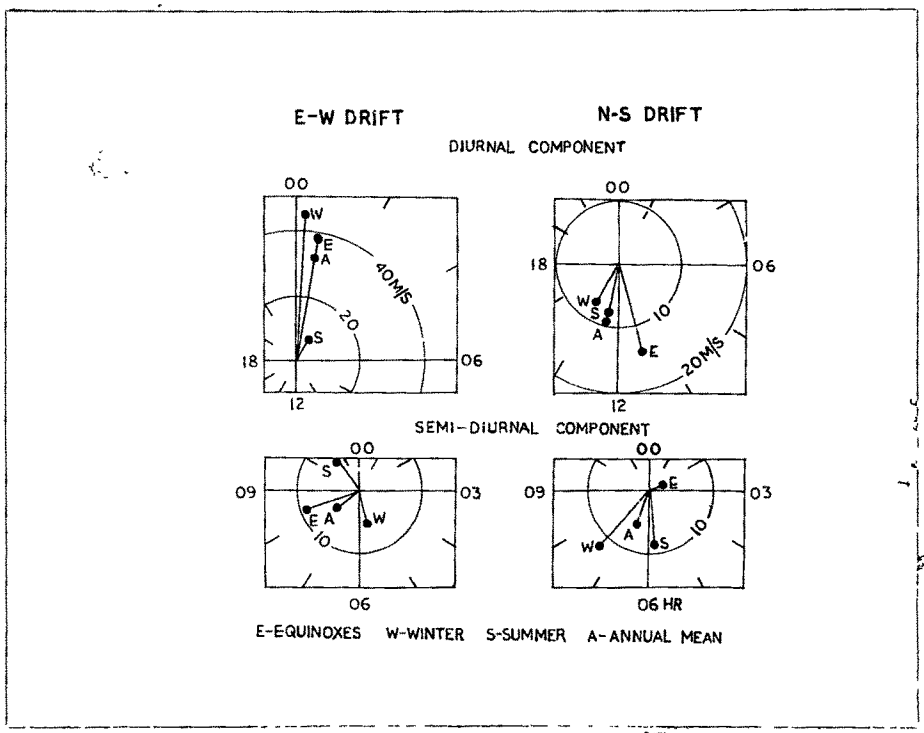

1960-62

Figure 4.8 Harmonic dial of E-W and N-S drift vectors in the F region, where the magnitude and time of maximum amplitude are plotted.

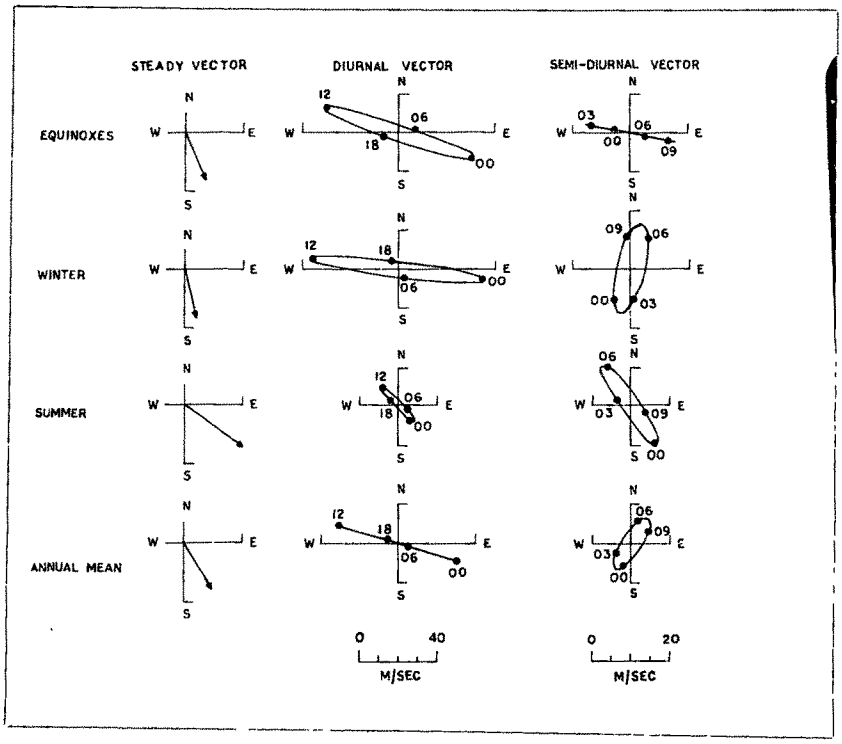

1960-62

Figure 4.9 Polar plots of steady, diurnal and semidiurnal drift vectors in the F region.

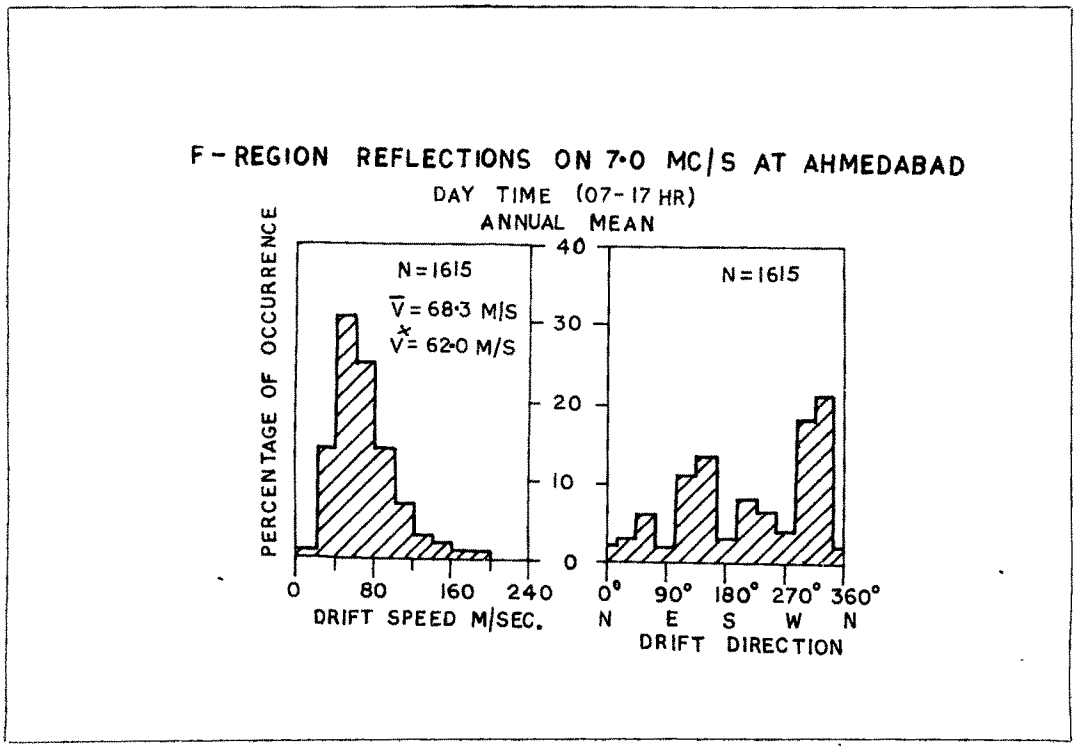

1959-62

(a) (b)

Figure 4.10 Histograms showing annual mean variation of F region drift speed and direction on 7.0 Mc/s during 1959-62 between 07-17 hours.

is found mostly towards N-W and S-E directions.

Figure 4.11 shows the distribution of drift speed and directions in different seasons. The speeds usually have maximum occurrence in the range 40-60 m/s; the average drift speed is 71 m/s in winter which is little higher than in other seasons. The average speed is minimum in summer, being 63 m/s.

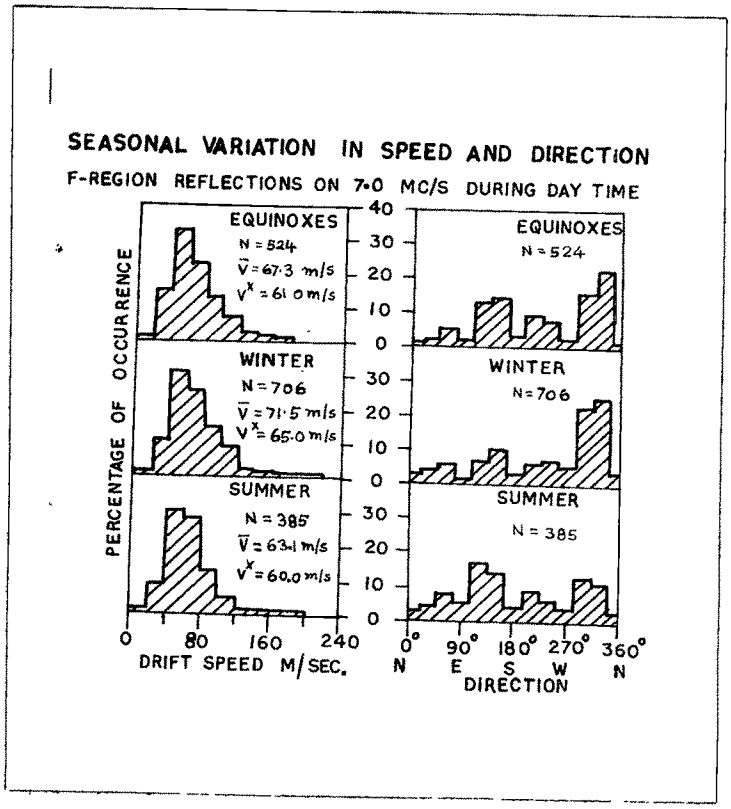

Figure 4.11 Histograms showing the seasonal variation of F region drift speed and direction on 7.0 Mc/s.

The direction of drift in majority of the cases is in the S-E and N-W quadrants in equinoxes and summer. In winter, the most probable direction is towards N-W.

Figure 4.12 shows the hourly average variation of speed during daytime. It can be seen that the speed is maximum between 09 and 14 hrs local time, and is minimum in early morning and evening hours.

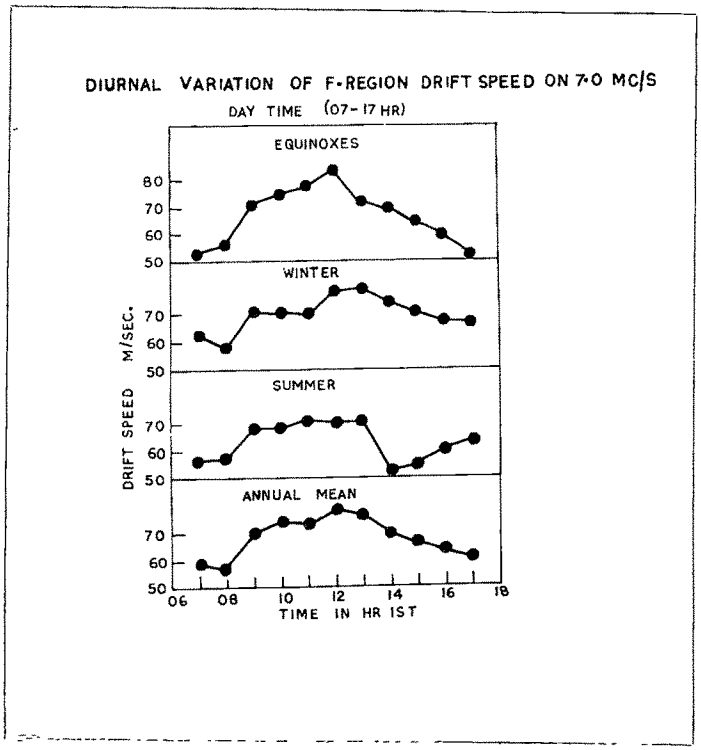

Figure 4.12 Curves showing the variation of average drift speed in the F region on 7.0 Mc/s between 07-17 hours.

Figure 4.13 shows the variation of drift direction at different hours of the day. The direction is towards N-W between 07-16 hrs and towards N-W and S-E at 17 hrs in winter. The directions are towards S-E between 07-10 hrs and it remains towards N-W and S-E between 11-17 hrs in summer. In equinoxes, the direction is towards S-E and N-W from 07-14 hrs and mainly towards N-W in the evening hours.

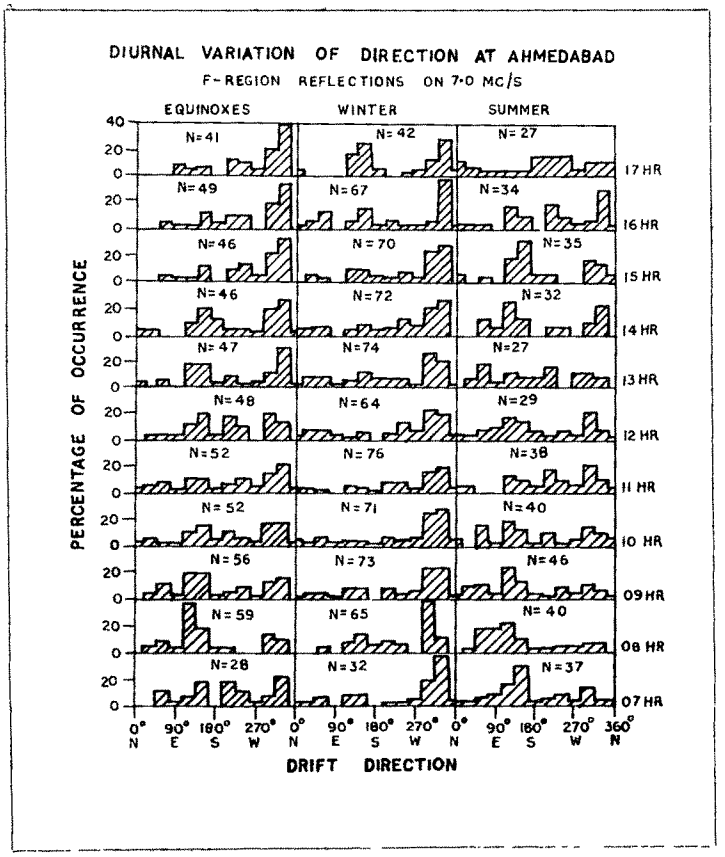

1959-62

Figure 4.13 Histograms showing hourly variation of F region drift direction on 7.0 Mc/s.

6. Discussion

If we glance at the values of drift speed from 1957 to 1962, we can get some idea of its variation with solar activity starting with the peak sunspot period 1957-58. We find that the average nighttime speed during 1957-59 was about 80 m/s which decreased to 65 m/s during 1960-62. The corresponding values during day were 71 m/s and 65 m/s respectively. This suggests that the average speed decreases with decrease of solar activity. A similar trend has been observed at Waltair [Rao and Rao (1964)] where the most probable drift speed was 95 m/s in 1956-58 and 85 m/s in 1960-62. At Yamagawa and Askhabad, the most probable range of drift speed is 60-80 m/s and at Semeiz and Gorky it is found to be 80-100 m/s.

However there is some difference in the nature of average hourly drift speed at Waltair and Ahmedabad. At Waltair the variation is mostly semidiurnal [Rao and Rao (1963)], whereas at Ahmedabad, it did not show any significant change with time during 1957-59 which agreed with Delhi observations [Mitra et al (1960)], but showed diurnal characteristic in summer and in winter and semidiurnal variation in equinoxes during 1960-62. The magnitude of the drift speed is seen to be higher at Waltair than at Ahmedabad which shows its latitude dependence.

Gross features of E-W and N-S components of drift at Waltair, Ahmedabad and Yamagawa are given in Table 4.3. It may

Table 4.3

Direction of E-W and N-S components with season at different places during 1956-59

Station		Winter		Equinoxes		Summer		Source
		E-W	N-S	E-W	N-S	E-W	N-S	
Waltair	Day	W	S	W	S	W	S	Rao and Rao (1959)
	Night	E	N	E	N	E	N	
Ahmedabad	Day	W	N	W	N	W	N	Patel (Present thesis)
	Night	E	S	E	S	E	N	
Yamagawa	Day	E	S	E	S	E	N	Tsukameto and Ogata (1959)
	Night	E	S	E	S	E	S	
	Direction of E-W and N-S components with season during 1960-62							
Waltair	Day	W	S	W	S	E	S	Rao and Rao (1963)
	Night	E	S	E	S	W	S	
Ahmedabad	Day	W	S	W	S	E	S	Patel (Present thesis)
	NIGHT	E	S	E	S	E	S	
Cambridge	Day	E	S	E	N	E	N	Briggs and Spencer (1954)
	Night	W	S	W	S	W	N	

be noted that latitudinally, Ahmedabad or Delhi and Yamagawa show transitional type of behaviour between Waltair and Cambridge. This is in general agreement with Martyn's theory (1955) which predicts a change of phase in the E-W component of F region drift at a geomagnetic latitude 35°. However the transition zone appears to be broad between 14° and 38° in the northern hemisphere if Ahmedabad and Yamagawa are considered to constitute that zone.

From the polar plots shown in Figure 4.9 for Ahmedabad and those given by Rao and Rao (1964) for Waltair and by Shimazaki (1959) for Yamagawa, we find that the diurnal vector rotates clockwise in all seasons at Waltair but only in winter at Ahmedabad. At Yamagawa it may be both ways, but generally is clockwise. The semidiurnal component at all the three places show clockwise and anticlockwise rotations equally frequently.

The drift speed is about the same when obtained from 5.7 Mc/s and 7.0 Mc/s reflections but the direction is mainly towards N-W and S-E on 7.0 Mc/s but mostly towards S-E on 5.7 Mc/s.

7. Summary and conclusions

We shall summarise the main points regarding the F region horizontal drift over Ahmedabad.

(1) The average drift speed is higher during night than during day and is higher in winter than in any other season

during 1957-59. Its mean value is 79 m/s during night and 65 m/s during day in 1957-59; whereas it is 64 m/s during night and 65 m/s during day in 1960-62.

(2) The average speed during 1960-62 is minimum during day and maximum during night in summer.

(3) Most frequent direction is towards N-W during day and N-W and S-E during night in 1957-59; it is not so well defined during day but is mainly towards S-E during night in 1960-62.

(4) There is no significant diurnal variation in the average speed in any season during 1957-59; but shows diurnal variation in summer and winter and semidiurnal variation in equinoxes during 1960-62.

(5) The E-W component of drift is consistently towards west during day and towards east during night from 1957 through 1962 except during summer of 1960-62 where it is towards east at all hours of the day.

(6) Generally, the N-S component is towards north during day and towards south during night in 1957-59, but is consistently towards south at all times during 1960-62.

(7) The composite diurnal vector of the E-W and N-S components traces an ellipse which rotates in a clockwise direction in winter and in an anticlockwise direction in equinoxes and summer.

(8) The composite semidiurnal vector of the E-W and N-S components also traces an ellipse and rotates in a clockwise direction in summer and in an anticlockwise direction in winter, and collapses into a straight line in equinoxes.

(9) There is no significant difference in drift speed on 5.7 and 7.0 Mc/s. The direction of drift seems to be mainly towards N-W and S-E on 7.0 Mc/s but mostly towards S-E on 5.7 Mc/s.

CHAPTER V

Steady and random velocities of ionospheric irregularities
Auto - and Cross - Correlations

1. Introduction

Mitra's method (1949) of similar fades assumes that the diffraction pattern produced on the ground by ionospheric irregularities does not change in the form as it moves past the observing points on the ground. It also assumes that the diffraction pattern is isotropic which means that its properties do not change along any direction at a fixed distance from the origin.

It is important to consider fading of a radio wave which has been singly reflected from the ionosphere and devise mathematical methods to analyse such records. Briggs et al (1950) introduced the method of auto - and cross - correlograms and demonstrated the usefulness of such concepts in the interpretation of complex fading patterns. Let us briefly review their method.

It is clear that fading could be produced by a movement of the diffraction patterns past the observing points as would happen if a horizontal wind is blowing in the ionosphere. The fading recorded at two points in the direction of wind would be exactly similar but displaced in time. Another way in which fading could be produced would be by random changes

in ionospheric irregularities without any drift; such a mechanism would produce random changes in the diffraction pattern on the ground and the fading at two nearby receivers would be similar. If receivers were separated from each other in any direction the fading becomes more and more dissimilar.

The two mechanisms mentioned above may operate simultaneously and would introduce changes of form in a moving diffraction pattern. It is possible to reduce from fading records taken at three points situated at the corners of a right-angle triangle (1) the steady velocity of the diffraction pattern moving on the ground, (2) the rate at which the pattern alters as it moves, (3) the size of the irregularities in the pattern. It is also possible to make some rough estimate of the shape of the irregularities if they are not isometric. For all these, it is found useful to consider the auto-correlation and cross-correlation functions of the fading records at the three receiver-points. Once we deduce the nature of the diffracting pattern, it could be connected with large scale movements in the ionosphere and associated changes in the pattern due to random movements therein. A full analysis of the amplitudes of reflected signals has been made by Briggs et al (1950), and this has been extended by Phillips and Spencer (1955) to include anisometric patterns. A comprehensive review of aspects of diffraction theory and their application to the ionosphere is given by Ratcliffe (1956).

2. Measurement of correlation

(1) A single time-record

A fading record is found to have random character like the curves in Figure 5.1. To study a variable of this kind, use can be made of auto-correlation function, i.e. the amplitude or phase correlation coefficients of the received signal. It is clear that the correlation coefficient of a sequence of amplitudes R_1, R_2 .... of the signal between time t and $t + \tau$, so that $R_i = R(t_i)$, and $R_i + 1 = R(t_i + T)$, is by definition given by function :-

$$\rho(0,0,\tau) = \frac{\overline{[R(0,0,t) - \bar{R}][R(0,0,t+\tau) - \bar{R}]}}{\overline{[R(0,0,t) - \bar{R}]^2}} \qquad (1)$$

where $\bar{R}$ is the mean value of R and $\rho(0,0,\tau)$ is the correlation coefficient of the envelope of the random oscillations and measures the correlation between values of R separated by a time interval τ . It has the value unity for time displacement $\tau = 0$ and generally decreases smoothly at first as τ increases from zero.

A typical auto-correlogram is shown in Figures 5.2(a) and 5.2(b). Clearly the value of τ at which $\rho(0,0,\tau)$ goes to zero is the time interval at which the two values of R have become completely independent.

In the analysis of fading of radio signals it is important to find a measure of the "speed of fading". It is

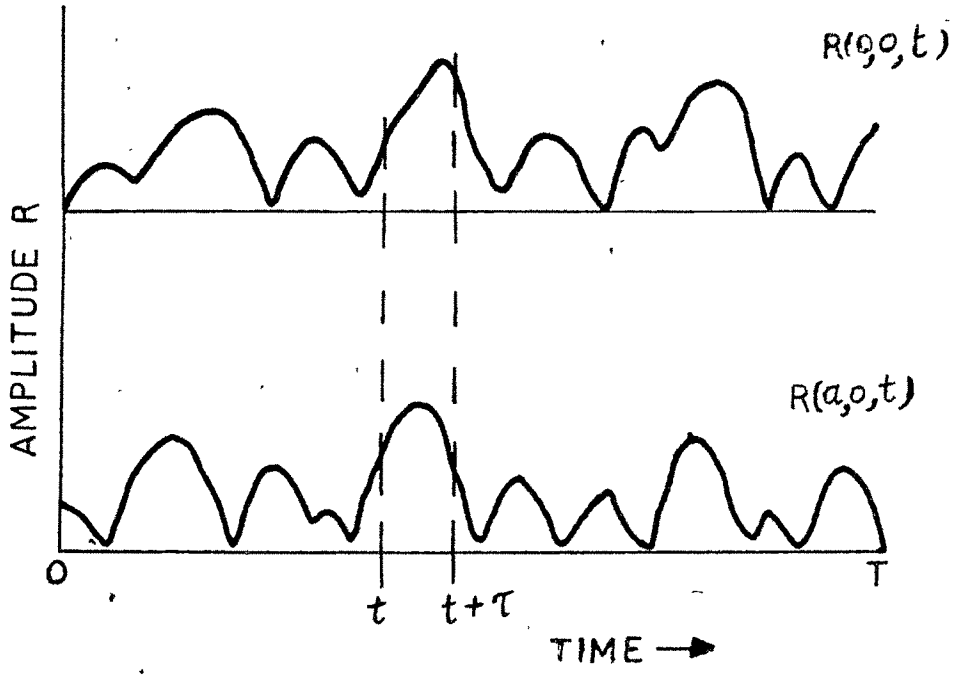

FIG. 5·1 FADING RECORDS AT TWO RECEIVERS

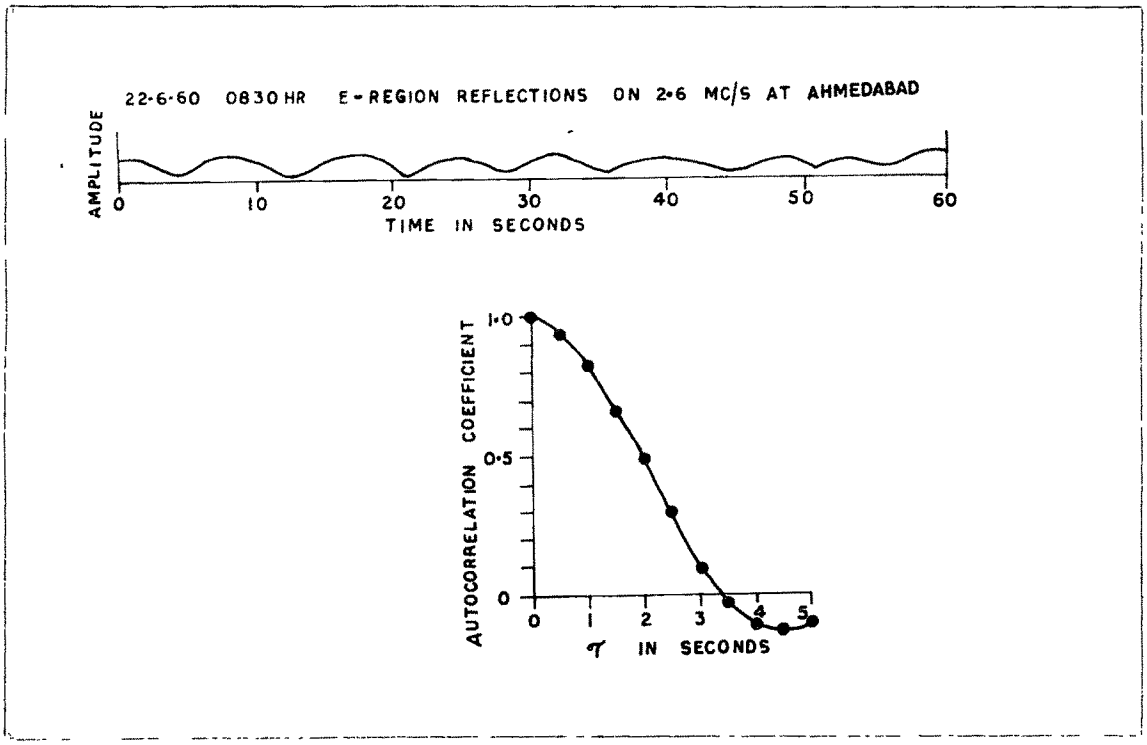

Figure 5.2(a) Fading curve on 2.6 Mc/s at 0830 hr on 22-6-60 and its auto-correlogram.

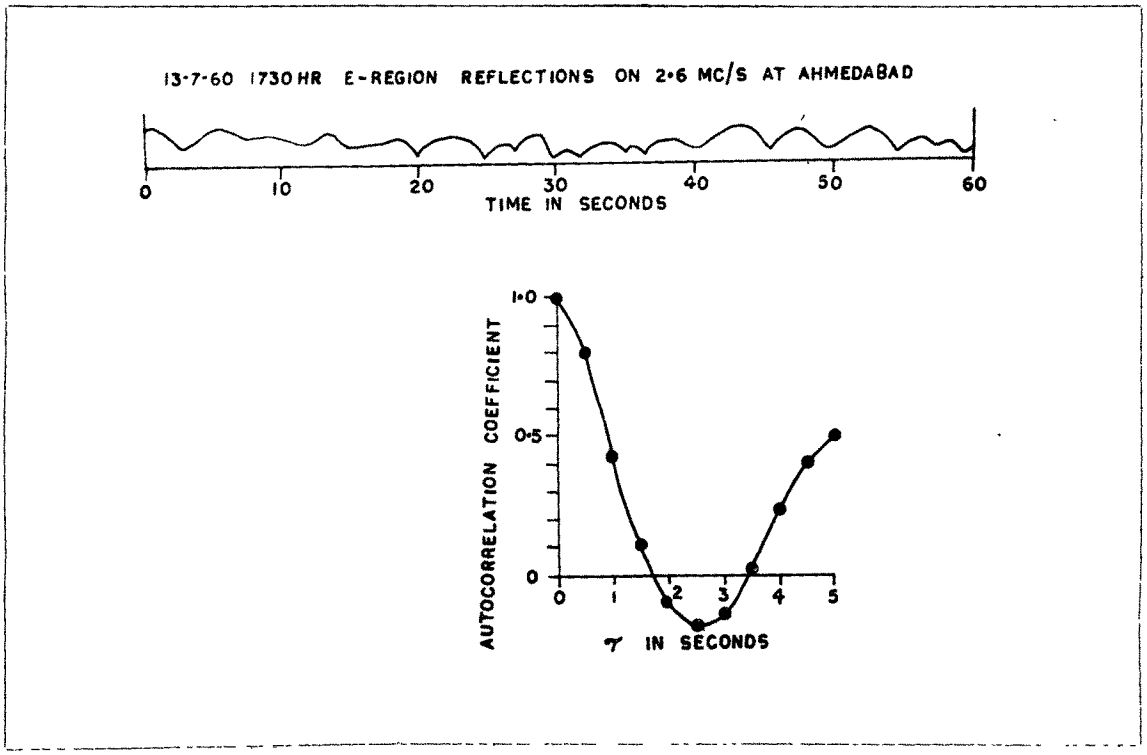

Figure 5.2(b) Fading curve on 2.6 Mc/s at 1730 hr on 13-7-60 and its auto-correlogram.

possible to derive it either from the function $\rho(0,0,\tau)$ as defined in equation (1) or with less labour in the following way :

$$S = \frac{\left|\overline{\frac{\partial R}{\partial t}}\right|}{\bar{R}} \qquad (2)$$

Here, the speed of fading S, is the mean rate of change of R, normalized to a constant mean value of R.

(2) Space variation and the two dimensional auto-correlation function

We may also measure the rate of variation R over the ground at a given instant and call it G, where

$$G = \frac{\left|\overline{\frac{\partial R}{\partial x}}\right|}{\bar{R}} \qquad (3)$$

where ∂x is the distance between two points at which R is measured at the same time. To start with, G may be assumed to be independent of the direction on the ground in which the variable x is measured.

Thus in practice the signal amplitude over the ground and in time could be represented by a function R (x,y,t) of the space coordinates x,y and the time coordinate t. We can simplify first the analysis by considering R as a function of 'a' and t and obtain the two-dimentional auto-correlation function of R(a,0,t) from equation (1). Thus

$$\rho(a,0,\tau)=\frac{\overline{[R(0,0,t)-\bar{R}][R(a,0,t+\tau)-\bar{R}]}}{[\overline{[R(0,0,t)-\bar{R}]^2}\,\overline{[R(a,0,t+\tau)-\bar{R}]^2}]^{\frac{1}{2}}} \qquad (4)$$

where $R(0,0,t)$ and $R(a,0,t+\tau)$ are the amplitudes of the signal at the origin at time t and at distance 'a' and $t+\tau$ respectively, 'a' being the separation between the pair of aerials. A bar drawn over a quantity signifies that the average of the quantity is taken over a time which is long compared to the time scale of the variations. The functional form of the correlation can be described mathematically as,

$$\rho(0) = 1$$
$$\rho(\tau_1) \geq \rho(\tau_2) \quad \text{for} \quad \tau_2 \geq \tau_1$$
$$\rho(\tau) = \rho(-\tau)$$

Equation (4) gives the cross-correlation between two records obtained at two aerials for different values of time difference τ. In this case $\rho(a,0,\tau)$ will not necessarily be peaked at $\tau = 0$. This might be expected since the cross-correlation function uses two time series not necessarily identical.

Suppose there is a systematic time shift between the two series, the peak cross-correlation may occur with a time lag $\tau = T_x$ in the fading records obtained with an E-W pair of aerials and a time lag $\tau = T_y$ in that with N-S pair of aerials. Thus, in general, the lag correlograms $\rho(a,0,T_x)$, $\rho(0,a,T_y)$ would be less than unity.

It is important to bear in mind that the use of this type of correlation analysis requires that the amplitude variations with time in a fading be statistically steady. This means that the mean amplitude and its standard deviation should not vary within the sampling time.

Some typical fading records and their correlograms

We shall compare here the results obtained by the method of similar fades and by the method of correlation functions. A few tracings of some typical fading records are shown at the top of Figures 5.3(a), 5.3(b) and 5.3(c). The auto - and cross-correlation function were calculated from equation (1) and (4) and are shown below the fading records. Inset is a table showing the drift speed and direction calculated by the method of similar fades and by the method of correlation functions. The same table is also typed below the figure. It may be seen that the results obtained by the two methods do not differ seriously in some type of records.

Groupings of the fading records were made as described below:-

(1) Fading records showing a high degree of similarity in the amplitude of fading and the individual time shifts between corresponding maxima or minima such as shown in Figure 5.3(a). The auto - and cross-correlation curves in this case vary smoothly with time. The speed and direction obtained by the two methods agree fairly well.

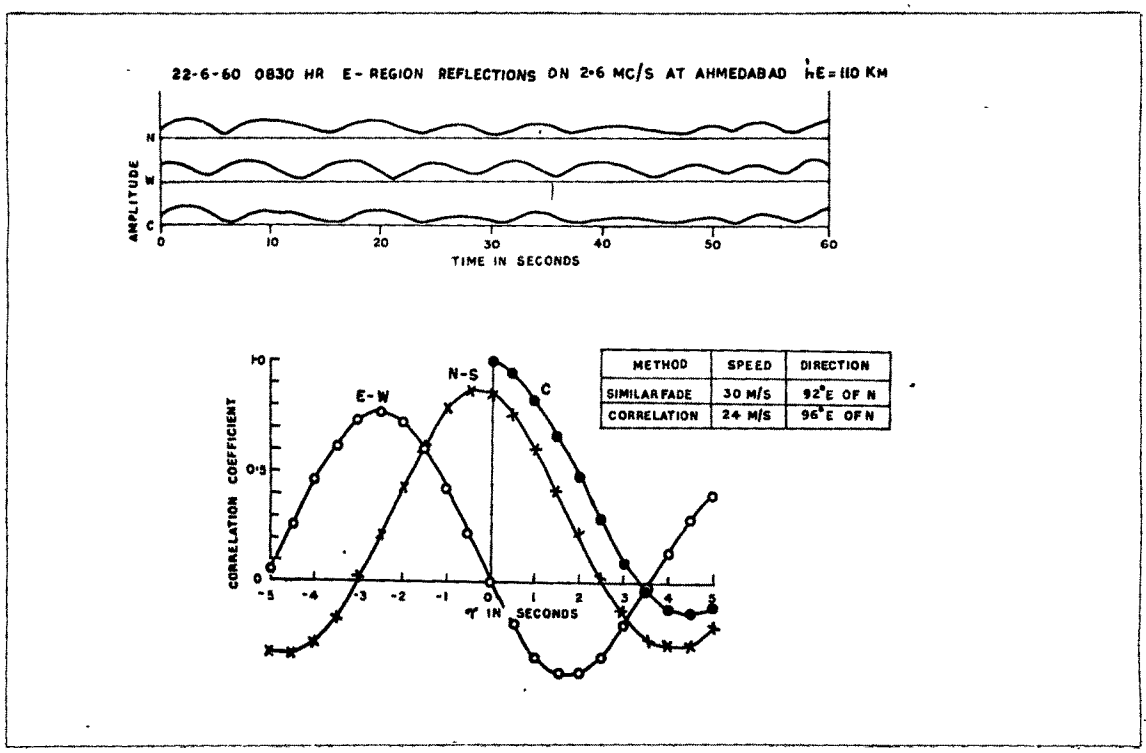

Figure 5.3(a) Fading curves on 2.6 Mc/s at 0830 hr on 22-6-60 and their auto - and cross-correlograms.

C-W forms E-W pair

N-C forms N-S pair.

Method	Speed	Direction
Correlation	24 m/s	96° E of N
Similar Fades	30 m/s	92° E of N

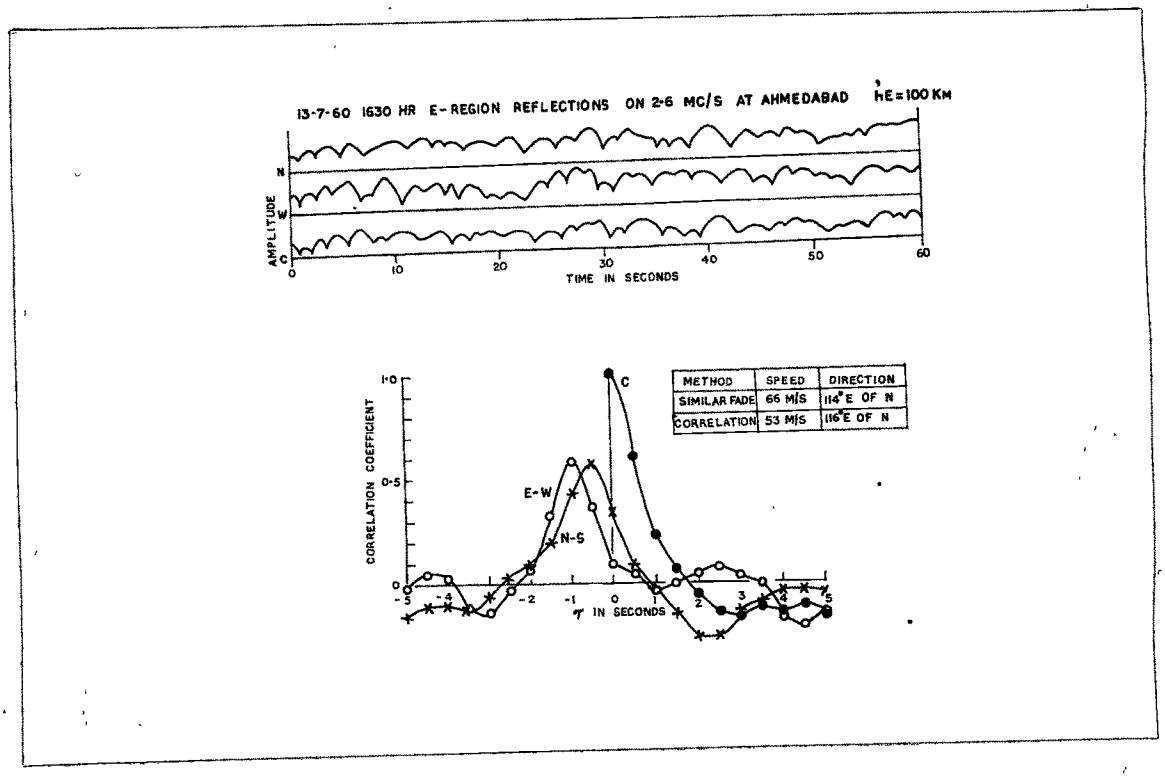

Figure 5.3(b) Fading curves on 2.6 Mc/s at 1630 hr on 13-7-60 and their auto - and cross-correlograms.
C-W forms E-W pair
N-C forms N-S pair.

Method	Speed	Direction
Correlation	53 m/s	116° E of N
Similar Fades	66 m/s	114° E of N

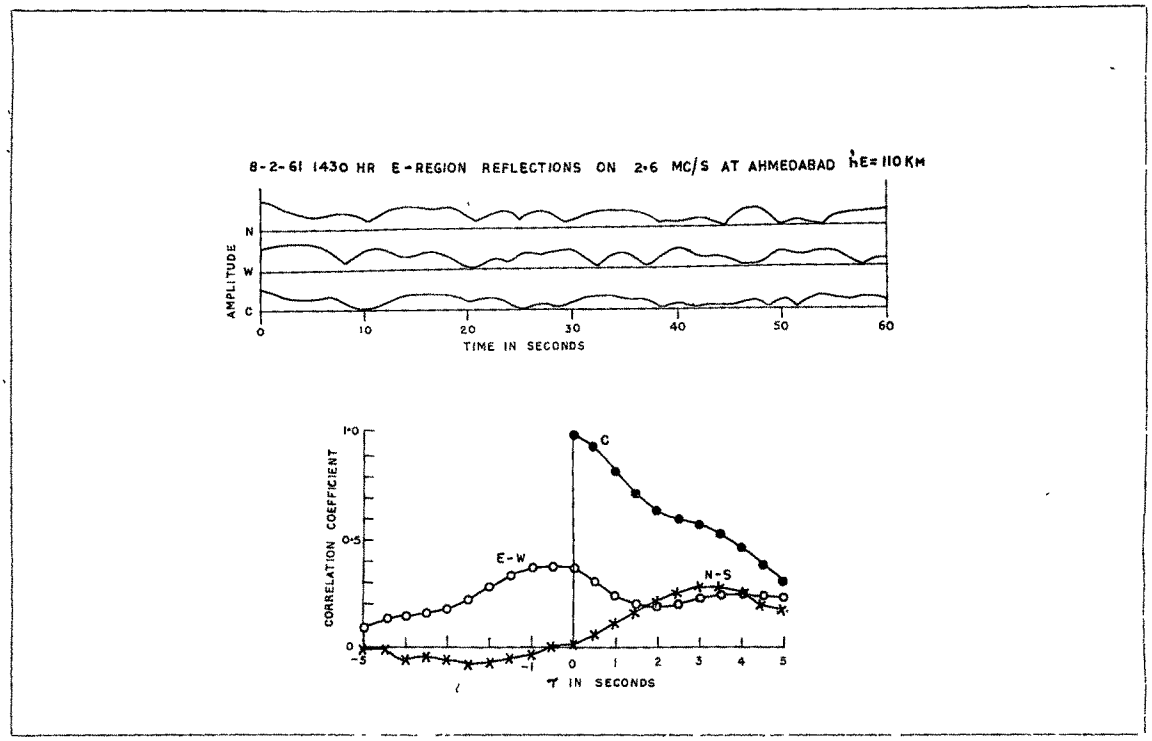

Figure 5.3(c) Fading curves on 2.6 Mc/s at 1430 hr on 8-2-61 and their auto - and cross-correlograms.
C-W forms E-W pair
N-C forms N-S pair.

(2) Fading records which do not show high degree of similarity, ~~as~~ are presented in Figure 5.3(b), but some similarity can still be seen between the records. The correlation is found to be less in this type but the results by both the methods are in tolerable agreement.

(3) Fading records which show random fading with few recognizable common features as are shown in Figure 5.3(c). Detection of corresponding maxima or minima is extremely difficult in such cases. The correlograms show poor correlation and hence such records may be rejected for analysis.

Results

Some 78 fading records obtained on 2.6 Mc/s from the E region at Ahmedabad during the period March 1960 - ~~May~~ February 1961 were selected for analysis. Of these, 17 records fell in group (3) and were rejected. The results of the remaining 61 records are presented below.

Variation of drift speed

Figure 5.4(a) shows the histograms of different ranges of drift speed obtained by the two methods. The most probable range is 40-60 m/s in both the cases with a small difference in the average speed. The error is likely to be larger in the range 60-100 m/s in the method of similar fades since the time delays measured are smaller in magnitude than those in the correlation method.

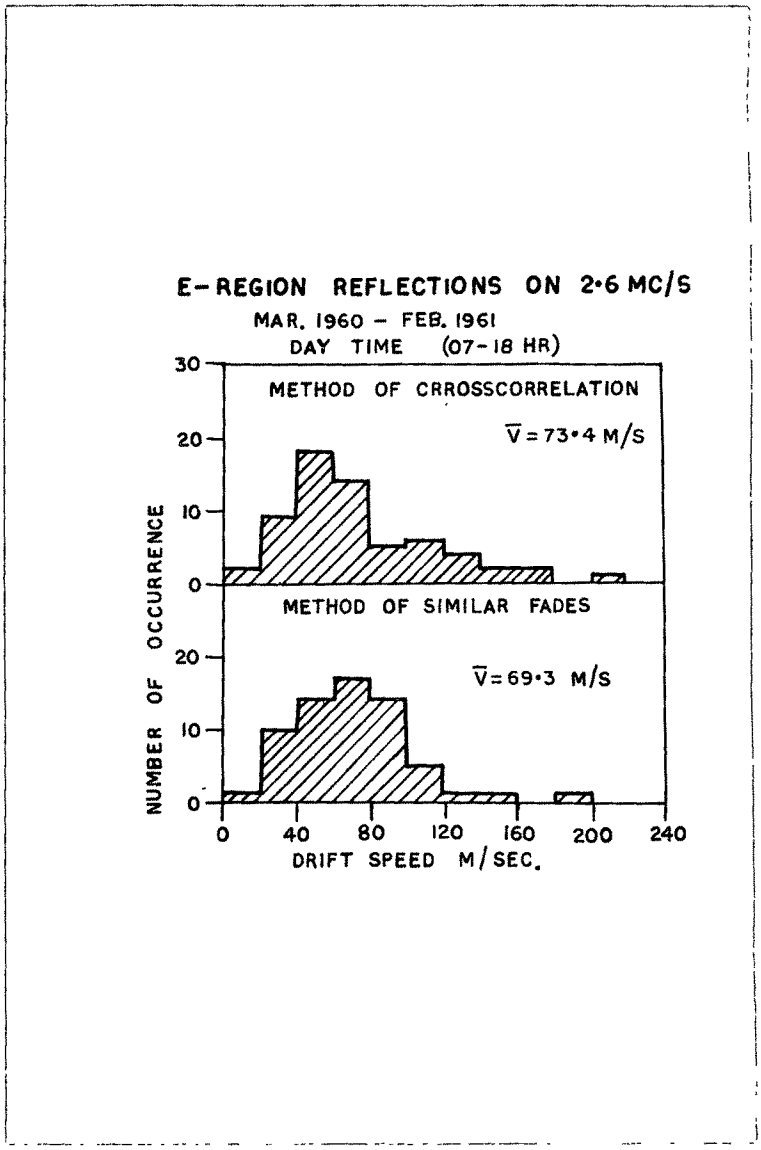

Figure 5.4(a) Histograms of drift speed obtained by method of cross-correlation and similar fades.

Figure 5.4(b) is a plot of drift speeds by the method of similar fades versus that by correlation functions. There is a good correlation at lower speeds.

Variation of drift direction

Figure 5.5(a) and 5.5(b) show similar plots of drift direction as calculated by the two methods. The results show tolerable agreement and hence it may be concluded that for a general statistical study, the less laborious method of similar fades may be adopted.

3. Amplitude and time analysis of a single downcoming wave

(1) Amplitude analysis

Ratcliffe (1948) gave an explanation of the rapid fading of the amplitude of singly reflected downcoming radio waves. He considered the ionosphere as a reflecting layer in which a large number of irregularities were imbedded in a horizontal plane. Each of these irregularities scatters part of the incident radio waves and if the irregularities are assumed to have a movement with a random velocity v in the line of sight the problem becomes similar to the motion of gas molecules in thermal agitation. The probability distribution of v can be easily worked out from Maxwell's theory as

$$P(v) = \frac{1}{\sqrt{2\pi}\, v_o} \exp\left(-\frac{v^2}{2v_o}\right) \qquad (5)$$

where v_o is the r.m.s. value of v.

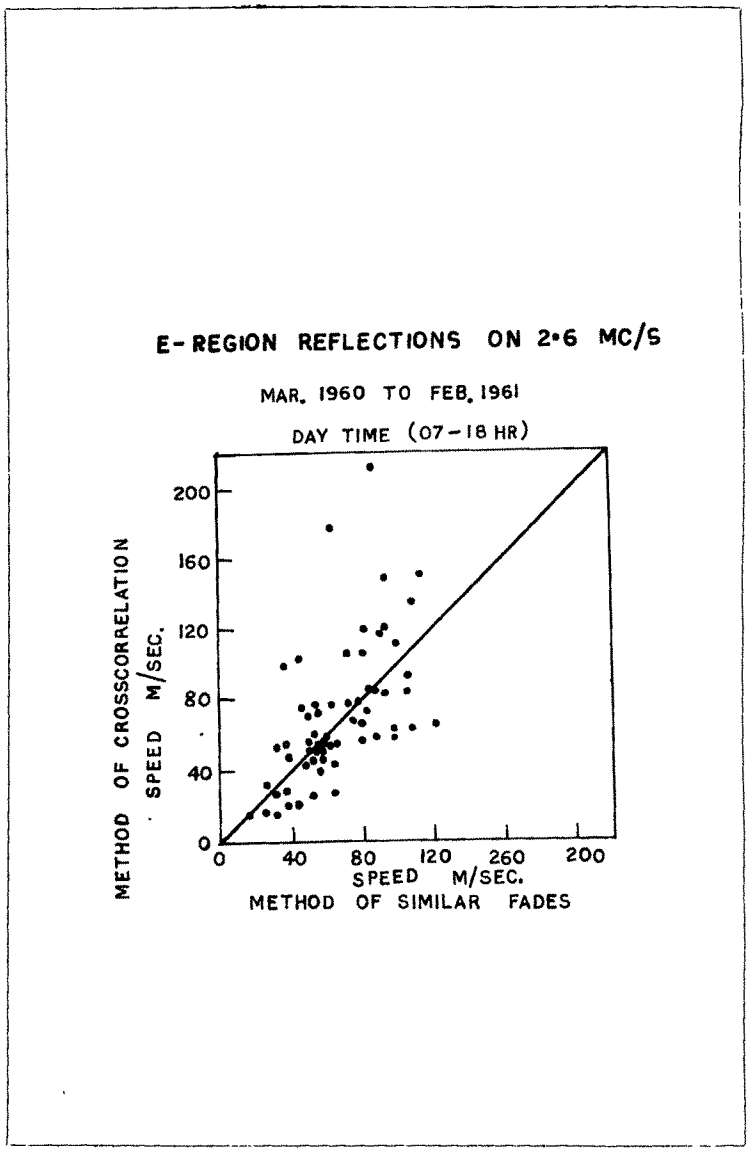

Figure 5.4(b) Plot of drift speeds by the method of similar fades versus that by correlation functions.

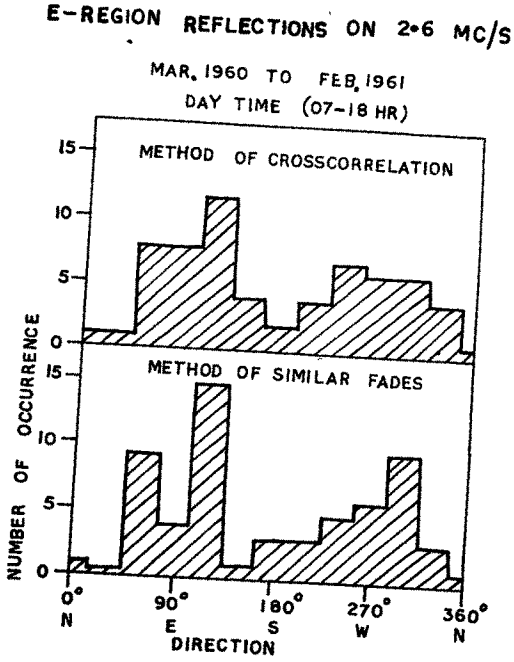

Figure 5.5(a) Histograms of drift direction obtained by method of correlation function and method of similar fades.

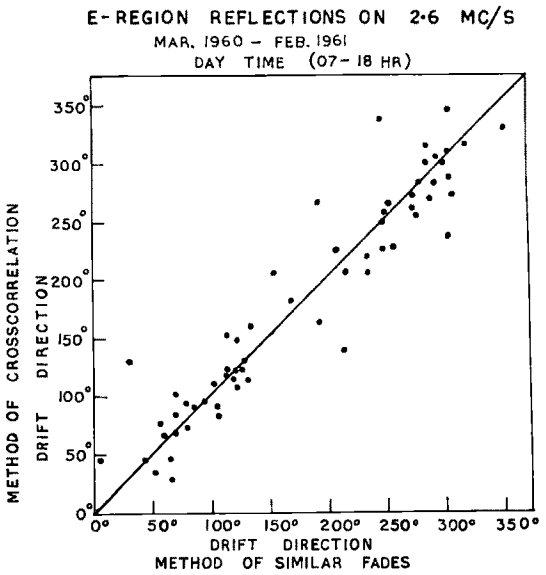

Figure 5.5(b) Plot of drift directions by the method of similar fades versus that by correlation functions.

The frequency of the scattered wave will suffer a doppler shift due to the motion of the irregularity and the change in frequency f is given by the wellknown Doppler formula

$$f = f_o \left(1 \pm \frac{2v}{c} \right) \qquad (6)$$

where f_o is the frequency of the incident wave, v is the velocity of the irregularity and c is the velocity of light. If v is small compared with c, the irregular change in frequency can be considered to be an irregular change in phase of a fixed frequency f_o.

The phase of the scattered wave from the individual irregularities or blobs can thus be considered to be distributed randomly and the fading of the received signal would be the result of the interference of a large number of wave-vectors with random phases. This problem is therefore similar to the "random walk" phenomenon. Lord Rayleigh showed that the probability P(R) of finding the amplitude of the resultant vector between R and R + dR in a random walk process is given by

$$P(R) = \frac{R}{\Psi} \exp \left(- \frac{R^2}{2\Psi} \right) \qquad (7)$$

where R is the instantaneous amplitude of the resultant vector, and Ψ is related to the amplitude $\bar{R}$, R_o and R_m as shown below :-

$$\bar{R} = \sqrt{\frac{\pi}{2} \Psi} \qquad (8)$$

$$R_o = \sqrt{2\Psi} \tag{9}$$

and

$$R_m = \sqrt{\Psi} \tag{10}$$

where $\bar{R}$ is the average value, R_o the r.m.s. value, and R_m the most probable value of the amplitude.

We see from equation (3) that if we plot $\ln\left[\frac{P(R)}{R}\right]$ vs. R^2, we should get a straight line.

A typical fading record which approximately follows the Rayleigh law of amplitude distribution is shown in Figure 5.6.

The distribution is different when the received signal is composed of a steady component specularly reflected from the layer and a random component contributed by time changes in the irregularities. For this situation, Rice (1945) modified equation (3) to the following form :

$$P(Q) = \frac{Q}{\Psi} \exp\left[-\frac{(Q^2 + B^2)}{\Psi} J_o\left(\frac{QB}{\Psi}\right)\right] \tag{11}$$

where B is the amplitude of the steady signal and Ψ is a function of the amplitude of random component as given by equations (4), (5) and (6) and $J_o(x)$ is the Bessel function of zero order. In general

$$Q^2 = B^2 + 2\Psi = B^2 + R_o^2 \tag{12}$$

That is, the mean square amplitude of the resultant is the

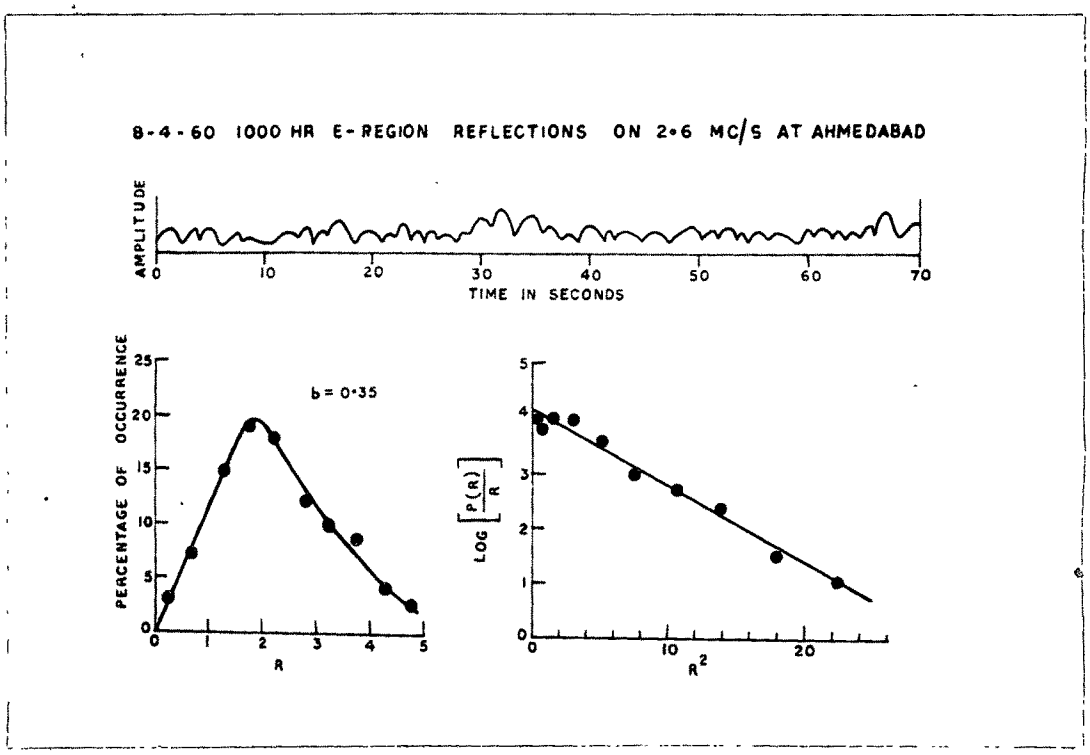

Figure 5.6 Fading record following Rayleigh law of amplitude distribution.

sum of the mean square values of the steady and random components. The general behaviour of P(Q) can be described by parameter b which is defined as

$$b = \frac{B}{\sqrt{\Psi}} = \frac{B}{R_m} \qquad (13)$$

Alpert (1963) has called this β , the turbidity factor. When $b < 1$, that is, when the steady signal is less than the random signal, equation (11) reduces approximately to Rayleigh type distribution.

If $b > 3$, McNicol (1949) has shown that equation (11) simplifies to

$$P(Q) \approx \frac{1}{\sqrt{2\pi\Psi}} \exp\left[-\frac{(Q - Q_m)^2}{2\Psi}\right] \qquad (14)$$

where Q_m is the most probable value of Q given by

$$Q_m = (b^2 + 1)^{\frac{1}{2}} \qquad (15)$$

A plot of $\ln\left[P(Q)\right]$ against $(Q-Q_m)^2$ will also be a straight line, if the assumptions are valid, and its slope gives the value of $\frac{1}{2\Psi}$. Thus knowing Ψ from the slope of the line and Q_m from experimental observations, b can be evaluated from equation (15). Two examples are shown in Figures 5.7(a) and 5.7(b).

(2) Time analysis

An approximate measure of the rate of fading can be

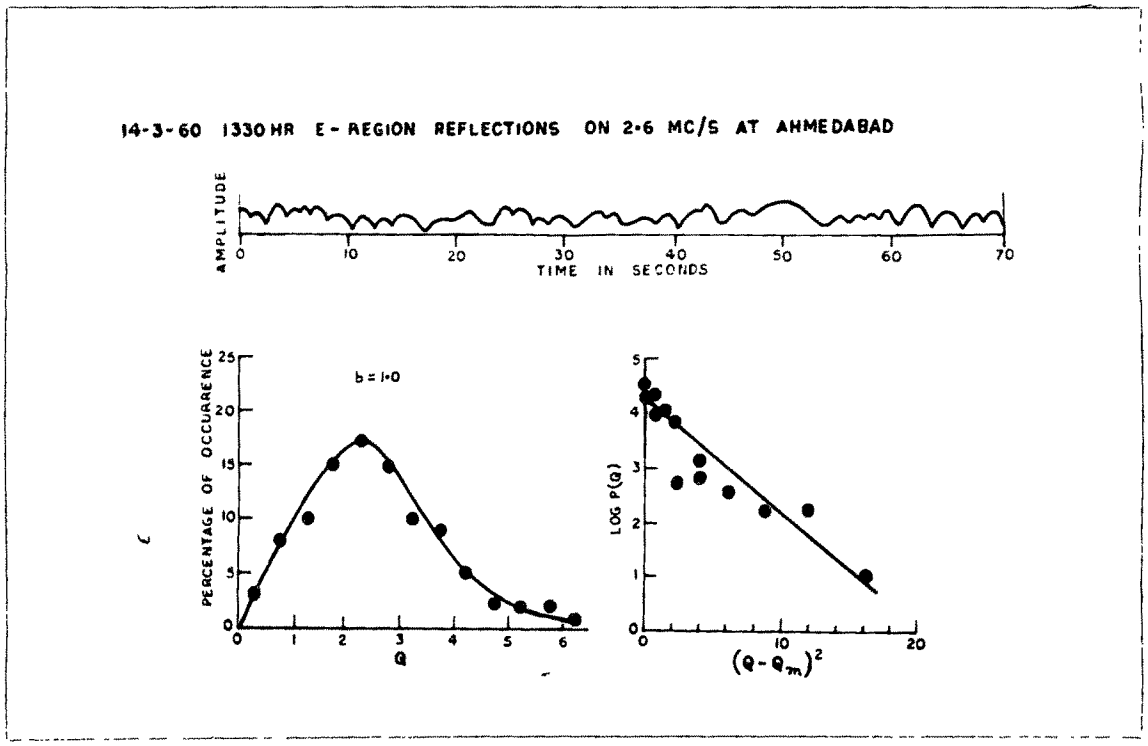

Figure 5.7(a) Fading curve and a plot of $\ln[P(Q)]$ against $(Q - Q_m)^2$.

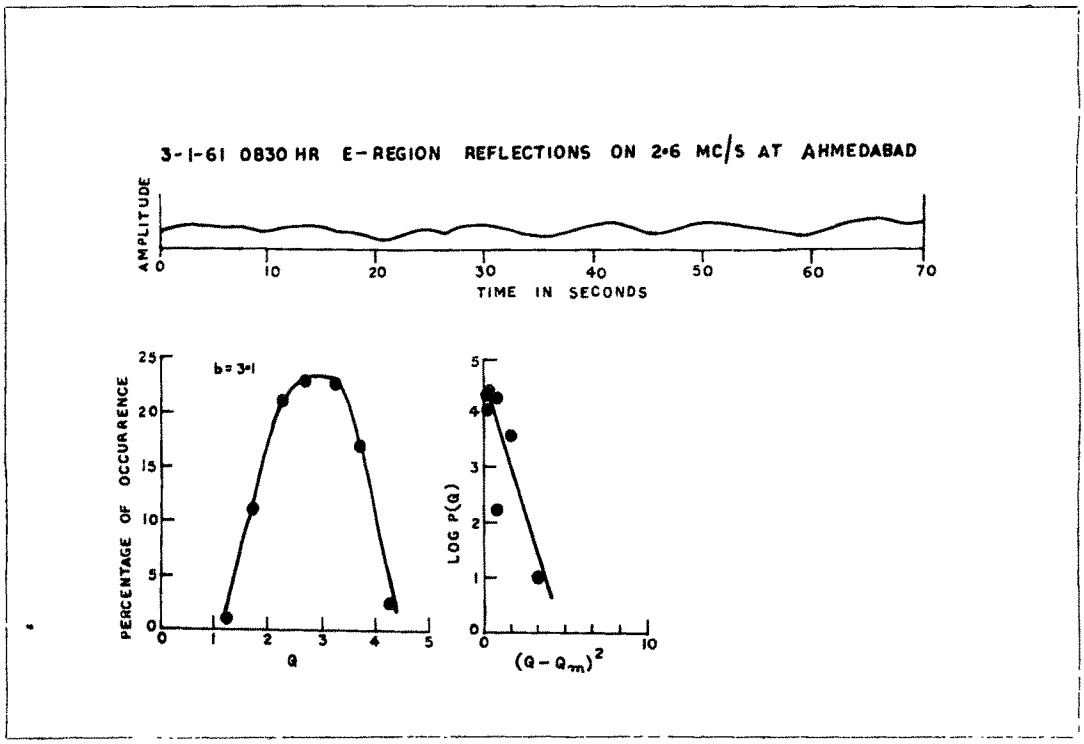

Figure 5.7(b) Fading curve and a plot of $\ln\left[P(Q)\right]$ against $(Q - Q_m)^2$.

made by counting the number of maxima N occuring in time t in a fading record. A more rigorous method has been suggested by Ratcliffe (1948) according to which the mean speed of fading S whose amplitudes follow the Rayleigh type distribution is given by

$$S = \frac{|\overline{\Delta R}|}{\overline{R}\tau} = \frac{8v_o}{\lambda} \qquad (16)$$

where $\overline{R}$ = mean amplitude of the fading curve

$|\overline{\Delta R}|$ = modulus of mean of the difference between successive amplitudes

τ = time interval between successive measured amplitudes using auto-correlation function

and v_o = r.m.s. value of random velocity in the line of sight.

Booker et al (1950) have derived a relation between power spectrum of the returned wave to the auto-correlation function $\rho(0,0,\tau)$ of the fading record. It is shown that in the presence of only random motions of the scattering center, the amplitude correlation coefficient is

$$\rho(0,0,\tau) = c \exp\left[-\frac{16\pi^2 v_o^2 \tau^2}{\lambda^2}\right] \qquad (17)$$

It can be seen from equation (17) that $\rho(0,0,\tau)$ reduces to $\frac{1}{e}$ at

$$\tau = \frac{\lambda}{4\pi v_o} \qquad (18)$$

Knowing the time τ at which the auto-correlation $\rho(0,0,\tau)$ falls to a value $\frac{1}{e}$ and the wavelength λ of the incident wave, v_o can be readily calculated from equation (18).

4. Results of amplitude and time analysis

Some fading records on 2.6 Mc/s obtained during March 1960 - February 1961 were selected for analysis. The total number of records selected was 310, out of which 249 were for the daytime (07-18 hrs) and 61 for the nighttime (19-05 hrs).

Table 5.1 shows the frequency of occurrence of different ranges of b for daytime and nighttime. The most frequently occuring value lies between 1.0-2.0 for day and 1.6-2.6 for night which means that specular reflection and scattered reflections are equally important during most of the time.

There is a small frequency of occurrences for $b < 1$, namely those with dominant random component, and quite a significant number for $b > 3$ indicating the dominance of a steady component.

There were about 51 day time cases and 14 nighttime cases where neither a Rayleigh nor a normal distribution curve could be fitted. These showed some mixed type of amplitude distribution, a few examples of which are shown in Figure 5.8.

Table 5.1

Frequency table of distribution of b during day and night

b = Steady signal/Most probable random signal

Range of b	Frequency of occurrence	
	Daytime (07-18 hr)	Nighttime (19-05 hr)
0.00-0.59	10	5
0.60-1.09	24	5
1.10-1.59	53	6
1.60-2.09	47	15
2.10-2.59	35	12
2.60-3.09	10	1
3.10-3.59	5	1
3.60-4.09	4	1
4.10-4.59	2	1
>4.6	8	-

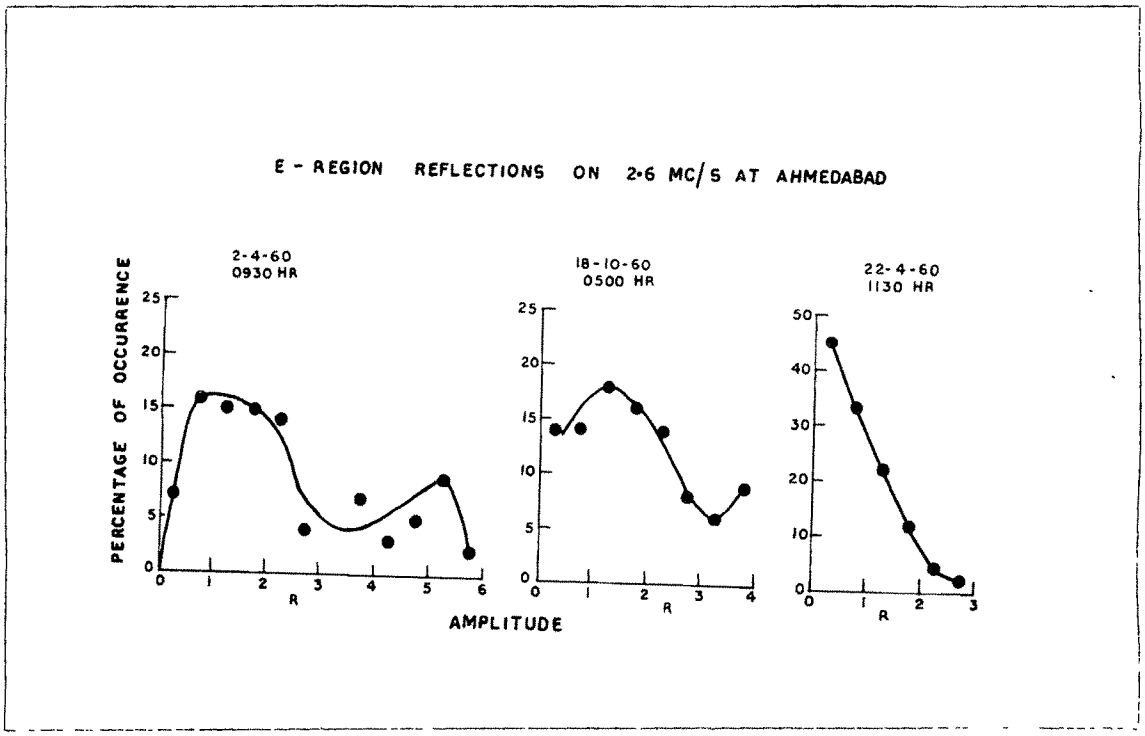

Figure 5.8 Examples of mixed type of amplitude distributions.

Table 5.2 gives the mean values of v_o for different ranges of $b \leq 2.09$ obtained by Ratcliffe's method and by the auto-correlation method. It can be seen that there is fair agreement between the two methods. It is interesting to note that v_o at night is less than that during day for $b \leqslant 1.09$ but is greater during night than during day when b is greater than 1.09.

5. Results obtained by other workers

Mitra and Srivastava (1957) reported that the amplitude distribution showed that the value of b ranged between 0.6 and 2.6. Dasgupta and Vij (1960) found that the distribution was of the Rayleigh type in the case of rapid fading and was of a double-hump type in the case of quasiperiodic fading.

The magnitude of v_o as reported by Mitra (1949) and Mitra and Srivastava (1957) ranges from 2 to 25 m/s, whereas Dasgupta and Vij (1960) and Khastgir and Singh (1960) obtained values of v_o to be less than 10 m/s. These may be compared to the values of v_o in Table 5.2 which is 7 to 8 m/s.

Table 5.2

Distribution of average value of v_o obtained by Ratcliffe's method and by the method of auto-correlation function against different values of b.

Range of b	DAYTIME (07-18 hr)			NIGHTTIME (19-05 hr)		
	Mean v_o by Ratcliffe's method m/s	Mean v_o by the method of auto-correlation function m/s	Number of observation	Mean v_o by Ratcliffe's method m/s	Mean v_o by the method of auto-correlation function m/s	Number of observations
0.00-0.59	7.9	7.9	10	7.4	6.0	5
0.60-1.09	7.2	6.1	24	5.7	4.7	5
1.10-1.59	7.0	6.2	53	10.4	10.2	6
1.60-2.09	6.5	6.6	47	8.3	8.9	15
2.10-2.59	-	7.3	35	-	11.1	12
2.60-3.09	-	6.8	10	-	-	-
3.10-3.59	-	4.5	5	-	-	-
3.60-4.09	-	3.9	4	-	-	-
4.10-4.59	-	3.0	2	-	-	-
>4.6	-	0.4	8	-	-	-

CHAPTER VI

Steady and random movement of ionospheric irregularities
Size of irregularity and angular spread of scattered waves

1. Drift velocity V, Fading velocity V_c' and characteristic velocity V_c

Let τ' and τ be the time lags observed on the auto - and cross-correlation for the same correlation level (Figure 6.1), then it can be shown by simple geometry (Briggs et al, 1950),

$$\tau'^2 - \tau^2 = \frac{a^2 - 2Va\tau}{V_c'^2} \qquad (1)$$

or
$$\frac{\tau'^2 - \tau^2}{\left(\frac{a^2}{V_c'^2}\right)} = 1 - \frac{2Va\tau}{\left(\frac{V_c'^2 a^2}{V_c'^2}\right)}$$

$$= 1 - \frac{\tau}{\left(\frac{a}{2V}\right)}$$

i.e.
$$\frac{\tau'^2 - \tau^2}{\left(\frac{a}{V_c'}\right)^2} + \frac{\tau}{\left(\frac{a}{2V}\right)} = 1 \qquad (2)$$

where V is the drift velocity and V_c' is the fading velocity of the pattern measured by a pair of aerials with separation distance 'a' along a particular direction.

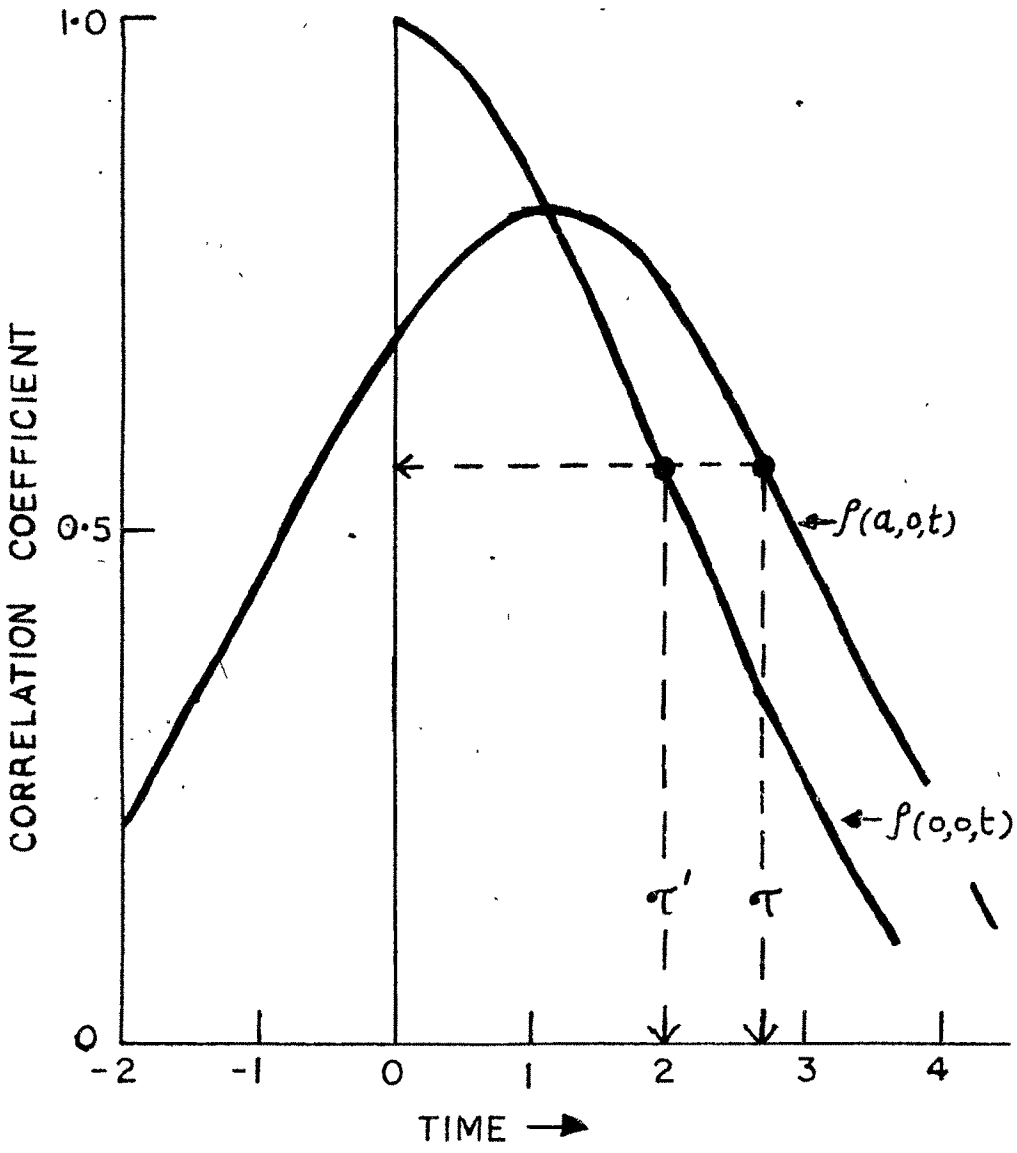

Figure 6.1 Correlograms defining τ' and τ

If we plot $(\tau'^2 - \tau^2)$ against τ , we should get a straight line according to equation (2). We shall call this line as BPS (Briggs, Phillips and Shinn) line. The intercepts of this line on the two axes can be easily shown to be equal to

$$\tau_x = \frac{a}{2V} \tag{3}$$

$$\tau_y^2 = \frac{a^2}{V_c'^2} \tag{4}$$

Thus, knowing τ_x, τ_y and 'a', V and V_c' can be calculated along a direction in which the aerials are fixed.

A typical set of BPS line for the pairs of aerials along E-W and N-S directions is shown in Figure 6.2. It can be seen that there is a good agreement between the theory and the experimental points. However the agreement is not so good in all the cases, so much so, 24 records were rejected out of 78 as it was not possible to draw a straight line through all the points. The quantities V, V_c' and V_c (which is the characteristic velocity found by the observer moving at drift velocity V) were calculated for the remaining 54 records using the BPS line technique for each pair of aerials along E-W, N-S and SW-NE directions.

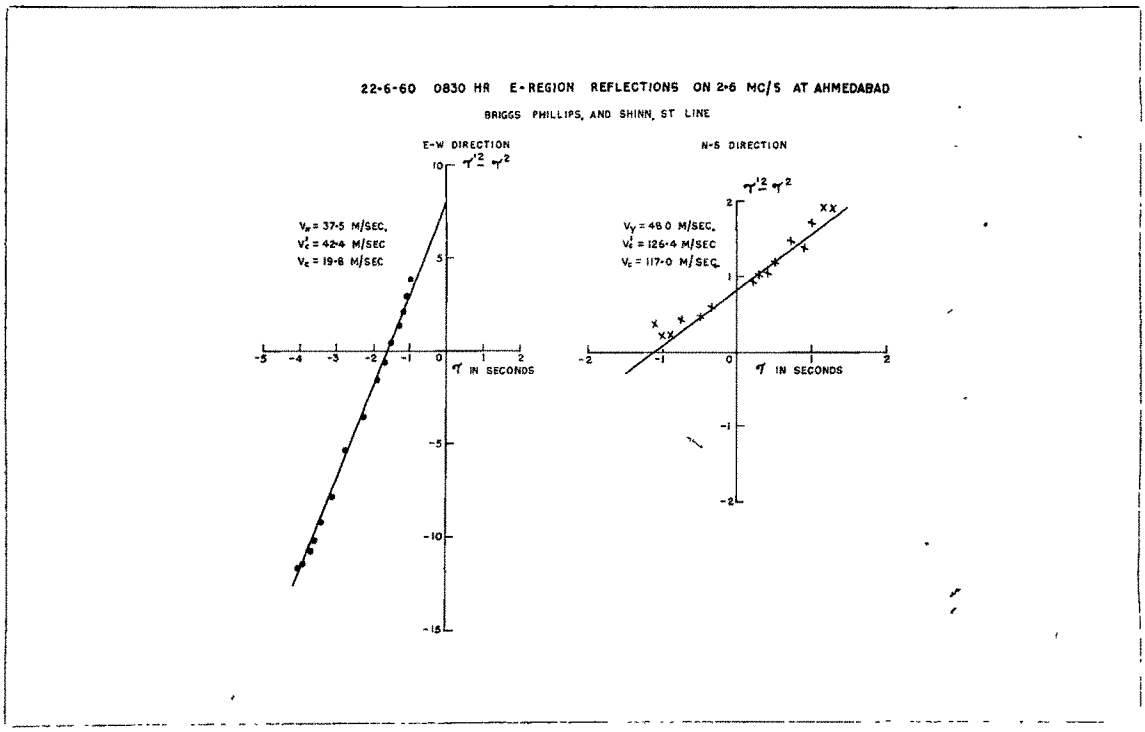

Figure 6.2 A typical set of BPS straight line for the pairs of aerials along E-W and N-S directions.

2. Results

Figure 6.3 shows the histograms of fading velocity V_c' along the E-W, N-S and SW-NE directions. The fading velocity varies in the range 20-140 m/s with a most probable range between 60-80 m/s along N-S and SW-NE direction and between 40-60 m/s along E-W direction. The mean values of V_c' are 65 m/s, 79 m/s and 68 m/s along ~~N-S~~ SW-NE, N-S and E-W direction respectively. The histograms show larger spread in V_c' along N-S than that along other directions.

Figure 6.4 shows a plot of V_c' along SW-NE and N-S direction versus that towards the E-W. It may be seen that V_c' shows similar features along E-W and SW-NE better than that along N-S direction.

3. Variation of the ratio $\frac{V_c}{V}$

The magnitude of the ratio of the characteristic velocity V_c to the true drift velocity V gives an idea of the effectiveness of V_c or V in producing random fading. This ratio is shown in the form of histograms in Figure 6.5 along the three principal directions. It can be seen that the most probable value of the ratio lies between 0.25 and 0.5 for the SW-NE direction and between 0.5 and 0.75 for N-S and E-W. The mean value of $\frac{V_c}{V}$ is about 1.0 which means that both V_c and V are equally effective in producing fading.

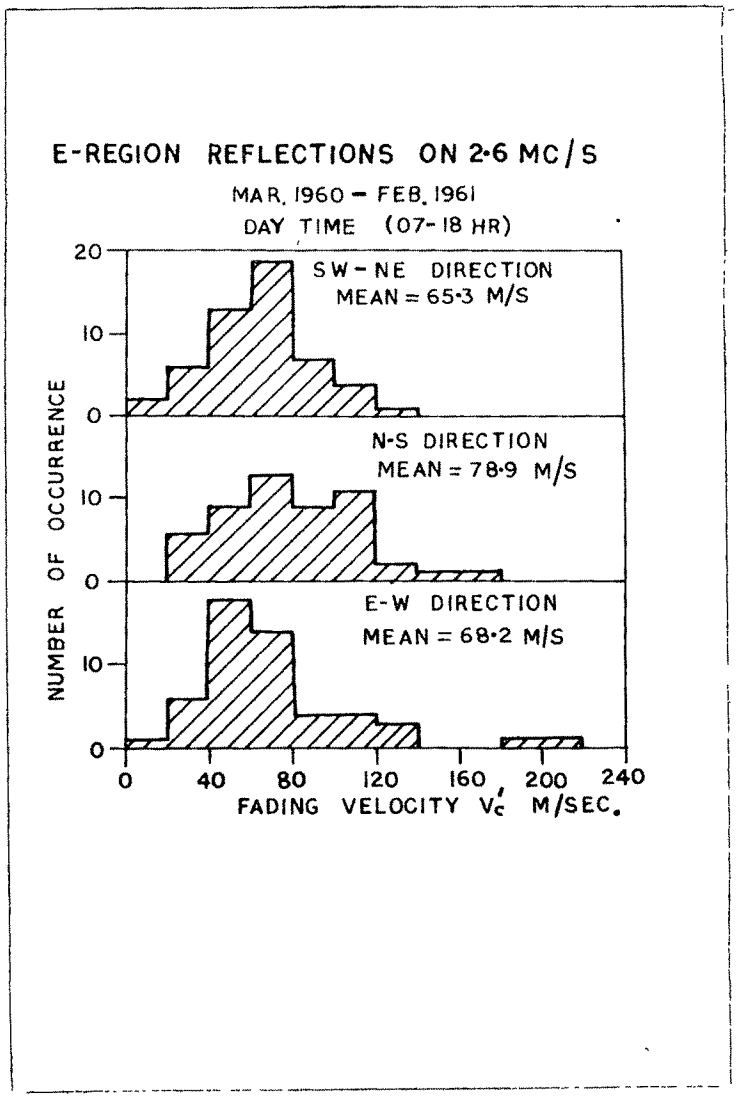

Figure 6.3 Histograms of fading velocity V_c' along the E-W, N-S and SW-NE directions.

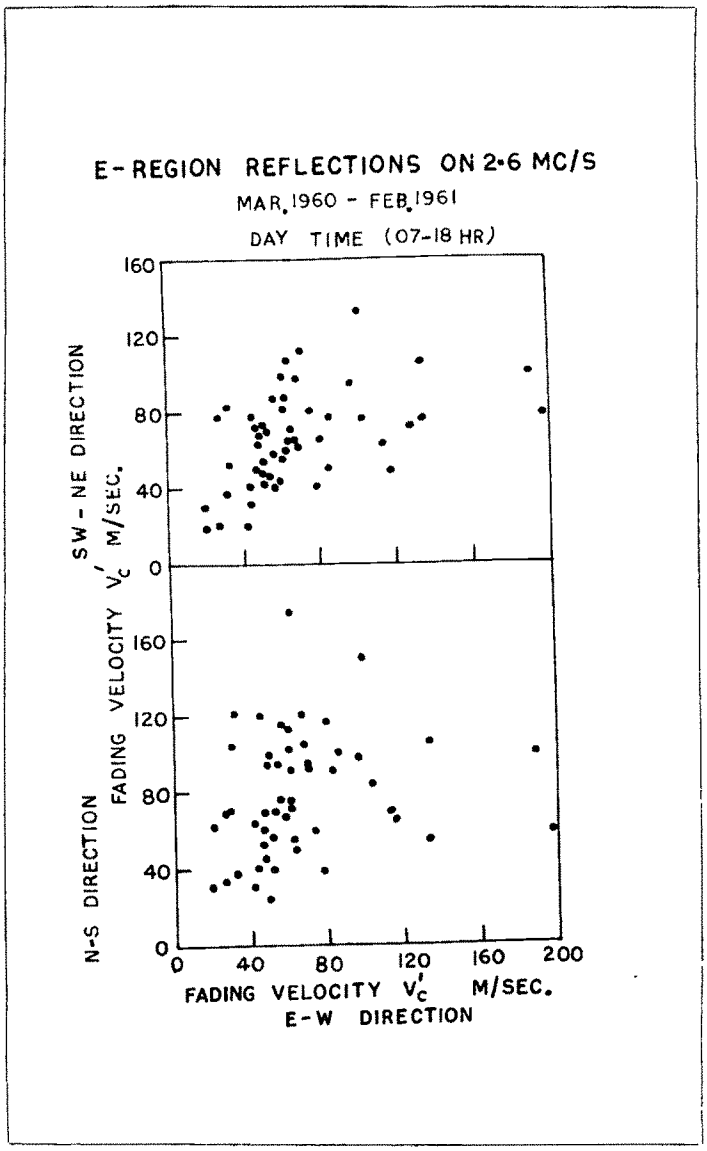

Figure 6.4 A plot of V_c' along SW-NE and N-S direction versus that towards the E-W.

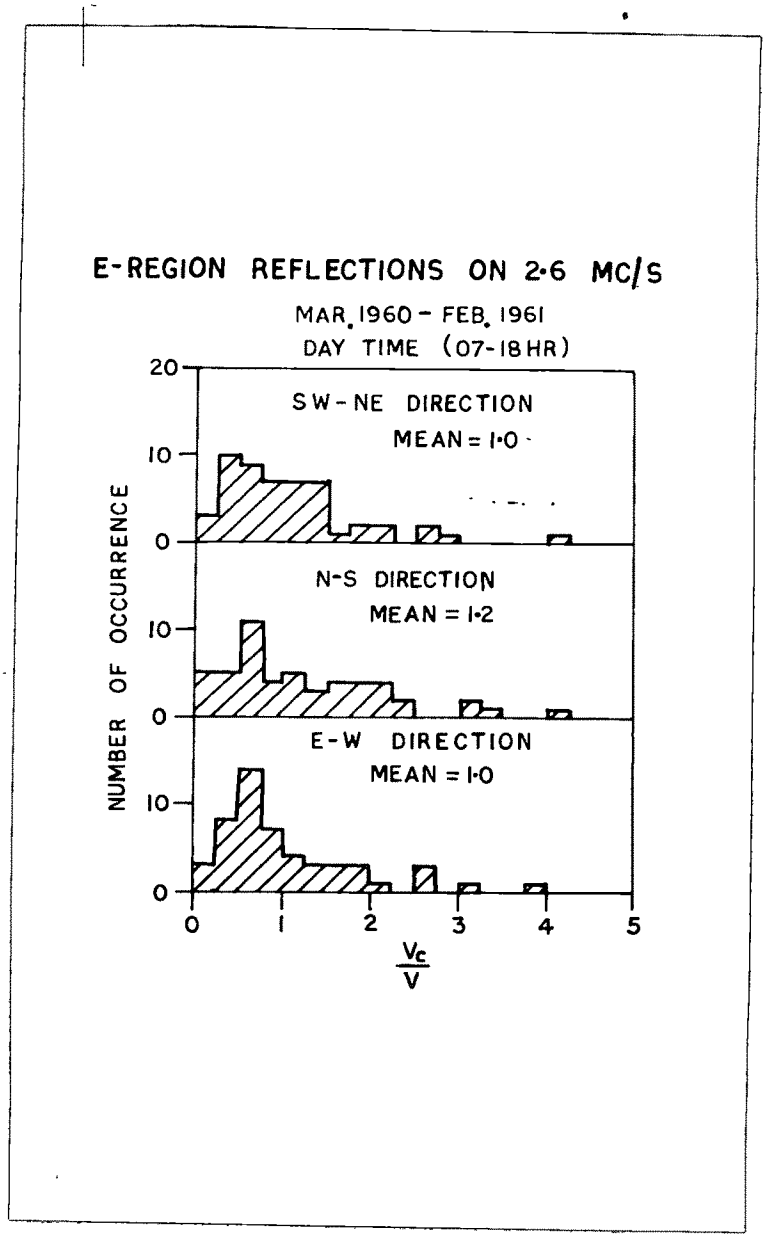

Figure 6.5 Histograms of $\frac{V_c}{V}$ along SW-NE, N-S and the E-W directions.

A mass plot of the ratio $\frac{V_c}{V}$ along SW-NE and along N-S direction against that along E-W shown in Figure 6.6 reveals a tendency for the SW-NE and E-W ratios to go together.

4. Variation of true drift speed V and its direction by the BPS method

Knowing the values of drift speed V_x and V_y along E-W and N-S directions respectively with the help of BPS line, the resultant speed and direction were calculated as follows

$$V = \sqrt{V_x^2 + V_y^2} \qquad (5)$$

and

$$\theta = \tan^{-1} \frac{V_y}{V_x} \qquad (6)$$

Figure 6.7 shows the histograms for V and ϕ which is equal to $(90^\circ - \theta)$ in degrees east of north for the E region during the period March 1960 - February 1961. It may be seen that the drift speed has a wide range from 20 to 160 m/s with a maximum occurrence between 60 and 80 m/s and the average about 76 m/s.

There is however no significant preferred direction of the drift though the N-E direction appears to be the least favoured.

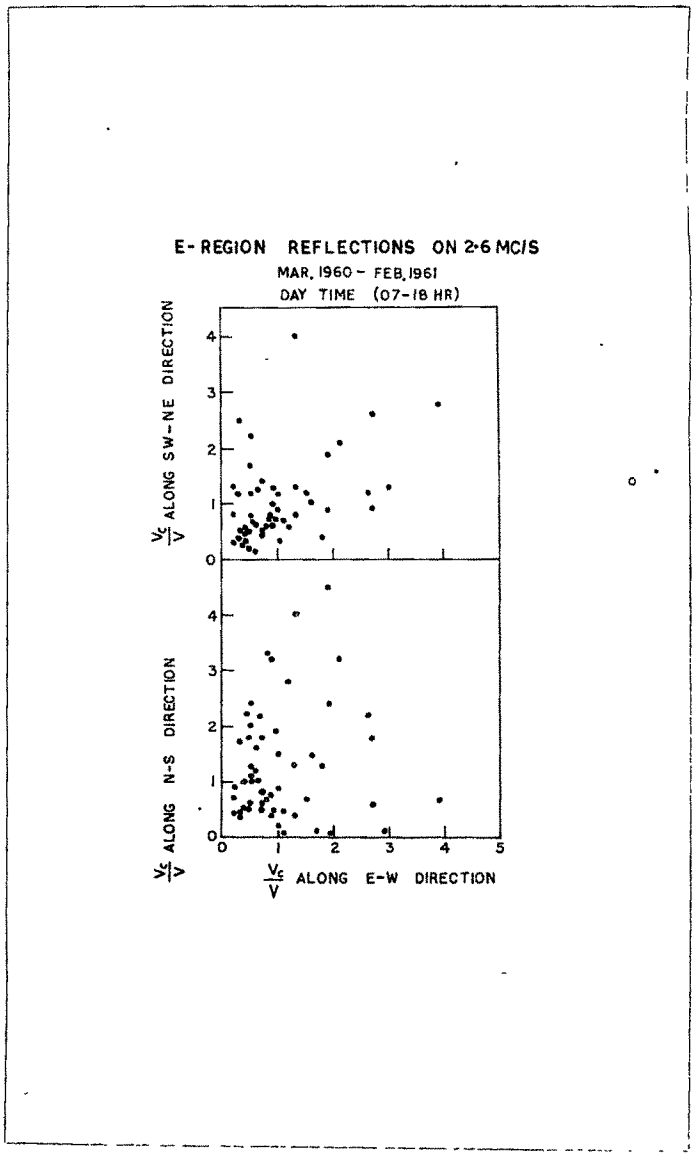

Figure 6.6 A mass plot of the ratio $\frac{V_c}{V}$ along SW-NE and along N-S direction against that along the E-W direction.

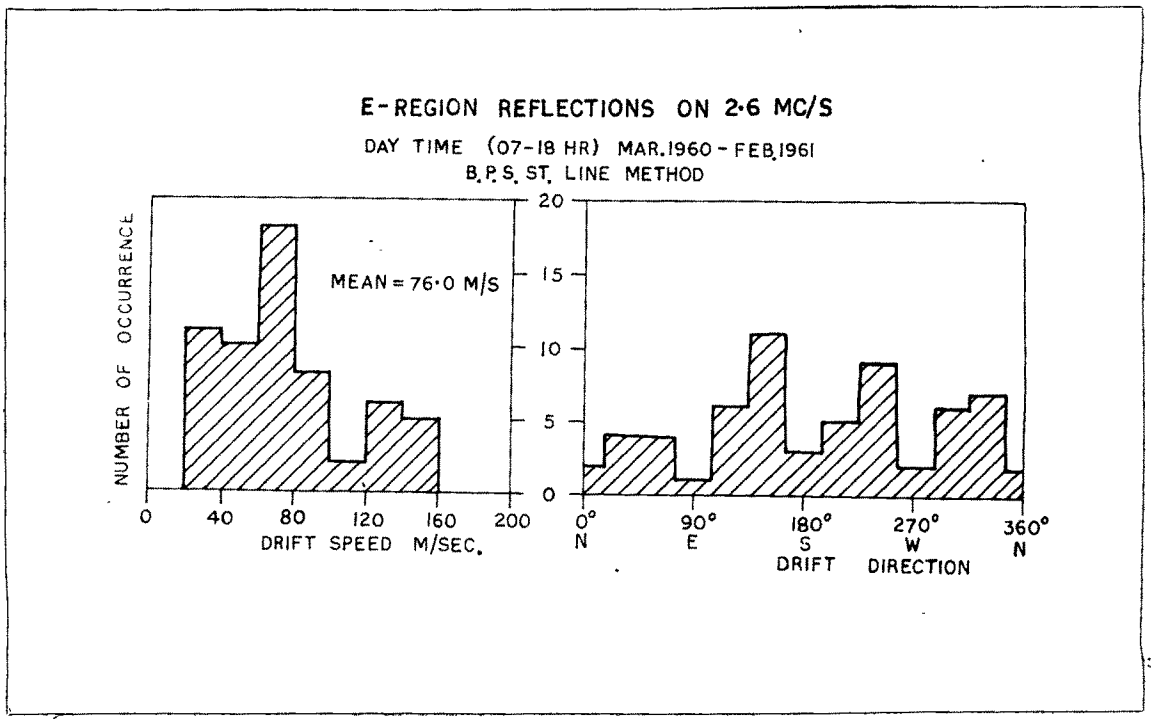

Figure 6.7 Histograms of drift speed and direction obtained by BPS method.

5. Comparison with other results

Fooks and Jones (1961) have reported the median value of $\frac{V_c}{V}$ to be 0.8 at Cambridge. Yerg (1956) found the ratio of the order of 2.5 at Puerto Rico and Rao and Rao (1964) obtained $\frac{V_c}{V}$ as 0.6 at Waltair which may be compared with 1.0 obtained at Ahmedabad.

6. Size of the irregularity Characteristic ellipse

We mentioned earlier that Briggs et al (1950) assumed the contours of constant correlation ρ in the $\rho(a,0,\tau)$ diagram to be ellipses concentric about the origin. Similarly when a two-dimentional ground is considered the contours of surfaces in the $\rho(x,y,\tau)$ diagram would represent similar concentric ellipsoids which intersect the x-y plane in circles.

The argument may be lent a physical meaning since the irregularities responsible for the scattering of the radio waves may be aligned along the magnetic field of the earth, and in such a situation the contours of constant correlation may take an elliptical shape. The diffraction pattern formed by contours of constant ρ may be taken as stretched circular pattern which can be defined by a "characteristic ellipse".

Let τ_1, τ_2 and τ_3 be the times at which the magnitude of the auto-correlation function $\rho(0,0,\tau)$ obtained from a single fading curve be equal to the cross-correlation function $\rho(a,0,0)$, $\rho(0,a,0)$ and $\rho(a,-a,0)$

between the three pairs of fading curves (see Figure 6.8), then the axial ratio γ of the semi-major to semi-minor axis of the equivalent ellipse (see Figure 6.9) and the tilt angle ψ of the semi-major axis 'ℓ' in degrees east of north can be calculated from the following relations :

$$\gamma^2 = \frac{A + (P^2 + Q^2)^{\frac{1}{2}}}{A - (P^2 + Q^2)^{\frac{1}{2}}} \qquad (7)$$

$$\tan 2\psi = \frac{P}{Q} \qquad (8)$$

Where $$P = \tau_1^2 + \tau_2^2 - \tau_3^2 \qquad (9)$$

$$Q = \tau_1^2 - \tau_2^2 \qquad (10)$$

and $$A = \tau_1^2 + \tau_2^2 \qquad (11)$$

7. Size of the characteristic ellipse

Let 'D' denote the size of the characteristic ellipse about x axis taken along pair of aerials in the E-W direction. D may be defined as (see Figure 6.9)

$$D = \left(\frac{a}{\tau_x}\right) \cdot \tau_s \qquad (12)$$

where 'a', as usual, is the separation between the aerials along x-axis. τ_x and τ_s were derived from the correlograms as illustrated in Figure 6.10 such that

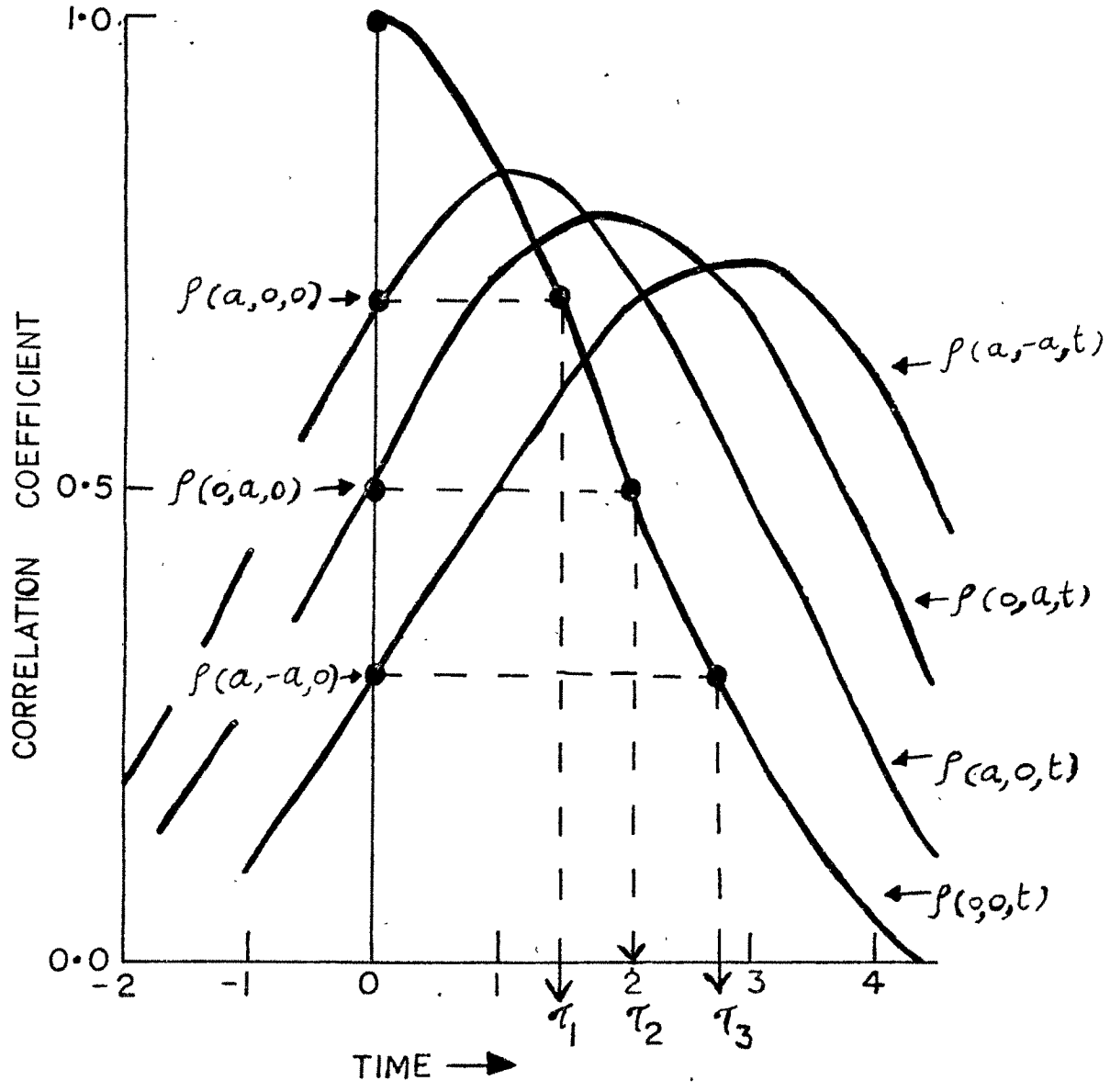

Figure 6.8 Illustration of auto- and -cross correlation curves and the definition of τ_1, τ_2 and τ_3

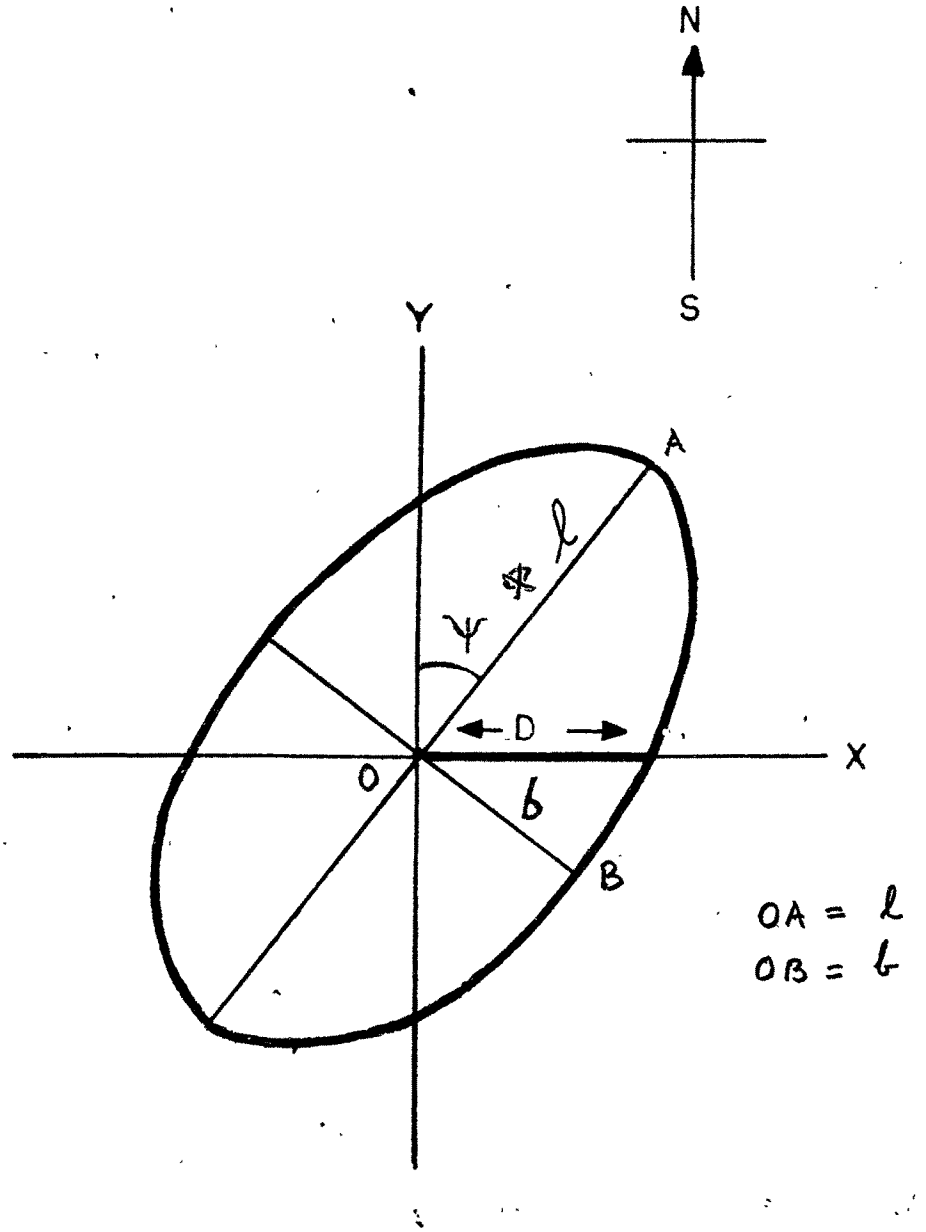

Figure 6.0 Characteristic ellipse due to irregularities

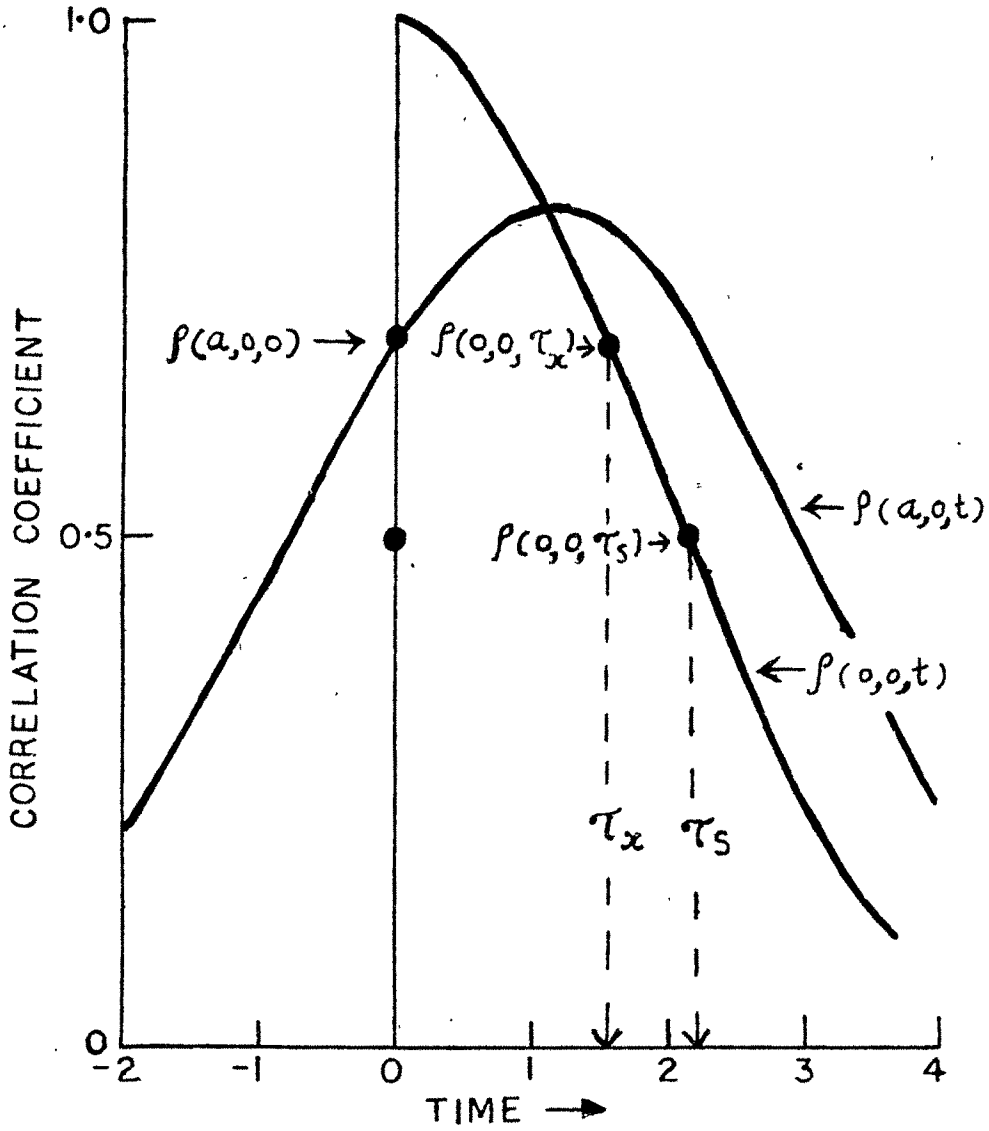

Figure 6.10 Correlograms defining τ_x and τ_s

$$\rho(\tau_s) = \rho(0,0,\tau) = 0.5 \qquad (13)$$

and $$\rho(a,0,0) = \rho(\tau_x) \qquad (14)$$

τ_s is the time at which the auto-correlation function $\rho(0,0,\tau)$ falls to a value 0.5 and τ_x is the time on the auto-correlogram when the cross-correlation level meets the zero time axis of the former.

Now the equation of an ellipse having ℓ and b as semi-major and semi-minor axis and inclined at an angle with the y-axis (north) can be written as

$$\frac{D^2 \sin^2}{b^2} + \frac{D^2 \cos^2\psi}{\ell^2} = 1 \qquad (15)$$

or $$\ell^2 = D^2 \cos^2\psi + \frac{\ell^2 D^2}{b^2} \sin^2\psi \qquad (16)$$

$$= D^2 \left[1 + \left(\frac{\ell^2}{b2} - 1\right) \sin^2\psi\right] \qquad (17)$$

Putting $\frac{\ell}{b} = r$, the axial ratio as defined in equation (7), we get from equation (17) the relation for the semi-major axis

$$\ell = D \left[1 + (r^2 - 1) \sin^2\psi\right]^{\frac{1}{2}} \qquad (18)$$

Knowing ℓ from equation (18), b can be calculated from (7) and thus all the parameters of an ellipse could be obtained.

Ambiguity in the tilt angle γ in the range $0^{\circ} \leq \gamma \leq 180^{\circ}$ is resolved by taking cos 2γ of the same sign as Q in equation (8). We shall present the results in the next section.

8. Results

Figure 6.11 shows the values of 'L' calculated from equation (18). Its length has a most frequent value between 100-150 meters and mean length 212 meters. The same may be compared with 240 meters at Waltair, 182 meters at Yamagawa, 173 meters at De Bilt and 293 meters at Halley Bay (Rao and Rao, 1963).

Figure 6.12 shows the histograms of γ and γ. We find that the most probable value of γ lies between 1.0 and 1.5 but the mean of all its values is 2.6. Similarly the tilt angle γ is most frequently observed along NE-SW or along SE-NW quadrant but not along N-S direction as may be expected. The following table 6.1 summarises the results obtained at Ahmedabad and elsewhere.

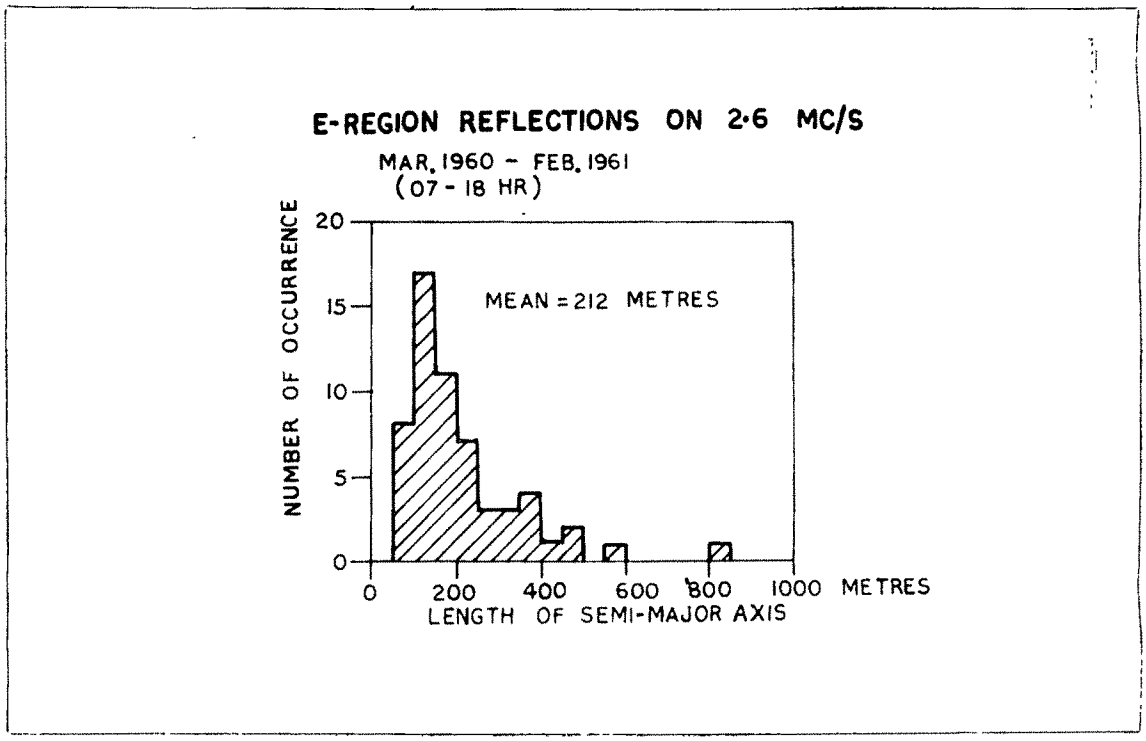

Figure 6.11 Length of semi-major axis 'ℓ' of characteristic ellipse.

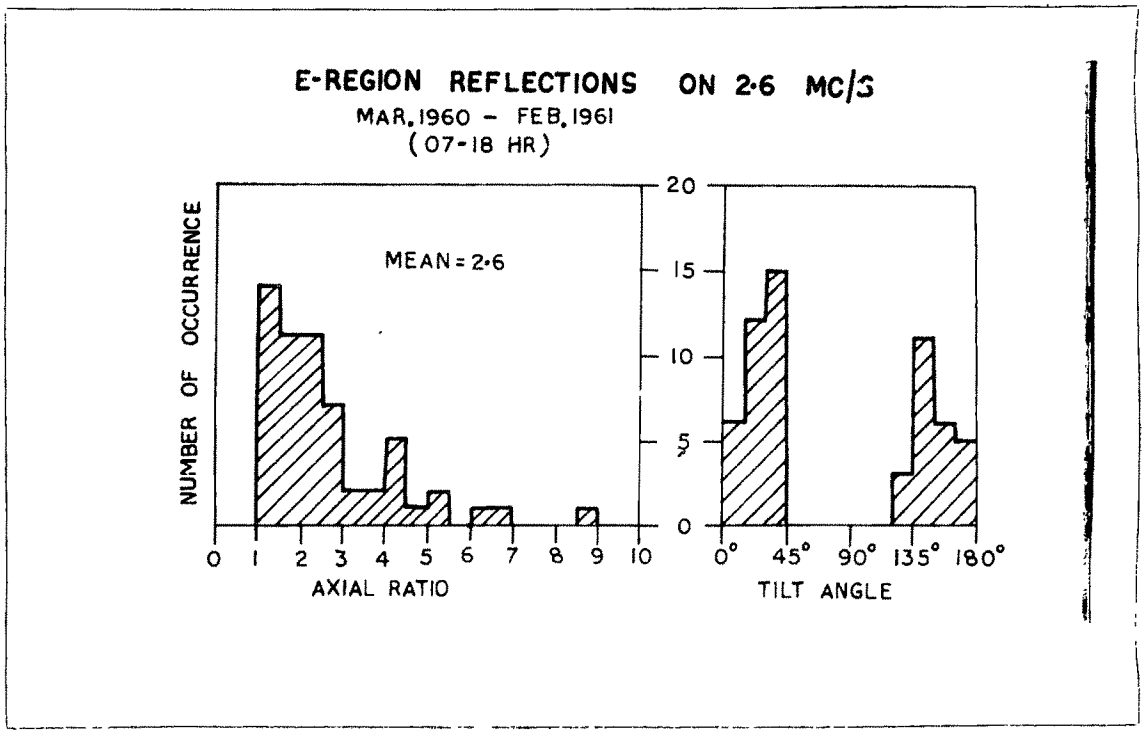

Figure 6.12 Axial ratio γ and tilt angle γ of the semi-major axis of characteristic ellipse.

Table 6.1

Properties of characteristic ellipse

Station	ℓ meters	$r = \frac{\ell}{b}$		$\frac{V_c}{V}$	Source
Ahmedabad	212	2.6	NE-SW or SE-NW	1.0	Patel (present thesis)
Waltair	240	2.1	N-S	0.7	Rao and Rao (1963)
Yamagawa	182	2.1	NW-SE	0.8	Rao and Rao (1963)
De Bilt	177	1.6	NW-SE	1.1	Rao and Rao (1963)
Halley Bay	293	2.4	NW-SE	1.4	Rao and Rao (1963)
Peurto Rico	-	1.8	-	2.5	Yerg (1956)
Cambridge	352	1.5	-	0.8	Fooks and Jones (1961)

It is gratifying that the results at Ahmedabad are in good agreement with those reported elsewhere.

9. Width of the angular spectrum of scattered waves

It was pointed out by Booker et al (1950) that the diffraction of radio waves by irregularities in the ionosphere will lead to an angular spread of the downcoming waves. Briggs (1950) considers the effect of the irregularities to spread out the reflection to a cone of rays over a range of angles $\pm \theta_0$ with respect to the vertical as shown in Figure 6.13 (see Al'pert, 1963, p.32).

If the irregularities move with a steady horizontal velocity V, the rays in the cone which travel at an angle θ_0 to the vertical will suffer on reflection a Doppler frequency shift $\pm \frac{2V}{\lambda} \sin \theta_0$. The frequency difference between the extreme rays in the cone would be $\frac{4V}{\lambda} \sin \theta_0$. Thus if Δn maxima occur in time Δt, the following result will be approximately true,

$$\frac{\Delta n}{\Delta t} = \frac{4V}{\lambda} \sin \theta_0 \qquad (19)$$

Putting $N = \frac{\Delta n}{\Delta t}$ we can write equation (19) as

$$N\lambda = 4V \sin \theta_0 \qquad (20)$$

Knowing N, the number of maxima or minima occurring per unit

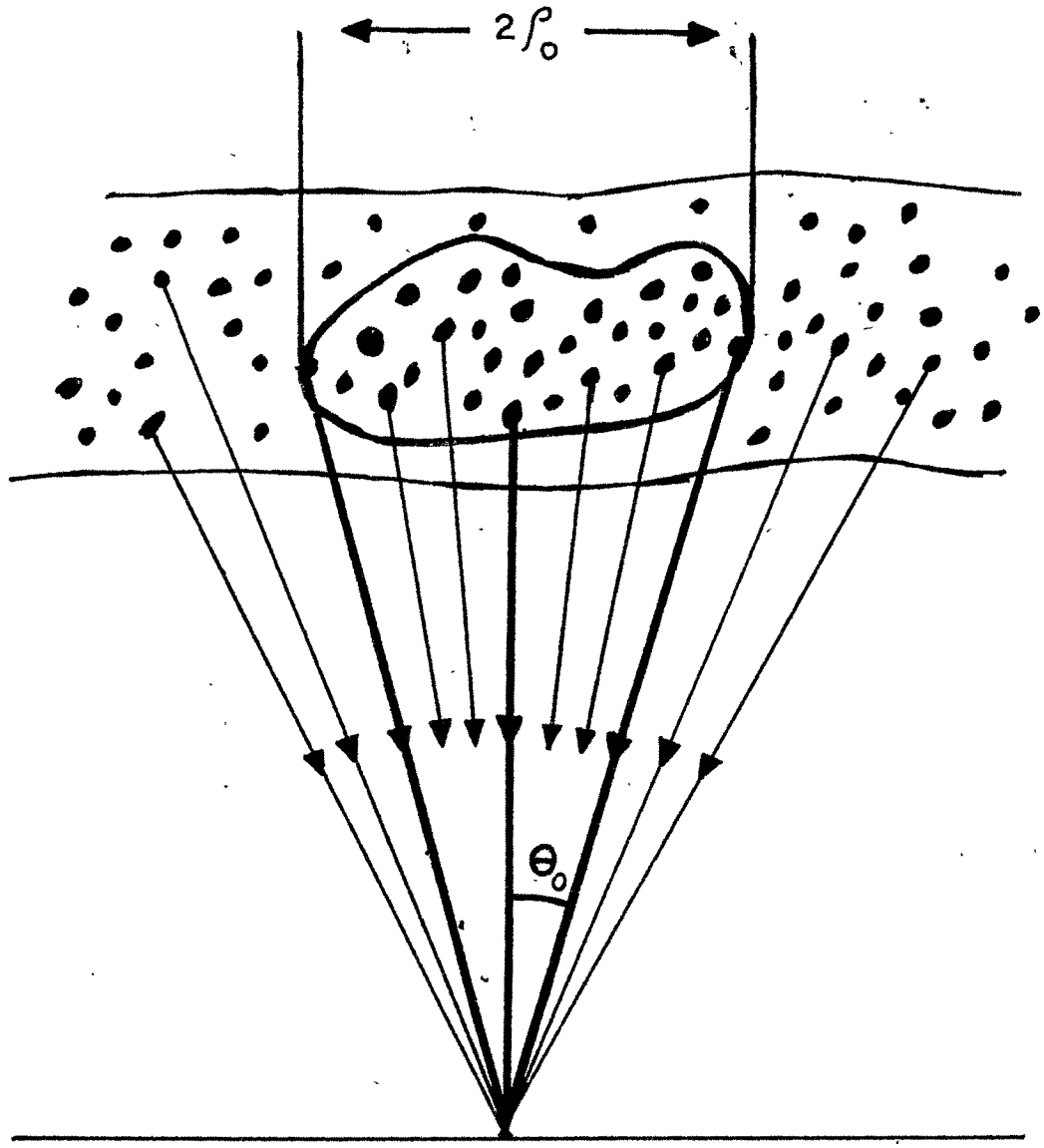

Figure 6.13 Schematic diagram of the structure of ionosphere showing single reflecting region giving rise to a single reflected signal at the point of observation

time in a fading record, the horizontal velocity V of the irregularities and the wavelength of the radio wave, we can calculate the semi-angle θ_0 of the cone of downcoming wave using equation (20). It can be easily seen that the graph of $N\lambda$ against V will follow a straight line passing through origin, the slope of which is given by 4 sin θ_0. θ_0 can thus be calculated.

The angular spread of the downcoming wave can be related to the radius ρ_0 of the irregularities according to the expression

$$\tan \theta_0 = \frac{\rho_0}{z} \qquad (21)$$

where z is the height of the irregularities above the ground.

For small values of angle θ_0 equation (21) can be expressed as

$$\rho_0 = z\theta_0 \qquad (22)$$

Further assuming that the linear dimensions of the irregularities are equal to the distance L at which the spatial correlation coefficient falls to e^{-1}, Al'pert (1963) has shown that,

$$L = \frac{\lambda}{2\pi\theta_0} \qquad (23)$$

Knowing λ and θ, L can be calculated from equation (23).

10. Analysis and results

Some of the records taken at Ahmedabad during the period March 1960 to February 1961 on 2.6 Mc/s were utilised for calculating the semi-angle θ_o, radius ρ_o and the dimension of the irregularities L in the E and F regions.

Reflections during daytime refer to the regular E region or the sporadic E and the reflections during the nighttime refer to the F region or the sporadic E. The horizontal velocity V of the irregularities was calculated by the method of similar fades as described in Chapter I, and the fading rate $N = \frac{\Delta n}{\Delta t}$ was obtained by counting the number Δn of clear maxima in the fading record in a certain time Δt. To varify the relation between $N\lambda$ and V the observations were divided into different groups according to the values of V lying between the limits 0-19, 20-39, 40-59 m/s ..... etc. The average values of N and V for each group were computed and graphs of $N\lambda$ against V are shown in Figure 6.14 for reflections from (a) E region during daytime, (b) E_s region during nighttime, (c) F region in the presence of E_s and (d) F region in the absence of E_s.

11. Relation between the fading rate and the drift speed

We see from Figure 6.14 that the points lie fairly well on a straight line passing through the origin thus confirming that $V \propto N\lambda$. The constant of proportionality

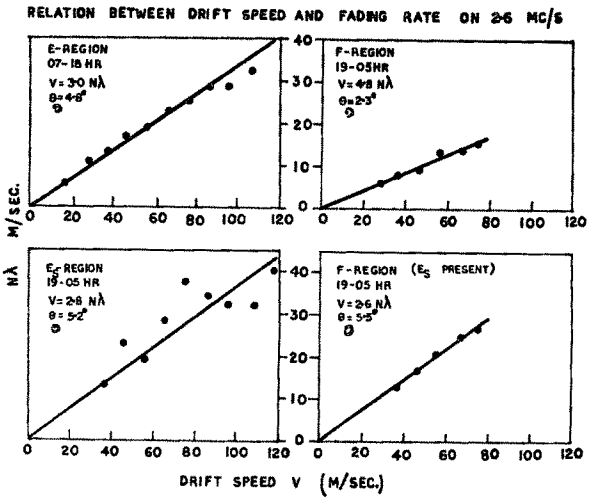

Figure 6.14 Graph of $N\lambda$ versus the steady drift velocity V of reflections on 2.6 Mc/s from E, E_s and F over Ahmedabad. E refers to day hours and E_s and F to night hours.

which is the inverse slope of the straight line is 3.0 for daytime E, 2.8 for nighttime E_s, 2.6 for nighttime F in presence of E_s and 4.8 for nighttime F without E_s. The values are of the same order as those derived by McNicol (1949) except for the F region reflections in the absence of E_s.

The semi-angle θ_o of the cone of downcoming wave is 4.8^o for daytime E, 5.2^o for nighttime E_s, 5.5^o for nighttime F with E_s present and, 2.3^o for the nighttime F without E_s. It is noteworthy that for the reflections from F region, the spread is smaller when there is no sporadic E than when the reflections pass through E_s.

12. Seasonal variation of the semi-angle θ_o of the cone of the downcoming wave

To find the seasonal variations in the magnitude of the semi-angle θ_o of the cone of the downcoming wave, θ_o was calculated for each observation using the relation $N\lambda = 4V \sin\theta_o$. Histograms showing the percentage occurrence of θ_o against the corresponding range of θ_o are plotted in Figure 6.15 for three seasons, equinoxes, winter and summer. The number of observations and the average value of θ_o are indicated in each diagram.

It can be seen from Figure 6.15 that the histograms for the daytime E observations show rapid rise and rapid fall whereas the histograms for the nighttime sporadic E observations

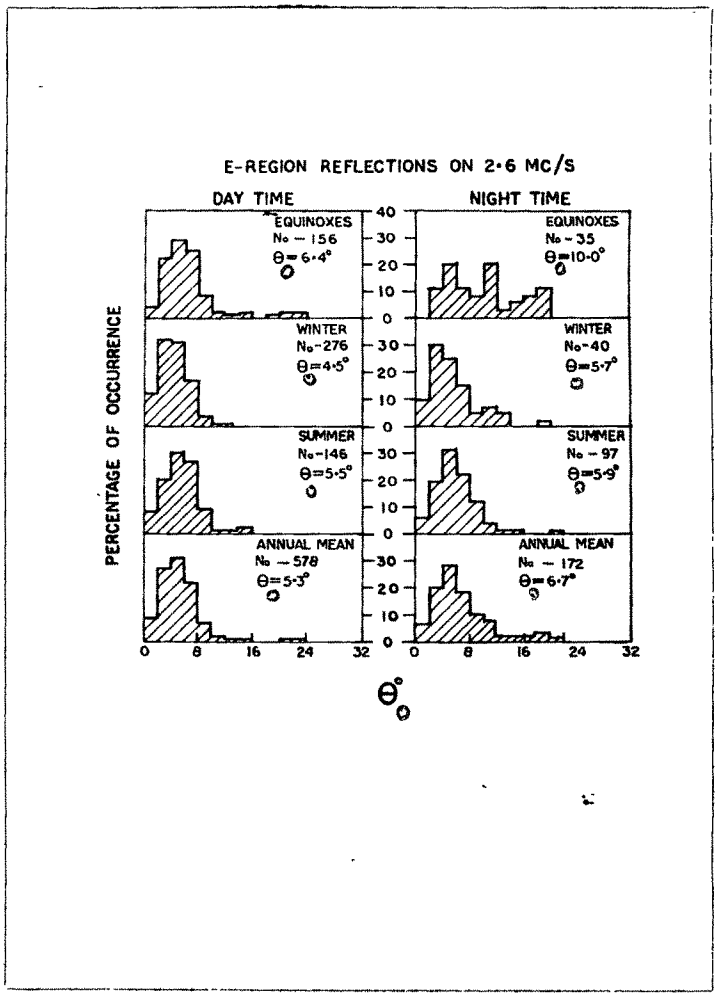

Figure 6.15 Histograms giving the percentage occurrence of the semi-angle of the cone of spread of radio waves of 2.6 Mc/s reflections from E.

show rapid rise and slower fall. The variation of θ_0 during night in the equinoctical months is large and ranges upto 20°. High values of θ_0 for E region reflections during daytime are also occasionally observed in equinoxes, the mean values being 6.4° for the daytime and 10.0° for the nighttime. The average values of θ_0 are smallest for the E region reflections in winter, being 4.5° during daytime and 5.7° during nighttime.

Figure 6.16(a) shows the histograms for the nighttime F region observations in the absence of sporadic E. Here θ_0 varies between 0° to 6°. The average value of θ_0 is found to be maximum in equinoxes being 3.9°, and is minimum in winter being 2.5°. The annual average value is 3.1°.

Figure 6.16(b) shows the annual average histogram for the F region observations taken in the presence of sporadic E. Seasonal variations of θ_0 for these observations were not calculated due to the smaller number of observations in each season. It can be seen that θ_0 for the F region observations taken in the presence of sporadic E varies between 2° to 8°. The average value of θ_0 is 4.7° which is higher than that for F region reflections in the absence of E_s.

The angle θ_0 for reflections from the E_s region itself during nighttime is 6.7°. Thus it is clear that the presence of sporadic E in the part of a ray reflected from the F region increases the semi-angle of the cone.

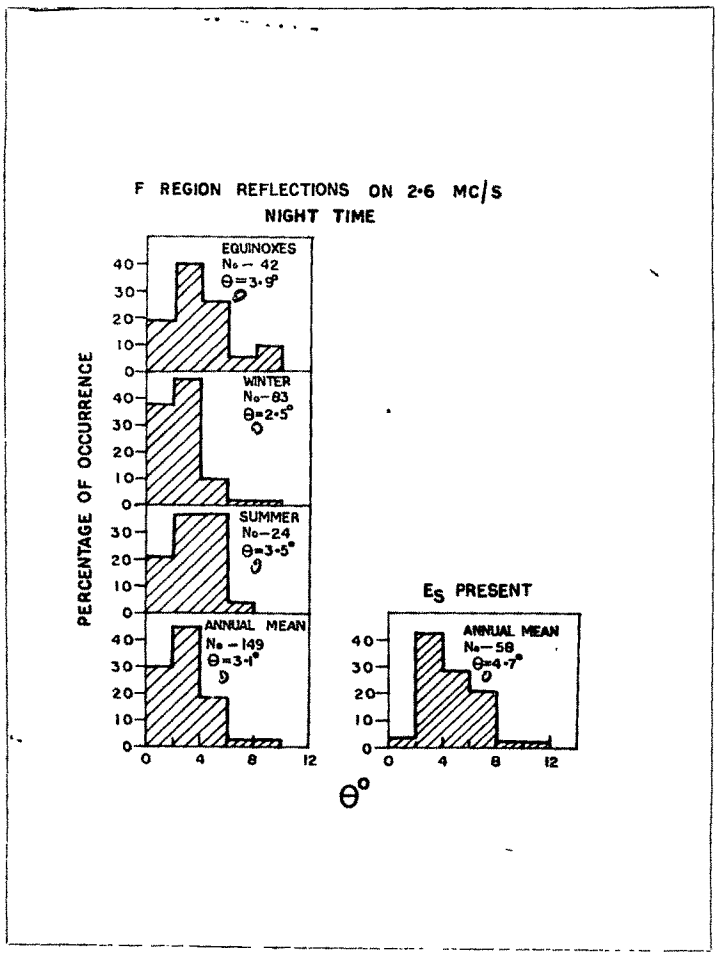

Figure 6.16 Histograms of the semi-angle θ_0 of the cone of downcoming waves of nighttime reflections from F region on 2.6 Mc/s.

13. Linear dimension of irregularities

The values of ρ_o and L calculated from equations (21) and (22) are shown in Table 6.2. The values of θ_o used to calculate ρ_o and L are taken from Figure 6.14. It can be seen from the table that the radius ρ_o is minimum for regular E layer and is maximum in the case of F region when E_s is present. The linear dimension of irregularities is about 200 metres in the E region and more than twice in the F region. The last point is doubtful since we do not know whether the result got vitiated in the presence of E_s.

14. Discussion

Briggs and Phillips (1950) estimated that the semi-angle of the spread of the downcoming wave at Cambridge was 5^o for E and F region reflections and about 7^o for sporadic E region reflections on 2.4 Mc/s. Rao and Rao (1961) found the semi-angle of the spread for F region reflections on 4.6 Mc/s at Waltair to be only 1^o which is smaller than the value obtained at Ahmedabad. It should be remembered that the observations on 4.6 Mc/s at Waltair refer to F region during day time, whereas those on 2.6 Mc/s at Ahmedabad refer to F region during nighttime.

Al'pert (1963) has shown that the radius of the reflecting zone approximately ranged from 2-10 km for the height range of 100-120 km and that the linear dimension of

the irregularities from 200-1000 metres as could be deduced from the results of Briggs and Phillips (1950) and Brameley (1951). These results are of the same order as obtained by us.

Table 6.2

Radius of the reflecting region and the dimension of the irregularities using the values of θ_o given in Figure 6.14.

Region	Height in km.	Spread angle θ °	Radius of the effective reflecting region. ρ_o, km.	Linear dimension of irregularities. L, m.
E (07-18 hr)	100	4.8°	8.3	218
E sporadic (19-05 hr)	100	5.2°	9.0	201
F (19-05 hr) without E_s	250	2.3°	10.0	456
F (19-05 hr) with E_s present	250	5.5°	24.0	190

CHAPTER VII

Summary and conclusions

We have dealt in some detail various aspects of the analysis of fading records and have given the results concerning horizontal drifts in the E and F regions of the ionosphere over Ahmedabad.

The essential points presented in each of the preceding chapters and some important general conclusions are summarised below.

In the first chapter a review of various methods of measuring horizontal drift of ionisation in the ionosphere is given. The method of similar fades of Mitra (1949) which has been adopted at different places in the world was also used at Ahmedabad. The results obtained by observing meteor trails and observations on scintillations of radio stars are briefly discussed.

In the second chapter the experimental set up at Ahmedabad is described. The author modified the transmitter to take observations on 4.5 Mc/s to 7.0 Mc/s. The various circuits employed in the transmitter, receiver and display units and the aerial system for the transmitter and the receiver are all described. The programme of observations established at Ahmedabad in 1960 and a few typical fading pictures at different frequencies reflected from E and F regions are illustrated at the end of the Chapter II.

In Chapter III, the results of analysis of fading records of reflections from E region are given for the period 1956-62. The analysis was carried out using the method of similar fades. The average value of the drift velocity at Ahmedabad (23° N) was found to be of the order of 80 m/s in 1957-59 and about 65 m/s in 1960-62. The most probable direction is towards N-W in winter daytime and summer nighttime. In other seasons the drift occurs towards N-W and S-E equally frequently. From the Fourier analysis it was found that the magnitude of the diurnal component was in general greater than the steady and semi-diurnal harmonic. The rotation of the diurnal drift vector with time was anticlockwise in winter and equinoxes, but clockwise in summer. In the case of semi-diurnal component, the rotation of the drift vector with time is in a clockwise fashion in winter and summer but in an anticlockwise direction in equinoxes. The direction of the N-S component of the drift was towards north during most of the time during 1956-59 and during part of the daytime in winter and equinoxes of 1959-62. It was towards south for the rest of the time in 1959-62. The E-W component of the drift was mostly towards west during daytime and towards east during nighttime with the exception of summer in 1959-62 when it was towards east all the time. The most frequent value for the drift velocity for Waltair (18° N) and Delhi (29° N) was about 75 m/s and 55 m/s respectively during the IGY.

In Chapter IV, the results of analysis of F region

drifts are presented. The observations were taken mostly on 2.6 Mc/s and 5.7 Mc/s. There was, however, no significant difference between the speed and direction values and so the results on these frequencies have been combined. The average speed decreases from about 79 m/s in 1957-59 to about 65 m/s in 1960-62. The average drift velocity was greater during night than during day in winter and summer in 1957-59, but the opposite was the case in 1960-62. It is interesting to note that the speeds are higher during night than during day from 1957 through 1962 in summer. The most probable direction was towards N-W in daytime and towards N-W and S-E in nighttime during 1957-59; whereas it was mostly towards S-E in daytime and nighttime during 1960-62. From the Fourier analysis, it was found that the magnitude of the steady component was generally higher in the northward drift, while the diurnal component was larger in the eastward drift than the semi-diurnal component. The rotation of the diurnal drift vector with time was in a clockwise direction in winter and in an anticlockwise direction in summer and equinoxes. The rotation of the semi-diurnal drift vector with time was clockwise in summer and anticlockwise in winter but was indeterminate in equinoxes. The N-S component of the drift was towards north during day and south during night in 1957-59, but was consistently towards south all the time during 1960-62. The E-W component of the drift was westward during day and eastward during night throughout 1957-62 except in summer of 1960-62 when it was mostly towards east and practically nil towards west. We have described

briefly the results of drift speed and direction obtained from observations on 7.0 Mc/s at Ahmedabad during daytime. The results generally agree with those obtained on 5.7 Mc/s.

Comparing F region drifts at Waltair and other places, we find that the mean drift velocity tends to decrease with decrease in solar activity which is in agreement with that found at Ahmedabad. The average hourly value when plotted with the time of the day showed semi-diurnal variation at Waltair, whereas it did not show any significant semi-diurnal periodicity at Ahmedabad or Delhi (Mitra et al, 1960) in 1957-59. In 1960-62, diurnal variation was significant in summer and winter and semi-diurnal variation in equinoxes. The results for Delhi for the latter period are not known and hence we do not know whether it had a variation similar to Ahmedabad or not. The magnitude of the drift speed was higher at Waltair than at Ahmedabad. So it appears that the speed increases towards equator and high latitudes with low speeds around Ahmedabad and Delhi zone.

From the study of directions of the E-W and the N-S components of drifts at various places, we find that Ahmedabad, Delhi and Yamagawa constitute a transition zone in the northern hemisphere as far as the E-W component is concerned. This is in accordance with Martyn's theory (1955) though the transition is not confined only to the geomagnetic latitude 35^{o}.

In Chapter V, the methods of auto - and cross-correlations are reviewed. The drift speed and direction

computed by full correlation analysis are presented and the results are compared with those computed by the method of Ratcliffe. Though the true drift velocity computed by the former method is somewhat lower than that obtained by the latter method, the results essentially remained unaltered and so we concluded that the method of similar fades is quite adequate to represent the general behaviour of the horizontal drift.

In the second part of Chapter V, we have given the type of amplitude distribution for some fading records. The distributions were generally either the Normal Gaussian or the Rayleigh type. But some records showed complex distribution. The ratio b of the amplitude of steady signal to the most probable amplitude of random signals gives a measure of the contribution of these two types of signals. We have shown that the most probable range of values of b is between 1.1 and 2.1 which means that the steady amplitude signal dominates over the R.M.S. value of the random amplitude signal at Ahmedabad.

The Chapter VI describes our attempt to work out the fine structure of the irregularities in the ionosphere. The ratio $\frac{V_c}{V}$ of equivalent random velocity to true drift velocity was of the order 1 at Ahmedabad indicating that both are equally important in producing the fading of reflected waves. From the semi-angle θ of a cone formed by the reflected rays from irregularities of an assumed ellipsoidal shape,

the linear dimension of such a characteristic ellipse have been estimated. The semi-major axis of the ellipse was of the order of 200 metres in the E region and greater than 400 metres in the F region.

Conclusions

The following are the main conclusions from the present study :-

1. The nighttime average drift velocities were greater than the average daytime drift velocities both in E and F regions.

2. There was no significant difference between the drift speed values obtained from the observations on any of the frequencies, 2.6 and 4.0-4.4 Mc/s or 5.7 and 7.0 Mc/s.

3. The average drift velocity was in general greater in the E region than in the F region.

4. Latitudinally the average drift velocity was lower in the Ahmedabad-Delhi region than at equatorial or high latitude station.

5. The most probable direction of horizontal drift was towards northwest during day and towards southeast during night.

6. No diurnal variation was apparent in E region drift speed in winter and equinoxes; but in summer there was a diurnal trend with minimum around noon and maximum around midnight. A semi-diurnal variation could be seen in winter during 1959-62.

7. There was no significant diurnal variation in the average F region drift speed in any season during 1957-59. However there appeared a diurnal variation in the drift speed in summer and winter and a semi-diurnal variation in equinoxes during 1960-62.

8. The E-W component of drift velocity was generally towards west during day and toward east during night both in E and F regions.

9. The N-S component of drift velocity was generally towards north during day and towards south during night in both the regions. However during 1960-62 the F region drift velocity was towards south all the time.

10. The rotation of diurnal vector with time in E region is anticlockwise in winter and equinoxes but clockwise in summer. The same vector in F region rotates clockwise in winter and anticlockwise in summer and equinoxes.

11. The rotation of semi-diurnal vector with time in E

and F regions is clockwise in winter and summer, but anticlockwise in equinoxes (in E region only).

12. The amplitude distribution of fading records was sometimes Rayleigh and Normal. There were also some mixed type with double humps or no hump at all.

13. The results obtained from auto - and cross-correlation techniques and from similar fades were not seriously different.

14. The ratio of random to true drift velocity was of the order of unity which meant that steady and random motions are equally prominent in causing fading of radio signals.

15. The semi-major axis of the characteristic ellipse assuming it as that due to irregularities that cause random fading was found to be of the order 200 metres in length in the E region and greater than 400 metres in the F region.

The effect of magnetic storms on the fading pattern could not be studied as the data on such occasions were not sufficient.

REFERENCES

Al'pert, Y.L.	1963	Radiowave Propagation and the Ionosphere, Consultants Bureau, New York, p.31-81.
Beynon, W.J.G. & Brown, G.M.	1957	Annals of the IGY, 3, 244.
Booker, H.G., Ratcliffe, J.A. & Shinn, D.H.	1950	Phil.Trans.Roy.Soc., A262, 579.
Bramley, E.N.	1953	Proc.Roy.Soc., A220, 39.
Bramley, E.N.	1951	Proc.Inst.Elect.Engrs., III, 198, 19.
Briggs, B.H.	1951	Proc.Phys.Soc., B64, 255.
Briggs, B.H.	1952	Private communication.
Briggs, B.H., Phillips, G.J. & Shinn, D.H.	1950	Proc.Phys.Soc., B63, 106.
Briggs, B.H. & Phillips, G.J.	1950	Proc.Phys.Soc., B63, 907.
Briggs, B.H. & Spencer, M.	1954	Rep.Prog.Phys., 17, 245.
Dasgupta, P. & Vij, K.K.	1960	J.Atmosph.Terr.Phys., 18, 265.
Elford, W.G.	1959	Planet.Space Sci., 1, 94.
Elford, W.G. & Robertson, D.S.	1953	J.Atmosph.Terr.Phys., 4, 271.
Fooks, G.F. & Jones, I.L.	1961	J.Atmosph.Terr.Phys., 20, 229.
Greenhow, J.S.	1954	Phil.Mag., 45, 364.

Greenhow, J.S. & Neufeld, E.L.	1955	Phil.Mag., 46, 546.
Greenhow, J.S. & Neufeld, E.L.	1961	Quart.J.R.Met.Soc., 87, 472.
Hewish, A.	1951	Proc.Roy.Soc., A209, 81.
Hines, C.O.	1963	Quart.J.R.Met.Soc., 89, 1.
Hoffmeister, C.	1946	Z.Meterologie., 1, 33.
Khastgir, S.R. & Sing, R.N.	1961	Ind.Jour.Phys., 34, 527.
Little, C.G. & Maxwell, A.	1951	Phil.Mag., 42, 267.
McNicol, R.W.E.	1949	Proc.Inst.Elect.Engrs., III, 96, 517.
Manning, L.A., Villard, O.G. & Peterson, A.M.	1950	Proc.Inst.Radio Engrs., 38, 877.
Martyn,D.F.	1955	Physics of the ionosphere. Phys.Soc., London, p.163.
Maxwell, A. & Little, C.G.	1952	Nature, 169, 746.
Mitra, S.N.	1949	Proc.Inst.Elect.Engrs., III, 96, 441.
Mitra,S.N.	1949	Proc.Inst.Elect.Engrs., III, 96, 505.
Mitra, S.N., Vij, K.K. & Dasgupta, P.	1960	J.Atmosph.Terr.Phys., 19, 172.
Mitra, S.N. & Srivastava, R.B.L.	1957	Ind.Jour.Phys., 31, 20.
Munro, G.H.	1948	Nature, 162, 886.
Munro, G.H.	1950	Proc.Roy.Soc., A202, 208.
Munro, G.H.	1953	Nature, 171, 193.
Nanda, N.G.	1955	M.Sc. Thesis (Gujarat University).

Oliver, C.P.	1942	Proc.Amer.Phil.Soc., 85, 93.
Oliver, C.P.	1947	Proc.Amer.Phil.Soc., 91, 315.
Pawsey, J.L.	1933	Proc.Camb.Phil.Soc., 31, 107.
Phillips, G.J. & Spencer, M.	1955	Proc.Phys.Soc., B63, 481.
Piggot, W.R. & Barclay, L.W.	1962	Proc.Intern.Conf.on Ionosphere, Phys.Soc., London, p.323.
Rao, B.R. & Rao, E.R.	1959	J.Atmosph.Terr.Phys., 14, 94.
Rao, A.S. & Rao, B.R.	1963	J.Atmosph.Terr.Phys., 25, 249.
Rao, A.S. & Rao, B.R.	1964	J.Atmosph.Terr.Phys., 26, 339.
Rao, E.B. & Rao, B.R.	1961	J.Sci.Indust.Res., India, 20B, 7, 307.
Rao, G.L.N. & Rao, B.R.	1963	J.Atmosph.Terr.Phys., 25, 553.
Rao, G.L.N. & Rao, B.R.	1964	J.Atmosph.Terr.Phys., 26, 213.
Rao, G.L.N. & Rao, B.R.	1965	J.Geophys.Res., 70, 667.
Rao, R.R. & Rao, B.R.	1961	J.Atmosph.Terr.Phys., 22, 81.
Ratcliffe, J.A.	1948	Nature, 162, 9.
Ratcliffe, J.A.	1954	J.Atmosph.Terr.Phys., 5, 173.
Ratcliffe, J.A.	1956	Rep.Prog.Phys., 19, 188.
Ratcliffe, J.A.	1960	Physics of the upper atmosphere, Acedemic Press, New York, p.448.
Rice, S.O.	1945	Bell Syst.Tech.J., 24, 46.
Robertson, D.A., Liddy, D.T. & Elford, W.G.	1953	J.Atmosph.Terr.Phys., 4, 255.